

Electronic Theses and Dissertations, 2004-2019

2014

Climate and landscape controls on seasonal water balance at the watershed scale

Xi Chen
University of Central Florida

 Part of the [Environmental Engineering Commons](#)
Find similar works at: <https://stars.library.ucf.edu/etd>
University of Central Florida Libraries <http://library.ucf.edu>

This Doctoral Dissertation (Open Access) is brought to you for free and open access by STARS. It has been accepted for inclusion in Electronic Theses and Dissertations, 2004-2019 by an authorized administrator of STARS. For more information, please contact STARS@ucf.edu.

STARS Citation

Chen, Xi, "Climate and landscape controls on seasonal water balance at the watershed scale" (2014).
Electronic Theses and Dissertations, 2004-2019. 4628.
<https://stars.library.ucf.edu/etd/4628>

CLIMATE AND LANDSCAPE CONTROLS ON SEASONAL WATER BALANCE AT THE
WATERSHED SCALE

by

XI CHEN
B.S. Nankai University, 2007
M.S. University of Kansas, 2009

A dissertation submitted in partial fulfillment of the requirements
for the degree of Doctor of Philosophy
in the Department of Civil, Environmental, and Construction Engineering
in the College of Engineering and Computer Science
at the University of Central Florida
Orlando, Florida

Summer Term
2014

Major Professor: Dingbao Wang

© 2014 Xi Chen

ABSTRACT

The main goal of this dissertation is to develop a seasonal water balance model for evaporation, runoff and water storage change based on observations from a large number of watersheds, and further to obtain a comprehensive understanding on the dominant physical controls on intra-annual water balance. Meanwhile, the method for estimating evaporation and water storage based on recession analysis is improved by quantifying the seasonal pattern of the partial contributing area and contributing storage to base flow during low flow seasons.

A new method for quantifying seasonality is developed in this research. The difference between precipitation and soil water storage change, defined as effective precipitation, is considered as the available water. As an analog to climate aridity index, the ratio between monthly potential evaporation and effective precipitation is defined as a monthly aridity index. Water-limited or energy-limited months are defined based on the threshold of 1. Water-limited or energy-limited seasons are defined by aggregating water-limited or energy-limited months, respectively.

Seasonal evaporation is modeled by extending the Budyko hypothesis, which is originally for mean annual water balance; while seasonal surface runoff and base flow are modeled by generalizing the proportionality hypothesis originating from the SCS curve number model for surface runoff at the event scale. The developed seasonal evaporation and runoff models are evaluated based on watersheds across the United States. For the extended Budyko model, 250 out of 277 study watersheds have a Nash-Sutcliffe efficiency (NSE) higher than 0.5, and for the seasonal runoff model, 179 out of 203 study watersheds have a NSE higher than 0.5.

Furthermore, the connection between the seasonal parameters of the developed model and a variety of physical factors in the study watersheds is investigated. For the extended Budyko model, vegetation is identified as an important physical factor that related to the seasonal model parameters. However, the relationship is only strong in water-limited seasons, due to the seasonality of the vegetation coverage. In the seasonal runoff model, the key controlling factors for wetting capacity and initial wetting are soil hydraulic conductivity and maximum rainfall intensity respectively. As for initial evaporation, vegetation is identified as the strongest controlling factor. Besides long-term climate, this research identifies the key controlling factors on seasonal water balance: the effects of soil water storage, vegetation, soil hydraulic conductivity, and storminess.

The developed model is applied to the Chipola River watershed and the Apalachicola River basin in Florida for assessing potential climate change impact on the seasonal water balance. The developed model performance is compared with a physically-based distributed hydrologic model of the Soil Water Assessment Tool, showing a good performance for seasonal runoff, evaporation and storage change.

I dedicate this dissertation to my fiancé, Yi Zhu. I met her three years ago in University of Central Florida. I was going through a struggling time back then and she came to my life with hope and joy. She brought out the best of me, helped me to accomplish goals that I would not achieve by myself. This is for you, my love.

ACKNOWLEDGMENTS

I want to express my sincere appreciation for my advisor Dr. Dingbao Wang. He is my mentor in the field of hydrology. Guided by his brilliant thoughts, I started my research in this area. He made the hydrologic research enjoyable during my doctoral study.

I want to thank Dr. Scott C. Hagen for his kindness and generosity. I really appreciate his help during my doctoral study. I thank him for the opportunity to collaborate with CHAMPS lab research group on different projects, and for the recommendation for the Fluid Mechanics instructor opportunity.

This research was funded in part under Award NA10NOS4780146 from the National Oceanic and Atmospheric Administration (NOAA) Center for Sponsored Coastal Ocean Research (CSCOR) and Award NA10OAR4170079 from the Florida Sea Grant.

I also want to thank my committee members, Dr. Manoj Chopra and Dr. David M. Sumner, for the comments and cooperation. Also, I would like to thank my colleagues: Mr. Seoyoung Kim, Mr. Debapi Ghosh, Mr. Han Xiao and Ms. Yin Tang for their support and help. Finally, I want to thank my family, my mother Yanqing Cui and my father Dequan Chen, my uncle Guangming Cui and my aunt Yanrong Cui for giving me the opportunity to pursue my master's and doctor's degree in the US.

TABLE OF CONTENTS

LIST OF FIGURES	x
LIST OF TABLES	xiii
CHAPTER 1: INTRODUCTION	1
1.1 Long-term Water Balance and Budyko Framework	1
1.2 Annual and Intra-annual Scale Water Balance.....	3
1.3 Runoff Simulation and Proportionality Hypothesis	4
1.4 Discharge-Storage Interaction and Recession Analysis.....	5
1.5 The Strength and Limitation of the “Top-Down” Approach	6
1.6 Human Impact and Socio-Hydrology	7
1.7 Research Objectives	7
CHAPTER 2: EXTENDED BUDYKO FRAMEWORK	9
2.1 Methodology	9
2.1.1 Data collection	9
2.1.2 Wet and dry months.....	10
2.1.3 Seasonal aridity index	12
2.1.4 Seasonal evaporation ratio	13
2.1.5 Budyko-type models at the seasonal scale.....	14
2.1.6 Modeling annual storage changes.....	17
2.1.7 Model performance evaluation	18
2.2 Results and Discussion.....	19
2.2.1 Storage change impact on inter-annual water balance.....	19
2.2.2 Performance of the modified seasonal Turc-Pike model.....	20
2.2.3 Estimation model parameters.....	22
2.2.4 Vegetation control on seasonal evaporation ratios	23
2.2.5 Estimation of annual storage changes.....	25
2.2.6 Impacts of evaporation data uncertainty	27
2.2.7 Physically-based processes versus co-evolution.....	28
CHAPTER 3: RUNOFF GENERATION AND PROPORTIONALITY HYPOTHESIS	30

3.1 Methodology	30
3.1.1 SCS curve number method and proportionality hypothesis	30
3.1.2 Modeling runoff generation at annual scale using proportionality hypothesis	31
3.1.3 Two-stage partition at the seasonal scale	33
3.1.4 Modeling seasonal runoff based on the proportionality hypothesis	34
3.1.5 Data collection	38
3.2 Results and Discussion	40
3.2.1 Model performance	40
3.2.2 Estimated model parameters for seasonal water balance	41
3.2.2.1 Wetting capacity	42
3.2.2.2 Initial wetting	45
3.2.2.3 Initial evaporation	48
CHAPTER 4: STORAGE DYNAMICS AND CONTRIBUTING AREA	51
4.1 Methodology	52
4.1.1 Recession analysis	52
4.1.2 Estimation of α and β	57
4.1.3 Data selection and S_m	57
4.2 Results and Discussion	58
4.2.1 Recession analysis and parameter α and β	58
4.2.2 Underestimation of evaporation from base flow recession analysis	59
4.2.3 Temporal variability of α	61
4.2.4 Temporal variability of β	62
4.2.5 Variability of storage-discharge relationship	65
CHAPTER 5: CASE STUDIES	67
5.1 Case Study at Chipola River Watershed	67
5.1.1 General information of Chipola River Watershed	67
5.1.2 Seasonal water balance simulation	68
5.1.3 Seasonal water balance projection	69
5.2 Case Study at Apalachicola River Watershed	71
5.2.1 Study area and data sources	71

5.2.2 SWAT model parameter calibration and validation	74
5.2.3 RCM selection and future climate change projection.....	76
5.2.4 Climate change projections.....	77
5.2.5 Projected climate changes.....	79
5.2.6 Model calibration and performance during the baseline period	81
5.2.7 Runoff and sediment load under climate change scenarios	85
5.2.8 Runoff and sediment load during extreme events under climate change	86
CHAPTER 6: SUMMARY.....	89
REFERENCES	91

LIST OF FIGURES

Figure 1: The hydrologic cycle. (1) Exchange between water and energy; (2) Runoff generation; (3) Storage dynamics; and (4) Human/water interaction.....	2
Figure 2: The spatial distribution of study watersheds which are categorized by the number of months in dry seasons.	10
Figure 3: Seasonal evaporation ratio versus seasonal aridity index and the fitted Turc-Pike lines for the Rocky River watershed located in North Carolina at the USGS gage 02126000 (Panel A), the Auglaize River watershed in Ohio at the USGS gage 04191500 (Panel B), the Oostanaula River watershed located in Georgia at the USGS gage 02387500 (Panel C), and the Clear Fork Brazos River watershed in Texas at the USGS gage 08085500 (Panel D).....	17
Figure 4: Three presentations of annual water balance: a) $1-Q/P$ versus E_p/P ; b) E/P versus E_p/P ; c) $E_p/(P-\Delta S)$ versus $E/(P-\Delta S)$	20
Figure 5: Histograms of coefficient of efficiency for the modified Ture-Pick model in wet season (Panel A) and dry season (Panel B)	22
Figure 6: Histogram of parameters of wet and dry seasons	23
Figure 7: Seasonal parameters of the modified Turc-Pike equation and the long-term average NDVI in dry seasons and wet seasons	26
Figure 8: Observed and estimated values of annual storage changes during the validation period (1993-2002) in watersheds with both wet and dry seasons (Panel A), dry seasons only (Panel B), and wet seasons only (Panel C)	27
Figure 9: Strength of the Newtonian view and the Darwinian method on modeling evaporation at varying time scale.	29
Figure 10: Monthly evaporation ratio versus monthly aridity index and the fitted Turc-Pike lines for the Rocky River watershed (Panel A), the Auglaize River watershed (Panel B), the Oostanaula River watershed (Panel C), and the Clear Fork Brazos River watershed (Panel D).	30
Figure 11: Conceptual scheme for the first-stage partition for modeling surface runoff.	36
Figure 12: Conceptual scheme for the first-stage partition for modeling base flow.	37
Figure 13: NSE values during the validation period in different seasons: (a) direct runoff simulation, (b) base flow simulation, and (c) total runoff simulation	41
Figure 14: Spatial distribution of wetting capacity in 203 study watersheds: (a) energy-limited seasons , and (b) water-limited seasons	43
Figure 15: Relationships of W_p vs. K_a (a) and W_p vs. T_r (b) in energy-limited seasons; and W_p vs. K_a (c) and W_p vs. $NDVI_{ave}$ (d) in water-limited seasons	44
Figure 16: Comparison of wetting capacity values from the runoff model and from the regression equations in (a) energy-limited seasons and (b) water-limited seasons.....	45
Figure 17: Spatial distribution of intial wetting in the: (a) energy-limited seasons, and (b) water-limited seasons	46

Figure 18: Relationships of (a) $\lambda_s W_p$ vs. i_{max} in the energy-limited seasons, (b) $\lambda_s W_p$ vs. i_{max} and (c) $\lambda_s W_p$ vs. $NDVI_{ave}$ in the water-limited seasons.....	46
Figure 19: Comparison of initial wetting estimated from the two-stage runoff model and the regression equations in: (a) the energy-limited seasons and (b) the water-limited seasons ...	47
Figure 20: Spatial distribution of initial evaporation: (a) energy-limited seasons, and (b) water-limited seasons.....	49
Figure 21: Correlation of (a) E_0 vs. N in the energy-limited seasons, (b) E_0 vs. $NDVI$ in the energy-limited seasons, (c) E_0 vs. N in the water-limited seasons, and (d) E_0 vs. $NDVI$ in the water-limited seasons.....	49
Figure 22: Comparison of initial evaporation values from the two-stage runoff model and from the regression equations: (a) energy-limited seasons and (b) water-limited seasons.	50
Figure 23: Locations of the 9 study watersheds with Spoon River watershed located in Illinois highlighted with dark blue.	51
Figure 24: $-dQ/dt$ versus Q and the lower envelope for the Spoon River water based on daily streamflow data during 01/01/1983-12/31/2003.....	53
Figure 25: Comparison between estimated evaporation from recession analysis and evaporation from remote sensed data	58
Figure 26: Estimated α versus discharge (Q) from the Spoon River watershed.....	61
Figure 27: Cumulative distribution function of α from all the study watersheds.	62
Figure 28: Cumulative distribution function of $\beta=S/TS$ from all the study watersheds	63
Figure 29: Correlation between $\Delta S/\Delta TS$ and α in the Spoon River watershed.....	63
Figure 30: The relationship between estimated β and observed shallow groundwater table depth at the Spoon River watershed	65
Figure 31: The impact of variable contributing storage on the total storage-discharge relationship at the Spoon River watershed	66
Figure 32: Chipola River Watershed	68
Figure 33: Simulationg results in Chipola River Watershed in terms of evaporation (a), storage change (b) and runoff (c) and their comparison with the observed values respectively.....	69
Figure 34: Projection results in Chipola River Watershed in terms of evaporation (a), storage change (b) and runoff (c) and their comparison with the present values respectively	70
Figure 35: The basin boundary, river network, ground surface elevations, and the locations of rainfall and streamflow observation in the Apalachicola River basin.	72
Figure 36: Land use/land cover map in 1992 (a); and soil map (b) in Apalachicola River basin	73
Figure 37: Comparison of observed values and RCM baseline projections of mean monthly precipitation (a) and temperature (b)	78
Figure 38: Comparison of observed values and RCM future projections of mean monthly precipitation (a) and temperature (b)	80
Figure 39: (a) Time series of simulated and observed streamflow at the gage 2359170; (b) time series of simulated and observed sediment load at the gage 2359170.....	83

Figure 40: (a) 1:1 plot of simulated runoff versus observed streamflow; (b) 1:1 plot of simulated and observed sediment load	84
Figure 41: The mean monthly changing rate of discharge (a) and sediment load (b) under climate change impact based HRM3-HADCM3 and RCM3-GFDL	86
Figure 42: Hyetograph of the sample storms at three different locations in the Apalachicola River basin at 3/2/1991	87
Figure 43: Future projections of discharge (a) and sediment load (b) during the extreme event under climate change impact projection	88

LIST OF TABLES

Table 1: Information of the chosen 18 watersheds	42
Table 2: Watershed name, USGS gage number, drainage area, climate aridity index (E_p/P), and estimated recession parameters for the 9 case study watersheds	54
Table 3: One recession event from the Spoon River watershed in Illinois.....	59
Table 4: One recession event from the Nodaway River watershed in Iowa.....	59
Table 5: Calibrated parameter values for the SWAT model.....	82

CHAPTER 1 INTRODUCTION

The hydrologic water cycle is the fundamental concept in hydrology. At watershed scale, the complex hydrologic system is mainly controlled by climate and landscape factors. Rainfall partition into runoff, evaporation, and soil water storage change and the physical controls of climate, soil, topography, and vegetation on the partition at different temporal and spatial scales are fundamental questions for hydrologists. As shown in Figure 1, within catchment scale, water balance involves the water and energy exchange between land and atmosphere, namely precipitation and evaporation; as well as the spatial movement of water at the land surface and within the land, namely surface runoff and base flow; and also the soil storage and discharge interaction, namely storage dynamics. A comprehensive understanding of the complex catchment water system would be of great value.

1.1 Long-Term Water Balance and Budyko Framework

With the increase of the temporal scale, the complexity of rainfall partition decreases since the temporal variability of hydrologic variables is filtered out in the time-averaged values. *Budyko* [1958; 1974] postulated that mean annual water balance, represented by the ratio between evaporation and precipitation (E/P), is dominantly controlled by the climate aridity index, which is the ratio between potential evaporation and precipitation (E_p/P). The time scale in the Budyko framework is defined as the long-term average over far more than one year [Donohue *et al.*, 2010]. Various functional forms have been developed for quantifying the

relation between E/P and E_p/P [Turc, 1954; Pike, 1964; Fu, 1981; Choudhury, 1999; Zhang *et al.*, 2001; Porporato *et al.*, 2004; Yang *et al.*, 2008; Gerrits *et al.*, 2009]. Furthermore, the effects of rainfall seasonality and soil water storage capacity [Milly, 1994a and 1994b; Potter *et al.*, 2005; Hickel and Zhang, 2006; Yokoo *et al.*, 2008; Gerrits *et al.*, 2009; Feng *et al.*, 2012], and vegetation dynamics [Zhang *et al.*, 2001; Donohue *et al.*, 2007] on mean annual water balance have been discussed as a complementary to the climate aridity index. The Budyko framework provides a useful tool to assess the impacts of climate and watershed characteristic changes on annual runoff [Donohue *et al.*, 2011; Roderick and Farquhar, 2011; Wang and Hejazi, 2011; Yang and Yang, 2011].

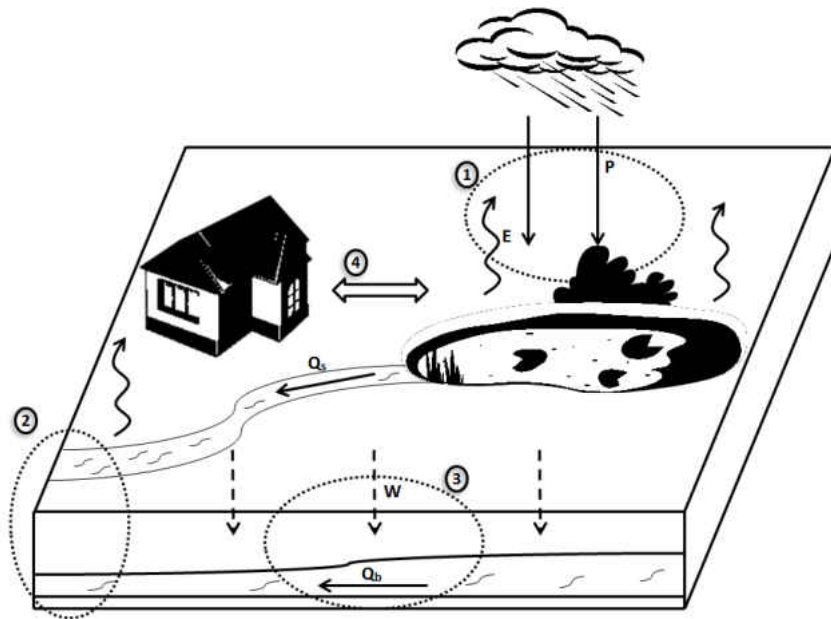


Figure 1: The hydrologic cycle. (1) Exchange between water and energy; (2) Runoff generation; (3) Storage dynamics; and (4) Human/water interaction.

1.2 Annual and Intra-Annual Scale Water Balance

The Budyko framework has been applied to inter-annual variability of rainfall partition in many studies [*Koster and Suarez, 1999; Sankarasubramanian and Vogel, 2002; Yang et al., 2007; Potter and Zhang; 2009; Cheng et al., 2011*]. Soil water storage changes have been found to be a significant component on the inter-annual variability of water balance at some study watersheds [*Milly and Dunne; 2002; Zhang et al., 2008; Donohue et al., 2010; Istanbuluoglu et al., 2012; Wang, 2012a*]. *Wang and Alimohammadi [2012]* estimated water storage changes as water balance residuals using remote sensing-based evaporation estimations and found that water storage carry-over is significant particularly for watersheds in arid regions. To consider the inter-annual soil water storage changes in the Budyko framework, *Wang [2012a]* suggested that effective rainfall, which is the difference between rainfall and soil water storage change, is taken as available water supply; and therefore rainfall in both the climate aridity index and the evaporation ratio is replaced by the computed effective rainfall.

Both rainfall seasonality and soil water storage change play a significant role on inter-annual variability of hydrologic responses [*Donohue et al., 2012*]. Soil water storage capacity, which filters the seasonal rainfall variability, can lower the runoff ratio [*Milly, 1993; Sankarasubramanian and Vogel, 2002 and 2003; Porporato et al., 2004; Fang et al., 2012*]. *Zhang et al. [2008]* extended the limit concept of Budyko hypothesis to generalized water demand and supply framework and the framework was applied to the water partition at two stages for developing monthly and daily water balance models. *Yokoo et al. [2008]* incorporated storage capacity index and drainability index to model water balance at the seasonal scale. *Jothityangkoon and Sivapalan [2009]* examined the effects of storminess on inter-annual

variability of water balance through the simulation of annual runoff in three semi-arid watersheds. *Zanardo et al.* [2012] studied the within-year rainfall variability controls on annual water balance in a diagnostic and data-driven approach.

1.3 Runoff Simulation and Proportionality Hypothesis

The mechanism of runoff generation is strongly related with hydrologic partitioning but with a higher timing sensitivity. *L'vovich* [1979] presented the two-stage hydrologic partitioning theory, which separated the water balance partitioning into surface runoff generation and base flow generation. To model surface runoff, curve number method was developed by the USDA Soil Conservation Service [USDA SCS, 1985]. As a widely used method to quantify surface runoff based on precipitation, curve number method described water balance partitioning with an empirical proportionality hypothesis [*Ponce and Hawkins*, 1996]. Based on *L'vovich's* two-stage theory, *Ponce and Shetty* [1995] proposed to use the proportional relation derived from curve number method to describe annual scale water balance. Following *Ponce and Shetty's* study, *Sivapalan et. al.* [2011] further explored the potential of proportionality in annual scale water balance. *Wang and Tang* [2014] showed that the proportionality is independent on time scales.

1.4 Discharge-Storage Interaction and Recession Analysis

The difficulties involved in measurement of water storage are due to the spatial variability of soil moisture and groundwater storage. Terrestrial water storage changes can be

identified by monitoring the variability in gravity field through Gravity Recovery and Climate Experiment (GRACE) satellite [Swenson *et al.*, 2006]. However, the spatial resolution of GRACE is too large to be applicable for watershed scale studies. Water storage changes can also be estimated by using point-based observations of groundwater level and soil moisture [Wang, 2012a] or water balance closure [Sayama *et al.*, 2011; Wang and Alimohammadi, 2012]. These methods are constrained by the data availability of soil moisture, groundwater and actual evaporation.

As a simple approach, the conceptual storage-discharge function derived from base flow recession has been used to estimate storage changes [e.g., Kirchner, 2009; Teuling *et al.*, 2010; Ajami *et al.*, 2011; Krakauer and Temimi, 2011], evaporation [e.g., Szilagyi *et al.*, 2007; Palmroth *et al.*, 2010], and leakage from and to bedrock [Wang, 2011]. The estimated evaporation and water storage dynamics from the lumped storage-discharge relationship are usually treated as the total values of the entire watershed. The underlying assumption is that all the subsurface storage in the watershed contributes to the streamflow observed at the outlet [Wang, 2012b]. The violation of this assumption may affect the evaporation and storage change estimation significantly, especially in large watersheds with considerable spatial heterogeneity of soil water storage.

However, the storage/discharge connectivity of a watershed varies spatially and temporally, especially during recession events. As a result, the storage-discharge function may also vary when total watershed storage is used in the lumped discharge model. The variable characteristic of storage-discharge function has been reported by several studies [e.g., Rupp *et al.*, 2009]. Using a linearized distributed model, Sloan [2000] found that total water storage and groundwater discharge is not a one-to-one relationship. Hysteresis relation between storage and

streamflow has been reported due to the variable hydrologic connectivity of water storage [Spence *et al.*, 2010]. Clark *et al.* [2011] demonstrated that a multi-valued storage-discharge relationship could be replicated by a simple lumped conceptual model with two parallel stores representing the saturated zone. Krakauer and Temimi [2011] reported that storage change estimated from base flow recession is underestimated compared with GRACE based estimation. A systematic investigation on the potential and limitation of one-to-one storage-discharge recession analysis in terms of evaporation and storage estimation would be beneficial as to improve the framework.

1.5 The Strength and Limitation of the “Top-Down” Approach

The development of hydrological model can be generally sorted into “top-down” approach and “bottom-up” approach. The currently dominating “bottom-up” approach is physical-process-based, which require a variety of input data. The approach focused in this study is “top-down” approach. The fundamental theories in this study, namely Budyko framework, proportionality hypothesis and recession analysis, are all developed based on “top-down” approach. While the “top-down” approach have the advantages of simpler model and lower requirement for input data comparing with “bottom-up” approach, two important questions should be considered as applying the approach: (1) how far the conceptual system can go down, temporally and spatially, and remain valid; (2) the difficulty of generalization. In fact, the limitation of the “top-down” approach is hard to be overcome without external assistance. The same statement can be applied on “bottom-up” approach as well. As a result, while the “top-down” approach is focusing on the simple dominating process and “bottom-up” approach is

focusing on complex individual processes and their interactions, a combination of the two approaches will probably be required to further the understanding of the hydrologic prediction issues [Sivapalan, *et al.*, 2003].

1.6 Human Impact and Socio-Hydrology

The purpose of hydrological model is to understand the physical controls behind the complex hydrologic processes and therefore to simulate and predict the trend of processes. As a result, the human impact is usually separated from all the natural factors and not included in the model, which is the case in this study. However, the interaction between natural water body and human activities is also one of the important aspects, if not the most, of the hydrologic system. In the large scale, climate change, which is potentially caused by human activities, is expected to change every aspect in the hydrological cycle. At the small scale, hydraulics projects and water management policies will have direct impact to local watersheds and the ecology system around them. With the idea of co-evolution of coupled human-water system, a new topic of socio-hydrology is interested by the hydrology science society [Sivapalan, *et al.*, 2012].

1.7. Research Objectives

The main goal of this study is to use “top-down” approach to simulate catchment scale hydrologic processes, in terms of water partitioning, runoff generation and storage dynamics, and therefore to improve the understanding on intra-annual water balance of watersheds.

The objectives of the study can be summarized as follow:

- (1) To develop seasonal and monthly evaporation model based on Budyko framework;
- (2) To develop seasonal and monthly runoff model based on proportionality hypothesis;
- (3) To combine the newly developed evaporation model and runoff model to obtain the complete water balance model at watershed scale;
- (4) To investigate the feasibility of recession analysis in terms of evaporation and storage change estimation;
- (5) To apply the water balance model on practical case study in Chipola River Watershed and to combine the water balance model with Regional Climate Model (RCM) projection to predict the future trend of evaporation and runoff.
- (6) To apply the Soil and Water Assessment Tools (SWAT) on the case study in Apalachicola River Watershed and to combine the hydrologic model with RCMs to project future streamflow and sediment load change under extreme events.

CHAPTER 2 EXTENDED BUDYKO FRAMEWORK

The first step of the study is to develop intra-annual evaporation model based on Budyko framework. As the time scale shortened from long-term mean annual, which Budyko hypothesis was based on, to intra-annual scale of seasonal and monthly, the number of controlling factors of the process increases. Storage change and seasonality are the two additional factors in the modified Budyko type model. The development of the model is described in detail as follows.

2.1 Methodology

2.1.1 Data collection

Daily precipitation, climatic potential evaporation, and runoff data from 1948 to 2003 are based on the Model Parameter Estimation Experiment (MOPEX) watersheds with low human interferences [Duan et al., 2006]. Daily actual evaporation and monthly potential evaporation from 1983 to 2006 are obtained from the data set provided by University of Montana [Zhang et al, 2010]. Actual evaporation data is derived from remote sensing data and provided at the gridded resolution of 8 km; and the potential evaporation was estimated using Priestley-Taylor method [Priestley and Taylor, 1972] at the same spatial resolution. The daily evaporation and monthly potential evaporation data are spatially averaged to the watershed scale values. This research is focused on the overlapped period of the two data sets from 1983 to 2003. As shown in Figure 2, 277 watersheds, for which there is no missing data during the entire period of 21 years, are selected as study watersheds for the model development.

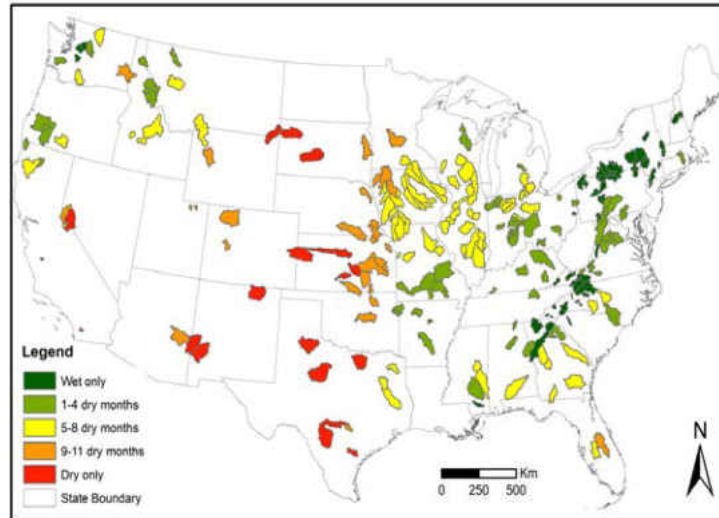


Figure 2: The spatial distribution of study watersheds which are categorized by the number of months in dry seasons.

2.1.2 Wet and dry months

The monthly aridity index, which follows the concept of climate aridity index, is the ratio of available energy to available water. For long-term water balance, water storage change is usually negligible compared with mean annual precipitation depth. Available energy is represented by potential evaporation, and water availability is represented by precipitation. However, water storage dynamics is significant at the monthly and seasonal scales, and therefore storage change needs to be considered for accounting available water supply. The available water supply in dry months includes not only precipitation but also the depletion of stored water in the watershed; while watershed storage is replenished by infiltrated rainfall in wet months, and the increased storage needs to be subtracted from precipitation. Following Wang [2012a], water availability is defined as effective precipitation $P_m - \Delta S_m$, and monthly aridity index (A_m) is defined as:

$$A_m = \frac{E_{P_m}}{P_m - \Delta S_m} \quad (2.1)$$

2.1.3 Seasonal aridity index

With the wet and dry months identified by equation (2.2), seasonal depths of precipitation, potential evaporation, runoff, and storage change are computed for each year by aggregating monthly values. For example, precipitation depth in the wet season (P_w) and the dry season (P_d) is computed by:

$$P_w = \sum_{i=1}^{n_w} P_{w_i} \quad (2.3.1)$$

$$P_d = \sum_{i=1}^{n_d} P_{d_i} \quad (2.3.2)$$

where n_w and n_d are the numbers of wet and dry months in a year and are constants for a given watershed. Similarly, the seasonal values for potential evaporation depth (E_{P_w} and E_{P_d}), runoff depth (Q_w and Q_d), and storage changes (ΔS_w and ΔS_d) are computed based on the monthly values in wet and dry seasons.

Following the definition of monthly aridity index, seasonal aridity indices for individual years are defined as:

$$A_w = \frac{E_{P_w}}{P_w - \Delta S_w} \quad (2.4.1)$$

$$A_d = \frac{E_{P_d}}{P_d - \Delta S_d} \quad (2.4.2)$$

where A_w and A_d are the seasonal aridity indices for wet and dry seasons, respectively. Climate seasonality is explicitly modeled in the seasonal aridity index since seasonal rainfall and potential evaporation depths are included in A_w and A_d . Seasonal water storage changes in equation (2.4) are hydrologic variables which are controlled by many factors such as soil water storage capacity and infiltration potential. The defined seasonal aridity indices are

hydroclimatic variables reflecting both climate seasonality and hydrologic characteristics of watersheds.

The values of seasonal aridity index for individual years are usually less than 1 for wet seasons and higher than 1 for dry seasons. It should be noted that this may not be valid for all the years, since the definition of dry and wet months is based on the mean monthly aridity index (equation 2.2). If the monthly aridity index for a year deviates significantly from its mean value, it is possible that the seasonal aridity indices are higher than one in wet seasons (or lower than one in dry seasons). It is possible that the mean monthly aridity indices for all 12 months are larger or smaller than 1 for some watersheds where the seasonality is not strong. For these watersheds, there is only one season (wet or dry), and the seasonal aridity index is the exact *equivalent* of the annual aridity index.

2.1.4 Seasonal evaporation ratio

In the Budyko framework, evaporation ratio is defined as the ratio between actual evaporation and water supply. Following the definition of seasonal aridity index, water supply is represented by the seasonal effective precipitation, and evaporation ratios for wet and dry seasons are modified as $\frac{E_w}{P_w - \Delta S_w}$ and $\frac{E_d}{P_d - \Delta S_d}$, respectively. In the next section, a Budyko-type function is extended to model the inter-annual relationship between the seasonal evaporation ratio and the seasonal aridity index defined above.

2.1.5 Budyko-type models at the seasonal scale

The semi-empirical equation proposed by *Budyko* [1974] is a non-parametric model for long-term water balance. To incorporate the effects of other factors on water balance, Budyko-type functions with a single parameter have been developed in the literature [*Fu*, 1981; *Zhang et al.*, 2001; *Yang et al.*, 2008]. One of the functional forms is the Turc-Pike equation:

$$\frac{E}{P} = \left[1 + \left(\frac{E_P}{P} \right)^{-v} \right]^{-1/v} \quad (2.5)$$

where v is the parameter which represents the effects of other factors such as vegetation, soil, and topography on the partition of precipitation. In this study, the Turc-Pike equation will be extended to model the dependence of the seasonal evaporation ratio on the seasonal aridity index.

The following two factors are considered in the extension of Budyko-type model to the seasonal scale: (1) the lower bound of the seasonal aridity index for a given watershed; and (2) the differentiation between dry and wet seasons. The Budyko equation provides an inter-comparison of water balance among watersheds. E/P approaches to zero when climate aridity index approaches to zero in equation (2.5). However, for a given watershed, the lower bound of seasonal aridity index may be a positive value or even higher than 1 in dry seasons. To characterize the possible non-zero lower bound of the seasonal aridity index, a shift along the horizontal axis is introduced to equation (2.5). On the other hand, two different sets of parameter values in equation (2.5) are used for wet and dry seasons for the purpose of differentiating the precipitation partitioning behavior in wet and dry conditions.

As a result, the following modified Turc-Pike equations are proposed to model the seasonal evaporation ratio in wet and dry seasons, respectively:

$$\frac{E_w}{P_w - \Delta S_w} = \left[1 + \left(\frac{E_{P_w}}{P_w - \Delta S_w} - \phi_w \right)^{-v_w} \right]^{-1/v_w} \quad (2.6.1)$$

$$\frac{E_d}{P_d - \Delta S_d} = \left[1 + \left(\frac{E_{P_d}}{P_d - \Delta S_d} - \phi_d \right)^{-v_d} \right]^{-1/v_d} \quad (2.6.2)$$

where v_w and v_d are the Turc-Pike coefficients in wet and dry seasons, respectively; and ϕ_w and ϕ_d are the corresponding lower bounds for the seasonal aridity indices. For the seasonal evaporation model, it is assumed that the functional form of the Budyko curve is applicable to seasonal time scale with the following modifications: (1) seasonal climate aridity index is defined as the ratio of potential evaporation to effective precipitation; (2) seasonal evaporation ratio is defined as the ratio of evaporation to effective precipitation; (3) the lower bound of seasonal climate aridity index can be more than zero.

For purposes of demonstration, Figure 3 plots the seasonal evaporation ratio versus seasonal aridity index for 4 selected watersheds, in which the parameters in equation (2.6) are estimated by fitting the observed data points. The Rocky River watershed located in North Carolina (Panel A) and the Auglaize River watershed in Ohio (Panel B) include both wet (diamond) and dry (circle) seasons. However, the Oostanaula River watershed located in Georgia (Panel C) only includes wet seasons, and the Clear Fork Brazos River watershed located in Texas (Panel D) only includes dry seasons. As shown in Figure 3, the data points in the wet and dry seasons in Panel A and Panel B do not follow the same Budyko-type curve. Two separate curves are necessary to model the evaporation ratio for the two seasons, respectively. If there is only one season for a watershed (Panel C or Panel D), one extended Budyko-type curve is used to model the annual evaporation ratio. Particularly for the Clear Fork Brazos River watershed, which is located in a dry region, the lower bound of seasonal aridity index is more than 2, and a Budyko-type curve with a horizontal shift fits the observations well.

Two parameters are needed to be estimated in the modified Budyko-type functions for each season. The values of v_w and v_d represent the physical controls of intra-seasonal rainfall (such as storminess) and watershed properties on seasonal evaporation and storage changes. The values of ϕ_w and ϕ_d can be interpreted as the lower limits of aridity index for wet and dry seasons. For a given watershed the value of ϕ_d should be higher than that of ϕ_w . Given the same seasonal aridity index in a watershed, the evaporation ratio in dry seasons should be higher than that in wet seasons. The values of ϕ_w and ϕ_d also represent the shifts of the 1:1 limit lines due to energy-limits. In the seasonal model of *Hickel and Zhang* [2006], when mean monthly rainfall exceeds potential evaporation during wet seasons, evaporation is assumed to occur at the potential rate for enabling a minimum-parameter formulation. The effect of this assumption appears to be minimal since they focus on mean annual water balance. However, this study focuses on the seasonal variability of evaporation and storage change, so the evaporation in wet seasons is modeled by equation (2.6.1). When a seasonal aridity index is smaller than 1 in the wet season, the upper bound of evaporation is equal to $E_{P_w} - \phi_w(P_w - \Delta S_w)$, which is usually smaller than E_{P_w} . On the other hand, in dry seasons with $A_d < 1 + \phi_d$, the upper limit of E_d is $E_{P_d} - \phi_d(P_d - \Delta S_d)$, which is smaller than the water supply ($P_d - \Delta S_d$). As a result, there is a smaller upper bound on seasonal evaporation in “energy-limited” conditions.

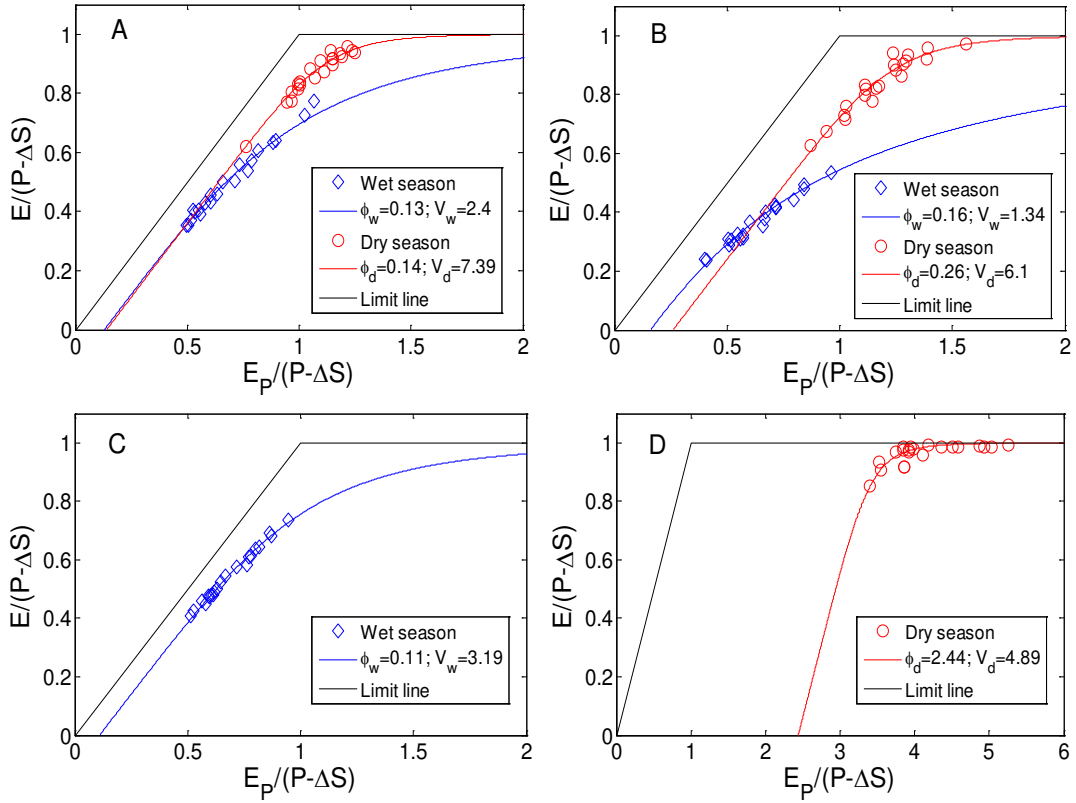


Figure 3: Seasonal evaporation ratio versus seasonal aridity index and the fitted Turc-Pike lines for the Rocky River watershed located in North Carolina at the USGS gage 02126000 (Panel A), the Auglaize River watershed in Ohio at the USGS gage 04191500 (Panel B), the Oostanaula River watershed located in Georgia at the USGS gage 02387500 (Panel C), and the Clear Fork Brazos River watershed in Texas at the USGS gage 08085500 (Panel D).

2.1.6 Modeling annual storage changes

Once the four parameters (v_w , v_d , ϕ_w and ϕ_d) for the seasonal evaporation model are obtained, the seasonal Budyko-type model developed in this study can be used to estimate annual storage changes and evaporation if precipitation, potential evaporation and runoff observations are available. Substituting $E_w = P_w - Q_w - \Delta S_w$ into equation (2.6), the following equations are obtained and can be used to estimate storage changes in wet and dry seasons:

$$1 - \frac{Q_w}{P_w - \Delta S_w} - \left[1 + \left(\frac{E_{P_w}}{P_w - \Delta S_w} - \phi_w \right)^{-v_w} \right]^{-1/v_w} = 0 \quad (2.7.1)$$

$$1 - \frac{Q_d}{P_d - \Delta S_d} - \left[1 + \left(\frac{E_{P_d}}{P_d - \Delta S_d} - \phi_d \right)^{-v_d} \right]^{-1/v_d} = 0 \quad (2.7.2)$$

The values of ΔS_w and ΔS_d can be solved numerically using equation (2.7), and annual storage changes (ΔS) can be computed as a summation of seasonal storage changes:

$$\Delta S = \Delta S_w + \Delta S_d \quad (2.8)$$

The annual evaporation can be computed as a residual of water balance once storage changes are estimated.

2.1.7 Model performance evaluation

The model performance is evaluated using two indicators: root mean square error (RMSE) and Nash-Sutcliffe efficiency (NSE). RMSE is calculated as:

$$RMSE = \sqrt{\frac{\sum_{i=1}^n (X_{o,i} - X_{m,i})^2}{n}} \quad (2.9)$$

where $X_{o,i}$ and $X_{m,i}$ are the observed and modeled values in the i^{th} year, respectively; n is the number of years. NSE shows the extent to which observed and modeled values follow the line with 1:1 slope [Moriassi *et al.*, 2007]. NSE is calculated as:

$$NSE = 1 - \frac{\sum_{i=1}^n (X_{o,i} - X_{m,i})^2}{\sum_{i=1}^n (X_{o,i} - \bar{X}_{o,i})^2} \quad (2.10)$$

NSE ranges from $-\infty$ to 1. Values close to 1 indicate higher model efficiency in predicting actual values [Legates and McCabe, 1999]. A positive NSE value is usually acceptable for a model [Moriassi *et al.*, 2007].

RMSE and NSE are applied to evaluate the fitness of the extended Budyko-type model and the performance of the model in estimating annual storage changes from equations (3.7) and (3.8). The fitness of the seasonal Budyko-type model is computed for all the watersheds in each season, and is compared among watersheds.

2.2 Results and Discussion

As formerly described, the seasonal Budyko type model is applied to the 277 case study watersheds shown in Figure 2. Based on the definition of wet and dry months, 203 watersheds have both wet and dry seasons, and 191 watersheds have consecutively dry months in summer seasons. The duration of dry seasons ranges from 1 to 11 months in these watersheds. 51 watersheds only have wet seasons, and most of them are located in the northeastern corner of the United States and the Appalachian Mountain area. 23 watersheds only have dry seasons and most of them are located in the High Plains.

2.2.1 Storage change impact on inter-annual water balance

The impact of storage change from year to year on the representation of Budyko hypothesis is assessed for the study watersheds. Figure 4 presents the water balance in the annual scale of all the study watersheds in the Budyko's framework with three different computations of aridity index or evaporation ratio. In Panel A, evaporation is estimated as the difference between precipitation and runoff. This representation is usually used when evaporation data is not available. Panel B represents E/P versus E_p/P . Such approach to

describe inter-annual water balance was presented by *Cheng et al.* [2011]. As shown in Panel B, if P is considered as water supply in the annual scale, E/P is higher than 1 in many cases. The uncertainty of E may contribute to this but is not enough to explain the high evaporation in extreme dry years. This result highlights the fact that available water supply is not limited to precipitation only, but storage changes also play a significant role in maintaining evaporation, especially for years with aridity indices higher than 1. Panel C shows the plot of $E/(P-\Delta S)$ versus $E_p/(P-\Delta S)$ when $P-\Delta S$ is used to represent available water instead of P . From this comparison, it can be interpreted that the Budyko hypothesis is applicable at the interannual scale, if the supply of energy and water are described accurately.

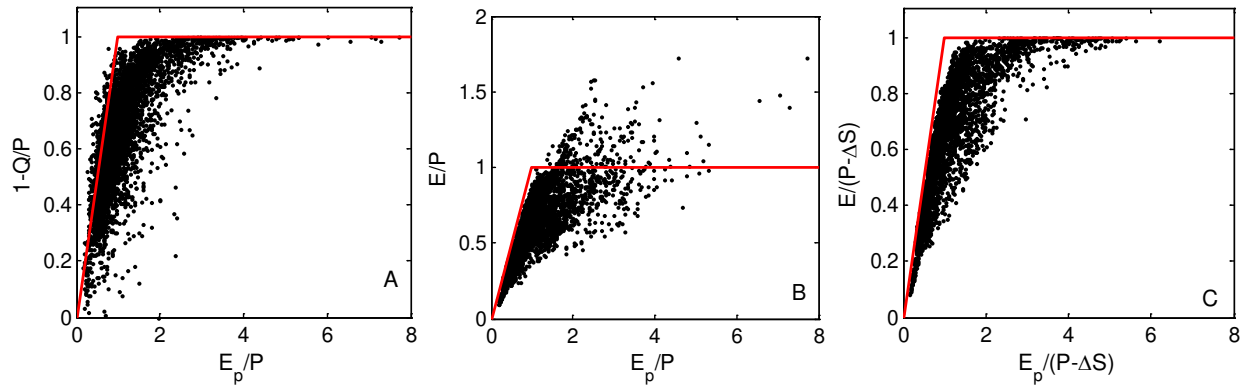


Figure 4: Three presentations of annual water balance: a) $1-Q/P$ versus E_p/P ; b) E/P versus E_p/P ; c) $E_p/(P-\Delta S)$ versus $E/(P-\Delta S)$.

2.2.2 Performance of the modified seasonal Turc-Pike model

The developed seasonal model based on the Budyko-type function in equation (3.6) is applied to the case study watersheds shown in Figure 2. The values of the four seasonal parameters (v_w , v_d , ϕ_w and ϕ_d) are estimated based on the available data for monthly precipitation, potential evaporation, evaporation, and runoff during 1983-2003. For example,

Figure 3 shows the modified Turc-Pike curves in wet and dry seasons that fit to the data points for 4 watersheds from the 277 case study watersheds. As shown in Figure 3A for the Rocky River watershed, parameters in wet seasons are estimated as $\phi_w=0.13$ and $v_w=2.40$, and parameters in dry seasons are estimated as $\phi_d=0.14$ and $v_d=7.39$. As shown in Figure 3B for the Auglaize River watershed, wet season parameters are estimated as $\phi_w=0.16$ and $v_w=1.34$, and dry season parameters are $\phi_d = 0.26$ and $v_d = 6.10$. To evaluate the performance of the model, NSE values are calculated for the Rocky River watershed and the Auglaize River watershed. The NSE values for the estimated seasonal evaporation ratio in wet seasons are 0.98 and 0.97 for the two watersheds, respectively; and the NSE values in dry seasons are 0.96 and 0.90. Figure 3C shows a fitted curve for the Oostanula River watershed in which all the 12 months are classified as wet seasons, and the value of NSE is 0.99. The estimated values are 0.11 and 3.19 for ϕ_w and v_w respectively. The Clear Fork Brazos River watershed in Figure 3D only includes the dry seasons and the values of ϕ_d and v_d for the fitted curve are 2.44 and 4.89, with a NSE value of 0.67.

To evaluate the overall performance of the model, the frequency distribution of NSE for all 277 case study watersheds was calculated and is presented in Figure 5. In wet seasons (Figure 5A), NSE values in 99% of watersheds are higher than 0.5, and NSE values in 81% of watersheds are higher than 0.9. In dry seasons (Figure 5B), NSE values in 90% of watersheds are higher than 0.5, and NSE values in 40% of watersheds are higher than 0.9. The model performance in wet seasons is generally better than that in dry seasons. The number of watersheds at the peak frequency is 139 with NSE value around 0.925~0.975 in wet seasons (Figure 5A); while the number of watersheds at the peak frequency is 59 with NSE value of

0.875~0.925 in dry seasons (Figure 5B). In general, the seasonal model in equation (2.6) works very well for the inter-annual water balance at the seasonal scale.

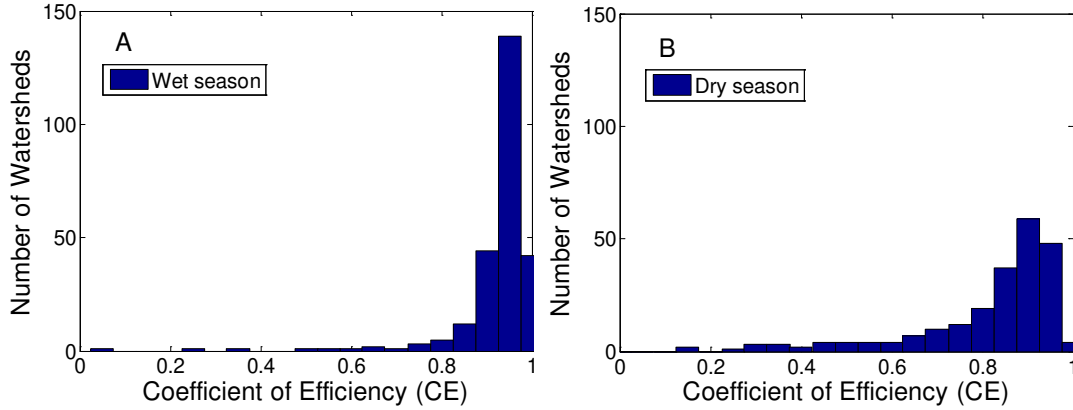


Figure 5: Histograms of coefficient of efficiency for the modified Ture-Pick model in wet season (Panel A) and dry season (Panel B).

2.2.3 Estimated model parameters

In the seasonal model, the evaporation ratio is a function of the seasonal aridity index and the parameters v_w and ϕ_w in wet seasons or v_d and ϕ_d in dry seasons. The values of the parameters reflect the dependence of seasonal evaporation and storage changes on other factors such as intra-seasonal rainfall, vegetation, soil properties, and topography in the watershed. Figure 6 shows the histograms of the four parameters (Panel A for the shift parameter ϕ_w in wet seasons and Panel B for the Turc-Pike parameter v_w ; Panel C for ϕ_d and Panel D for v_d). The maximum value of ϕ_w is 0.42 but the maximum value of ϕ_d is 2.74. Values of ϕ_w have the highest frequency around 0.1 while values of ϕ_d have the highest frequency around 0.25. This is due to the higher value of minimum aridity index in dry seasons compared with wet seasons. Values of v_w have the highest frequency around 1.5, though, in some cases, values higher than 10 were observed; values of v_d have the highest frequency around 5. The value of v_d is usually

larger than that of v_w for a given watershed. The parameter values of v in dry seasons are more dispersed compared with those in wet seasons.

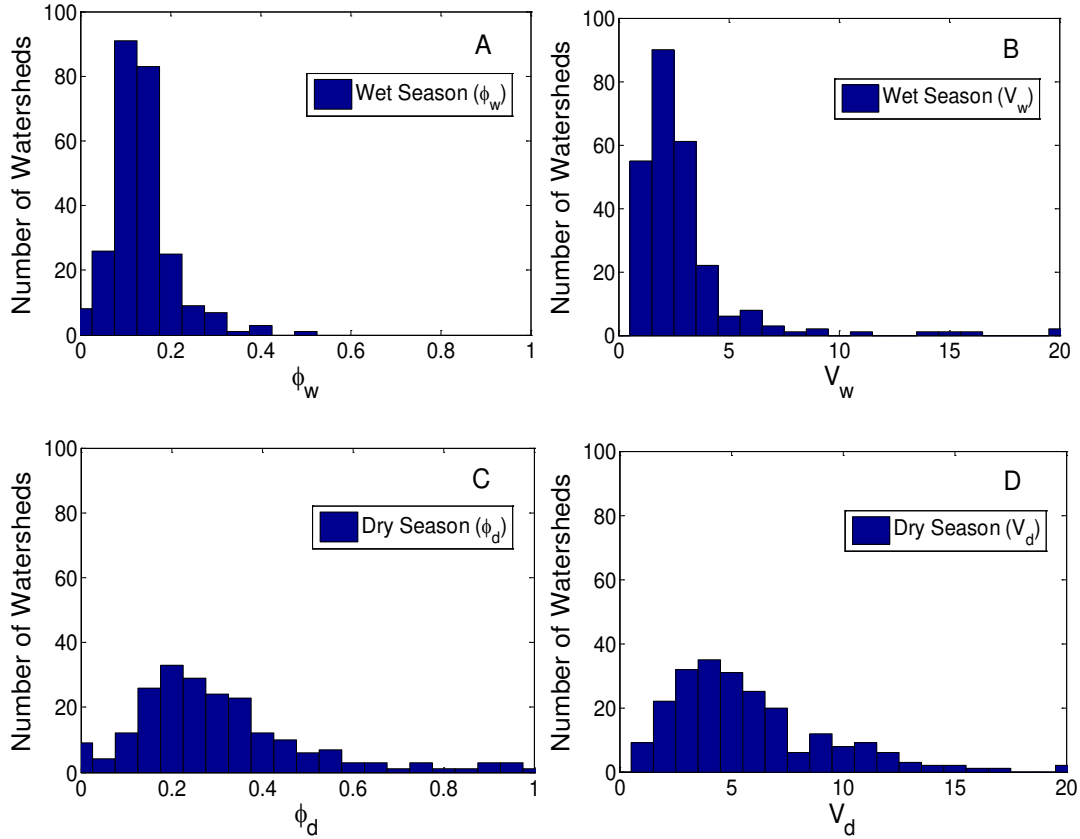


Figure 6: Histogram of parameters of wet and dry seasons.

2.2.4 Vegetation control on seasonal evaporation ratios

Climate seasonality and vegetation adaption controls on annual water balance have been one of the focused research areas in recent years [Feng *et al.*, 2012; Gentine *et al.*, 2012; Xu *et al.*, 2012]. Vegetation control on seasonal evaporation and storage change is explored in wet and dry seasons separately in this study. Normalized Difference Vegetation Index (NDVI) is used as a proxy for vegetation. Bimonthly NDVI data based on the Advanced Very High Resolution

Radiometer (AVHRR) imagery from the Global Inventory Modeling and Mapping Studies (GIMMS) can be downloaded at <http://glcf.umiacs.umd.edu/data/gimms/> [Tucker *et al.*, 2005]. Averaged values of NDVI at the monthly and seasonal scales are computed for each of the study watersheds.

Vegetation affects the seasonal water balance through both evaporation and soil moisture dynamics. Strong correlations exist between monthly average NDVI and evaporation. The percentage of watersheds where the correlation coefficients (r) between monthly NDVI and evaporation are higher than 0.5 is 96% in wet seasons and 73% in dry seasons. To quantify the potential interaction between vegetation and evaporation in wet and dry seasons, a bivariate Granger causality test [Granger, 1969; Engle and Granger, 1987; Detto *et al.*, 2012] is conducted between monthly NDVI and evaporation. A 10% significance level is used in the Granger test. In dry seasons, evaporation is the cause and NDVI is the effect in 71% of the watersheds, and NDVI is the cause and evaporation is the effect in 59% of the watersheds. In wet seasons, evaporation is the cause and NDVI is the effect in 92% of the watersheds, and NDVI is the cause and evaporation is the effect in 81% of the watersheds. These results on the Granger causality test show the interaction and feedback between vegetation and evaporation. Vegetation controls seasonal water balance not only by evaporation but also by soil moisture dynamics. In the developed seasonal model of equation (2.6), seasonal storage changes have been included into the seasonal aridity index. The controls of other factors such as vegetation, rainfall intensity and infiltration capacity are reflected by the parameters, and the corresponding controls may be different with wet and dry seasons. To evaluate the vegetation control on seasonal water balance, Figure 7 plots the dependence of ϕ_d , v_d , ϕ_w , and v_w as a function of long-term average seasonal NDVI values for all 277 watersheds. Strong correlation between

NDVI and dry season parameters is identified. As shown in Figure 7A, when NDVI is smaller than 0.5, ϕ_d is not sensitive to NDVI ($r=-0.273$). The absolute value of correlation coefficient between NDVI and ϕ_d increases when NDVI is larger than 0.5 ($r=-0.679$). As discussed earlier, ϕ_d corresponds to the lower bound of the dry season aridity index. According to Figure 7A, watersheds with higher NDVI have lower bounds of aridity index in dry seasons. This is due to the fact that higher vegetation coverage has a greater potential to deplete soil water storage during drought periods, which in turn induces smaller values of the dry season aridity index, $\frac{E_{Pd}}{P_d-\Delta S_d}$. As shown in Figure 7B, v_d increases with NDVI and the correlation coefficient between NDVI and v_d is 0.557. Higher values of v_d correspond to higher evaporation ratios, $\frac{E_d}{P_d-\Delta S_d}$. However, the relationships between NDVI and the wet season parameters are non-monotonic as shown in Figures 7C and 7D. The correlation coefficient is -0.24 in Figure 7C and 0.01 in Figure 7D, respectively. It seems that a maximum value of ϕ_w occurs around NDVI = 0.4.

2.2.5 Estimation of annual storage changes

As mentioned before, once the values of parameters for each watershed are estimated, the seasonal model developed in this study can be used to estimate annual evaporation and storage changes when precipitation, potential evaporation and runoff data are available. Storage changes are estimated by equations (2.7) for wet and dry seasons, which are then aggregated to annual storage changes by equation (2.8). The model's performance on modeling storage changes is evaluated by dividing the historical data into calibration (1983-1992) and validation (1993-2002) periods. The four parameters in equation (2.6) are estimated based on observations during the

calibration period. The annual storage changes during the validation period are computed and compared with the “observed” annual storage changes estimated by water balance closure. The comparison is presented in Figure 8: Panel A for watersheds with both wet and dry seasons, Panel B for watersheds with dry seasons only, and Panel C for watersheds with wet seasons only. In panel A, the average RMSE is 27 mm for dry seasons and 21 mm for wet seasons. The average value of RMSE is 54 mm for Panel B and 18 mm for Panel C. The overall average RMSE of annual storage changes for these 277 watersheds is 24 mm. The performance in wet seasons is better than in dry seasons, especially when comparing wet season only watersheds to dry season only watersheds.

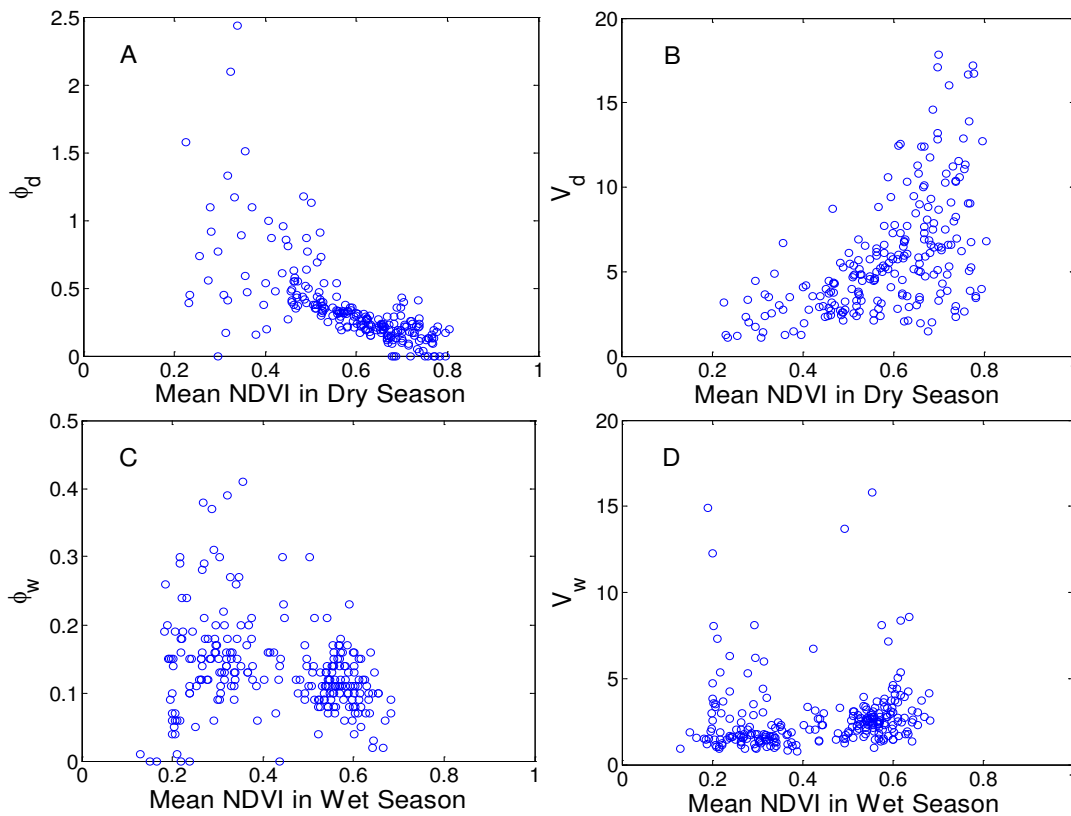


Figure 7: Seasonal parameters of the modified Turc-Pike equation and the long-term average NDVI in dry seasons and wet seasons.

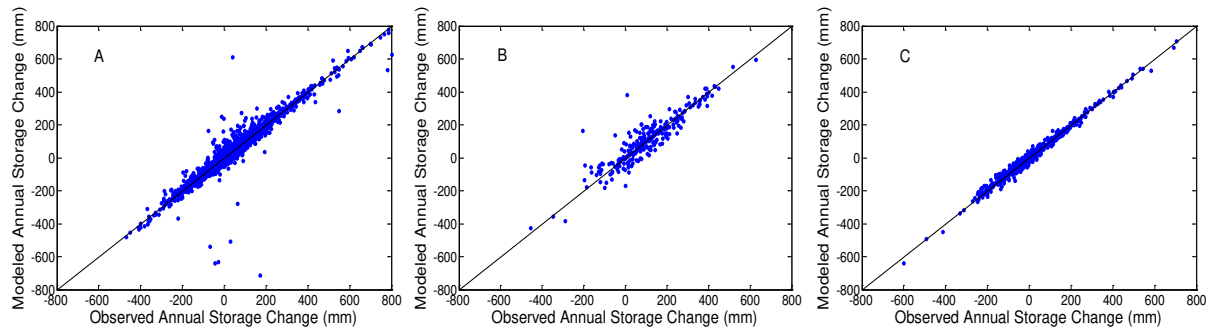


Figure 8: Observed and estimated values of annual storage changes during the validation period (1993-2002) in watersheds with both wet and dry seasons (Panel A), dry seasons only (Panel B), and wet seasons only (Panel C).

2.2.6 Impacts of evaporation data uncertainty

The uncertainties in observations, particularly evaporation estimation from remote sensing data, may contribute to the unrealistic storage change and further decrease the performance of the extended seasonal Budyko model. The observed storage changes are up to 800 mm in a few watersheds as shown in Figure 8 and this may be unrealistic. To evaluate the impacts of evaporation data uncertainty on the results, 158 watersheds from the total 277 watersheds discussed by Wang and Alimohammadi [2012], where the difference of long-term average annual evaporation between remote sensing-based and water balance-based estimation is within $\pm 10\%$, are selected for further investigation. The magnitude of observed annual storage changes in the 158 watersheds decreases significantly and the storage change values range from -400 mm to 400 mm. The average value of NSE over the 277 watersheds is 0.958 for wet seasons and 0.878 for dry seasons (Figure 5). The average value of NSE over the 158 watersheds increases to 0.968 for wet seasons and 0.882 for dry seasons. It indicates that the impact of the evaporation data uncertainty is not very significant on the seasonal model performance.

2.2.7 Physically-based processes versus co-evolution

The Budyko hypothesis on mean annual water balance results from the co-evolution of watershed vegetation and soils with climate [Gentine *et al.*, 2012; Troch *et al.*, 2013]. As demonstrated in Figure 9, the strength of co-evolution (Darwinian view) will become weaker with reducing time scales, and physical processes-based models (Newtonian view) for evaporation will take over at the small time scale (e.g., daily). Harman and Troch [2013] review the success of Darwinian method in hydrologic science and call for synthesis of the Darwinian and Newtonian approaches as a remaining goal. Great progresses are expected if the Newtonian approach can be reconciled with the Darwinian view [Sivapalan, 2005; Troch *et al.*, 2013]. One purpose of this work is to assess the strength of co-evolution view, presented by Budyko framework, on modeling evaporation at the shorter time scale. Figure 10 shows the monthly evaporation ratio versus monthly aridity index for the four watersheds shown previously in Figure 3. From seasonal to monthly scale, NSE values decrease from 0.98 to 0.90 (wet) and 0.97 to 0.84 (dry) for Rocky River watershed, from 0.98 to 0.64 (wet) and 0.95 to 0.46 (dry) for Auglaize River watershed. NSE values for Oostanaula River watershed decrease from 0.99 to 0.92 at all the wet months; particularly NSE values for Clear Fork Brazos River decrease from 0.68 to -2.09 for all the dry months. The performance of the extended Turc-Pike equation declines significantly from seasonal to monthly scales. Therefore, the strength of Darwinian approach for modeling evaporation may be not compelling at the monthly scale.

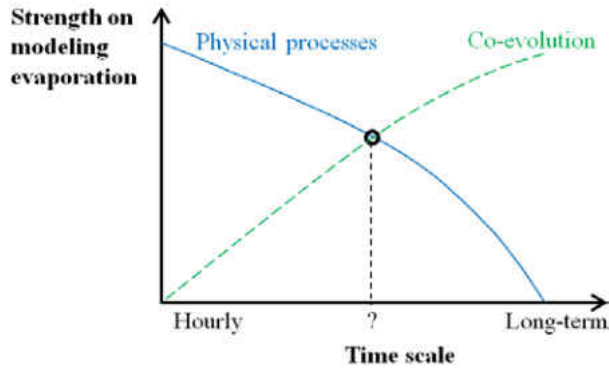


Figure 9: Strength of the Newtonian view and the Darwinian method on modeling evaporation at varying time scale.

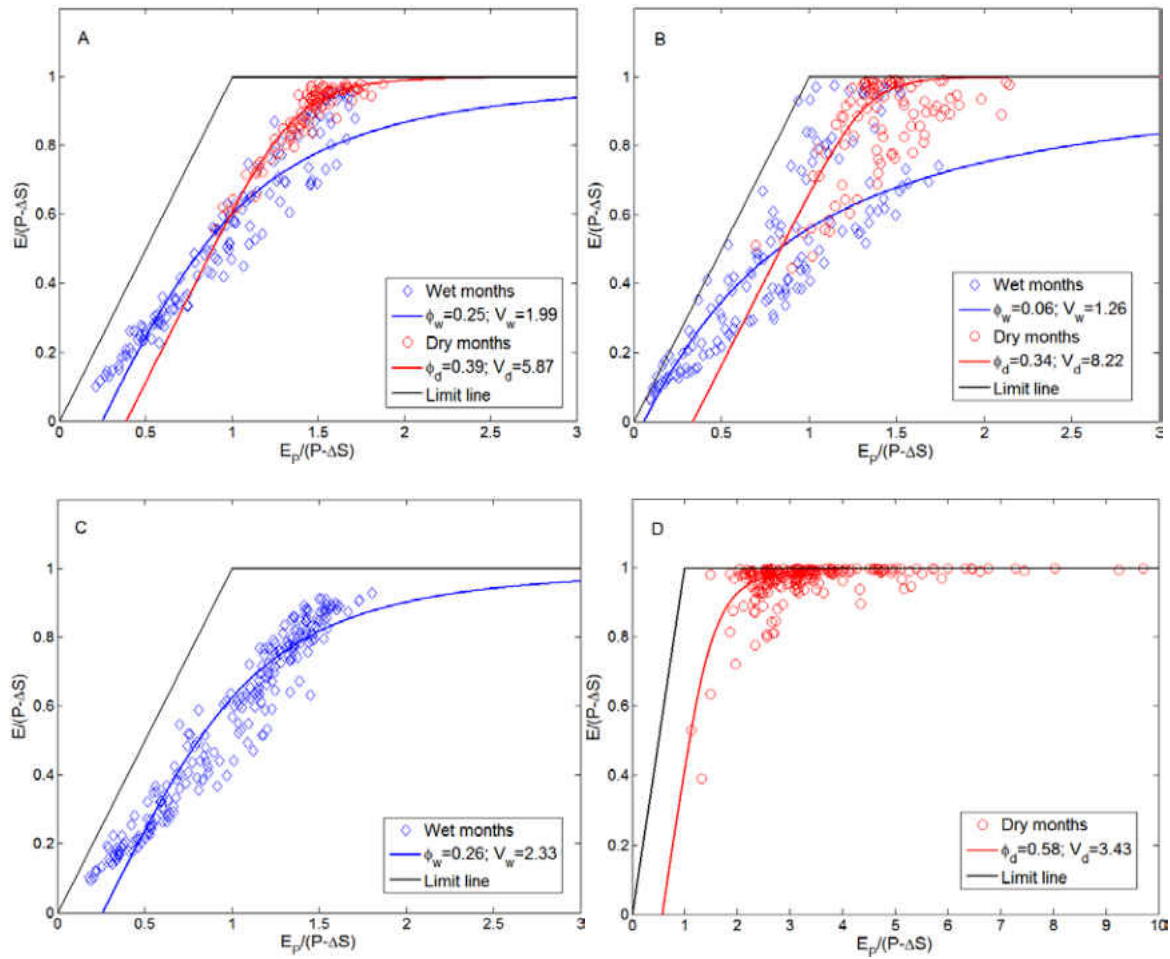


Figure 10: Monthly evaporation ratio versus monthly aridity index and the fitted Turc-Pike lines for the Rocky River watershed (Panel A), the Auglaize River watershed (Panel B), the Oostanaula River watershed (Panel C), and the Clear Fork Brazos River watershed (Panel D).

CHAPTER 3 RUNOFF GENERATION AND PROPORTIONALITY HYPOTHESES

The runoff simulation model at seasonal and monthly scale is developed based on the proportionality hypothesis, which is derived from SCS curve number method originally by *Ponce and Shetty* [1995].

3.1 Methodology

3.1.1 SCS curve number method and proportionality hypothesis

The SCS curve number method was developed for estimating surface runoff at the event scale [USDA SCS, 1985]. At the early stage of a rainfall event, rainfall (P) is abstracted by interception and surface retention and denoted as initial abstraction I_a . The remaining rainfall ($P - I_a$) is partitioned into continuing abstraction (F_a) and surface runoff (Q_s). Based on the data from a large number of observed watersheds, this partition follows the following proportionality formula:

$$\frac{F_a}{S} = \frac{Q_s}{P - I_a} \quad (3.1)$$

where S is the potential value of F_a and dependent on the capacity of soil wetting; similarly $P - I_a$ is the potential value of Q_s when F_a approaches to zero. Substituting $F_a = P - I_a - Q_s$ into equation (3.1) and assuming that I_a is a percentage of S (i.e., $I_a = \lambda_s S$), the SCS equation for computing surface runoff is obtained:

$$Q_s = \frac{(P-\lambda_s)^2}{P+(1-\lambda)S} \quad (3.2)$$

The basis of the curve number method is the proportionality relationship in equation (3.1). The time scale for the SCS curve number method is the duration of a rainfall-runoff event. Since the duration of rainfall event varies, the underlying assumption of the SCS curve number method is that equation (3.1) is independent on the time interval over which the partition occurs. This proportionality hypothesis can be generalized as follows. For a given time interval, the total amount of available water Z is allocated to X and Y . The potential values of X and Y are X_p and Y_p , respectively. The allocation is determined by the following proportionality equation:

$$\frac{X}{X_p} = \frac{Y}{Y_p} \quad (3.3)$$

For example, the proportionality relationship has been shown to be applicable at the annual scale [Ponce and Shetty, 1995; Sivapalan et al., 2011]. In this study, the proportionality relationship is tested at the seasonal scale considering water storage change in the quantification of available water.

3.1.2 Modeling runoff generation at annual scale using proportionality hypothesis

At the annual scale, precipitation is partitioned into runoff and evaporation when soil water storage change is negligible compared with other fluxes:

$$P = Q + E \quad (3.4)$$

L'vovich [1979] decomposed this partition into two stages. At the first stage, precipitation is partitioned into surface runoff and soil wetting (W):

$$P = Q_s + W \quad (3.5)$$

At the second stage, the soil wetting is partitioned into base flow (Q_b) and evaporation (E):

$$W = Q_b + E \quad (3.6)$$

The total runoff Q is the sum of Q_s and Q_b . By applying this empirical theory to many watersheds across the world, *L'vovich* [1979] observed a pattern: during the generation of Q_s and Q_b , an initial abstraction will occur until a certain amount of water has been supplied, in other words, the flow generation will not occur until the water supply reach a certain level; on the other hand, the amount of W and E from rainfall partitioning has a upper limit while the generation of Q_s and Q_b does not have upper limit.

Based on the two-stage runoff modeling concept by *L'vovich* [1979], *Ponce and Shetty* [1995] extended the SCS formula (equation 3.2) to the annual scale by generalizing the proportionality hypothesis. Initial soil wetting is represented as a percentage (λ_s) of soil wetting capacity (W_p). $\lambda_s W_p$ is the precipitation threshold for generating surface runoff. When $P > \lambda_s W_p$,

$$Q_s = \frac{(P - \lambda_s W_p)^2}{P + (1 - 2\lambda_s) W_p} \quad (3.7)$$

It should be noted that the functional difference between $(1 - \lambda)$ in equation (3.2) and $(1 - 2\lambda_s)$ in equation (3.7) is due to the definition of S and W_p . S is the maximum value of continuing wetting; while W_p is the maximum value of total wetting.

As an analog to surface flow, soil wetting threshold for base flow generation is defined as $\lambda_b V_p$. When $W > \lambda_b V_p$, base flow is computed by [Ponce and Shetty, 1995]:

$$Q_b = \frac{(W - \lambda_b V_p)^2}{W + (1 - 2\lambda_b)V_p} \quad (3.8)$$

This similarity of runoff generation in terms of surface runoff and base flow has been discussed in Sivapalan *et al.* [2011]. As Sivapalan *et al.* pointed out, this hydrologic similarity, which is presented by equation (3.7) and (3.8), has the probability to be universally applicable to different temporal and spatial scales.

3.1.3 Two-stage partition at the seasonal scale

Different from annual scale, water balance and rainfall partitioning at the seasonal or shorter temporal scales are affected by soil water storage changes. As described in Sivapalan *et al.* [2011], storage carryover between years is one of the reasons for the uncertainty of annual water balance variability. For seasonal water balance, storage change (ΔS) becomes more significant, and therefore has to be considered as a part of the water balance. As a result, the water balance in equation (3.4) becomes:

$$P = Q + E + \Delta S \quad (3.9)$$

Soil water storage change is included into the definition of seasonality and the proportionality relationship.

Seasonality is determined based on the monthly aridity index which is defined as $\frac{E_p}{P - \Delta S}$ [Chen *et al.*, 2013]. The monthly aridity index is an extension of the mean annual climate aridity

index $\left(\frac{E_p}{P}\right)$ in the Budyko framework [Budyko, 1958; 1974]. Dry months $\left(\frac{E_p}{P-\Delta S} > 1\right)$ and wet months $\left(\frac{E_p}{P-\Delta S} \leq 1\right)$ are determined by the mean monthly aridity index so that dry and wet months are fixed for a given watershed. By aggregating all the dry months in each year, dry seasons are identified; similarly, wet seasons can be identified as well.

The behavior of runoff generation in dry seasons and wet seasons can be different in a given watershed. As a result, the two-stage rainfall partitioning concept by *L'vovich* [1979] is applied to dry seasons and wet seasons separately. At the first stage, precipitation is partitioned into surface runoff and soil wetting, and the partitioning equation is same as equation (3.5) at the annual scale. At the second stage, soil water storage change needs to be taken account into the available water, similar with seasonal aridity index. The available water, represented by the difference between wetting and storage change, is partitioned into evaporation and base flow:

$$W - \Delta S = Q_b + E \quad (3.10)$$

The seasonal precipitation partition can be modeled based on the generalized proportionality hypothesis.

3.1.4 Modeling seasonal runoff based on the proportionality hypothesis

The simplified surface runoff generation process is illustrated in Figure 11. The precipitation is partitioning into wetting W and surface runoff Q_s , while initial abstraction $\lambda_s W_p$ is the amount of water that is not competing with Q_s . Continuing soil wetting and surface runoff

competes for the available water of $P - \lambda_s W_p$, and this partition is quantified by the following proportional relationship:

$$\frac{P - \lambda_s W_p - Q_s}{W_p - \lambda_s W_p} = \frac{Q_s}{P - \lambda_s W_p} \quad (3.11)$$

Based on this proportional relationship, surface runoff at the seasonal scale can be computed for wet and dry seasons respectively. For example, surface runoff in wet seasons can be computed by the following equation, of which the functional form is same as equation (3.7):

$$Q_s = \begin{cases} 0 & \text{if } P \leq \lambda_s^w W_p^w \\ \frac{(P - \lambda_s^w W_p^w)^2}{P + (1 - 2\lambda_s^w) W_p^w} & \text{if } P > \lambda_s^w W_p^w \end{cases} \quad (3.12.1)$$

where superscript w is used to denote wet seasons; W_p^w represents soil wetting capacities in wet seasons; $\lambda_s^w W_p^w$ represents initial soil wetting in wet seasons. Correspondingly, surface runoff in dry seasons is computed by:

$$Q_s = \begin{cases} 0 & \text{if } P \leq \lambda_s^d W_p^d \\ \frac{(P - \lambda_s^d W_p^d)^2}{P + (1 - 2\lambda_s^d) W_p^d} & \text{if } P > \lambda_s^d W_p^d \end{cases} \quad (3.12.2)$$

where superscript d represents dry seasons, and λ_s^d and W_p^d are corresponding parameters in dry seasons. The equations are similar with the equations on the annual scale as shown in equation (3.7). The only difference is that the seasonal surface runoff equations are separated into dry seasons and wet seasons.

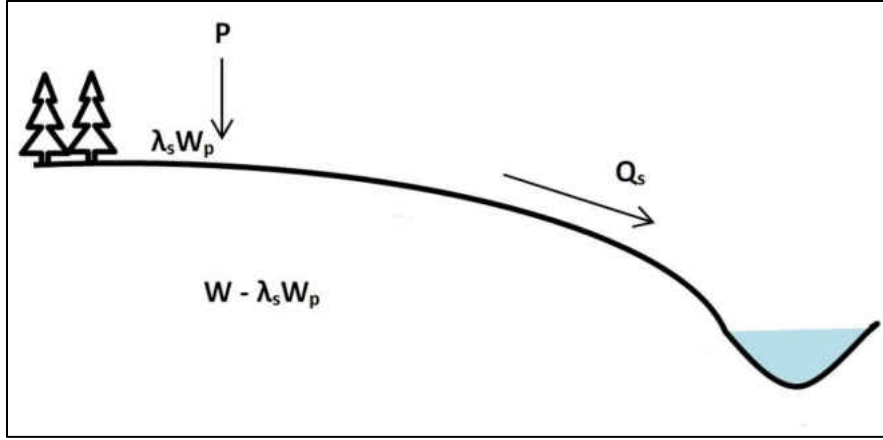


Figure 11: Conceptual scheme for the first-stage partition for modeling surface runoff.

However, the base flow equation at the seasonal scale is different from base flow equation at the annual scale. At the second stage, the available water for the competition between base flow and evaporation is $W - \Delta S$ as shown in equation (3.10). Analog to initial soil wetting, initial evaporation is defined as a percentage of potential evaporation: $\lambda_b E_p$. Continuing evaporation and base flow compete for the available water of $W - \Delta S - \lambda_b E_p$. The potential value for continuing evaporation is $E_p - \lambda_b E_p$; the potential value for base flow is $W - \Delta S - \lambda_b E_p$ when continuing evaporation approaches to zero. Therefore, the second-stage partition is quantified by the following equation based on the proportionality relationship:

$$\frac{E - \lambda_b E_p}{E_p - \lambda_b E_p} = \frac{Q_b}{W - \Delta S - \lambda_b E_p} \quad (3.13)$$

Substituting $E = W - \Delta S - Q_b$ into the equation (3.13), the base flow equation is obtained:

$$Q_b = \frac{(W - \Delta S - \lambda_b E_p)^2}{W - \Delta S + (1 - 2\lambda_b) E_p} \quad (3.14)$$

Similarly, base flows can be modeled in wet and dry seasons respectively. In dry seasons, base flow is computed by the following equation:

$$Q_b = \begin{cases} 0 & \text{if } P \leq \lambda_b^d E_p \\ \frac{(W - \Delta S - \lambda_b^d E_p)^2}{W - \Delta S + (1 - 2\lambda_b^d) E_p} & \text{if } P > \lambda_b^d E_p \end{cases} \quad (3.15.1)$$

Base flow in wet seasons is computed by:

$$Q_b = \begin{cases} 0 & \text{if } P \leq \lambda_b^w E_p \\ \frac{(W - \Delta S - \lambda_b^w E_p)^2}{W - \Delta S + (1 - 2\lambda_b^w) E_p} & \text{if } P > \lambda_b^w E_p \end{cases} \quad (3.15.2)$$

As shown, two differences exist between equations (3.15) and (3.8): 1) Storage change is included into the equation (3.15); 2) The variable E_p in equation (3.15) replaces V_p in equation (3.8). V_p is a fixed parameter, while E_p is obtained from observed data that varies over time.

Figure 12 illustrates the conceptual scheme of base flow generation.

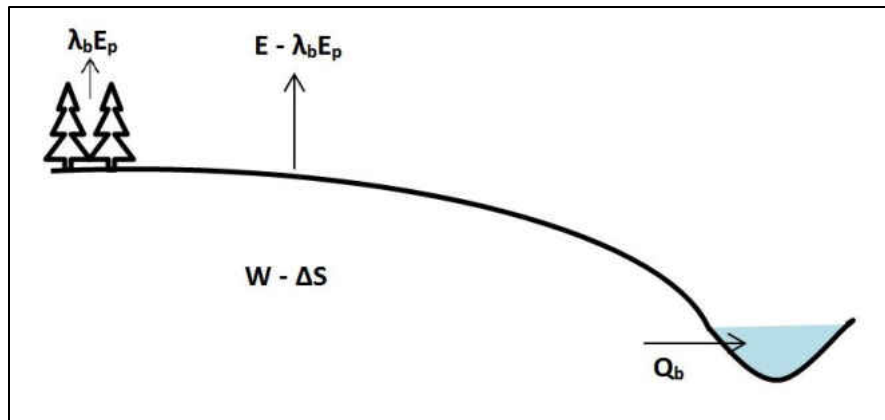


Figure 12: Conceptual scheme for the first-stage partition for modeling base flow.

In summary, the seasonal surface runoff and base flow can be modeled by equations (3.12) and (3.15) obtained from proportional relationships. There are three parameters for wet seasons (λ_s^w , W_p^w , and λ_b^w) and three parameters for dry seasons (λ_s^d , W_p^d , and λ_b^d).

3.1.5 Data collection

The daily data from 1983 to 2002 including precipitation and runoff are obtained from the Model Parameter Estimation Experiment (MOPEX) database [Duan *et al.*, 2006]. Daily evaporation and monthly potential evaporation during the same period is obtained from Zhang *et al.* [2010]. The daily runoff data is separated into surface runoff and base flow using one-parameter digital filter method with the filter parameter value of 0.925 [Nathan and McMahon, 1990; Sivapalan, *et al.*, 2011]. Daily precipitation, actual evaporation, surface runoff and base flow are aggregated to monthly values. The monthly values of storage change are estimated as residuals of water balance closure ($\Delta S = P - Q - E$). On the other hand, monthly values of soil wetting are computed by equation (3.5). Energy-limited and water-limited months are aggregated into seasonal values on annual bases, respectively.

Based on the definition of seasonal aridity index, the study watersheds are classified into three categories: 1) all the twelve months are energy-limited; 2) all the twelve months are water-limited; and 3) both energy-limited and water-limited seasons exist [Chen *et al.*, 2013]. Since water balance at the watersheds with single season is equivalent to annual water balance, 203 watersheds with both seasons are selected for analysis in this study.

In order to identify the rainfall variability control on seasonal water balance, the following storminess characteristics are quantified based on the daily rainfall data: the number of rainfall event per year (N), the maximum rainfall intensity (i_{max}) [mm/day], the average rainfall

intensity (i) [mm/day]; the average duration of rainfall events (T_r) [day], and the average between-event period (T_b) [day]. A rainfall event, based on which the storm duration and the between-event duration is computed, is defined as a period with continuous rainfall depth greater than 5 mm/day [Robinson and Sivapalan, 1997; Jothityangkoon and Sivapalan, 2009]. The number of event per year is counted for the two seasons respectively. The maximum rainfall intensity is obtained by identifying the maximum intensity event for each year (in energy-limited season or water-limited season) and then taking the average value over the years.

Watershed properties including vegetation, topography and soil are analyzed based on the available databases. The seasonal average value of Normalized Difference Vegetation Index (NDVI), as an indicator of vegetation coverage, is computed for both seasons. The slope is computed based on the 30 m Digital Elevation Model (DEM) from National Elevation Dataset [Gesch, 2007]. The following data from SSURGO [USDA, 2007] are calculated and aggregated to the watershed scale: the top layer porosity (ϕ_s) [%], the soil depth (D) [mm], the total soil water storage capacity (C) [mm], the saturated hydraulic conductivity (K_s) in the top soil layer [mm/hour] and the vertical average saturated hydraulic conductivity (K_a) [mm/hour]. The soil depth and saturated hydraulic conductivity are obtained directly from the soil database. Porosity for each soil layer is calculated based on the bulk density. The value for K_a is obtained by computing the depth weighted average saturated hydraulic conductivity for each horizontal soil unit (called “component” in SSURGO database), which is aggregated to the watershed value through the soil map unit.

3.2 Results and Discussion

The proposed two-stage seasonal runoff model is applied to the study watersheds. The parameter values are estimated during the calibration period (1983-1992). Nash-Sutcliffe efficiency coefficient (NSE) [Nash and Sutcliffe, 1970] is computed as an indicator of model performance:

$$NSE = 1 - \frac{\sum_{i=1}^n (Q_{obs}^i - Q_{est}^i)^2}{\sum_{i=1}^n (Q_{obs}^i - Q_{ave})^2} \quad (3.16)$$

where Q_{obs} is the observed runoff; Q_{ave} is the average value of observed runoff; Q_{est} is the modeled runoff ; n is the number of years during the calibration period. The values of NSE can range from $-\infty$ to 1. NSE=1 corresponds to a perfect model performance, and NSE=0 indicates that the model estimations are as accurate as the mean of the observed data. The set of parameters are estimated by maximizing the NSE values during the calibration period. NSE is also computed during the validation period of 1993-2002.

3.2.1 Model performance

The exceedance probability of the NSE values for surface runoff (Q_s), base flow(Q_b), and total runoff (Q) for the study watersheds are shown in Figure 13, respectively. The exceedance probability corresponding to the NSE value of 0.5 is 46% (75%) in water-limited seasons and 51% (84%) in energy-limited seasons for surface runoff (base flow), whereas the exceedance probability of NSE=0.5 for total runoff increases to 88% in water-limited seasons and 95% in energy-limited seasons. In general, the NSE values for base flow are higher than those for

surface runoff; the performance in energy-limited seasons, which is usually in the summer when the rainfall intensity is high, is higher than that in water-limited seasons.

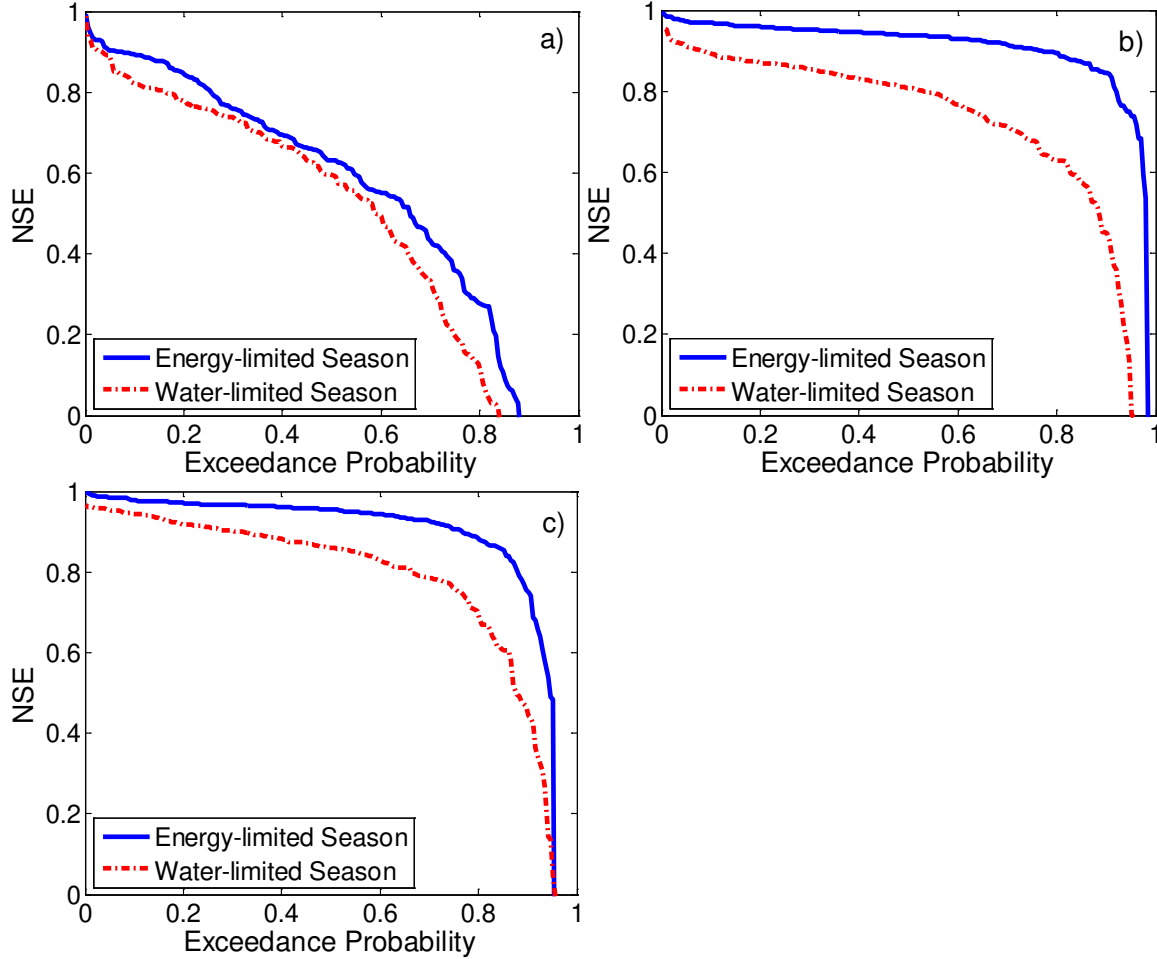


Figure 13: NSE values during the validation period in different seasons: (a) direct runoff simulation, (b) base flow simulation, and (c) total runoff simulation.

3.2.2 Estimated model parameters for seasonal water balance

The values of the model parameters (λ_s^w , W_p^w , and λ_b^w for water-limited seasons and λ_s^e , W_p^e , and λ_b^e for energy-limited seasons) are estimated through the calibration procedure. As examples, the parameter values for 18 watersheds from different geographic regions are shown

in Table 1. The values of these parameters, as well as their dependence on rainfall characteristics and watershed properties, are discussed in the following sections.

Table 1: Information of the chosen 18 watersheds

Gage ID	Region	State	Drainage Area (km ²)	E_p/P	W_p^w (mm)	λ_s^w	λ_b^w	W_p^d (mm)	λ_s^d	λ_b^d
01574000	Northeast	PA	1321	0.81	1500	0.12	0.18	2100	0.07	0.59
01127000	Northeast	CT	1847	0.55	7400	0	0.08	2100	0	0.63
01559000	Northeast	PA	2113	0.78	4300	0.01	0.25	3500	0	0.68
02018000	Appalachia	VA	852	0.71	3300	0.03	0.46	1500	0.07	0.77
01610000	Appalachia	WV	8104	0.75	3200	0.07	0.48	1800	0.01	0.78
02273000	Southeast	FL	7475	0.94	3300	0	0.76	17400	0.01	0.63
02228000	Southeast	GA	7226	0.87	5700	0	0.54	4800	0.09	0.63
02456500	Southeast	AL	2292	0.65	2700	0.13	0.4	3100	0.03	0.68
05570000	Midwest	IL	4237	1.05	700	0.13	0.17	2600	0.12	0.41
07183000	Midwest	KS	9643	1.37	400	0	0.14	3500	0.1	0.28
09497500	Southwest	AZ	7379	2.11	1000	0.08	0.74	5400	0.02	0.18
08172000	Southwest	TX	2170	1.60	800	0.04	0.21	2300	0.26	0.19
14113000	Northwest	WA	3359	0.79	9200	0.02	0	14400	0.03	0.11
14321000	Northwest	OR	9539	0.53	6900	0	0.17	3600	0	0.43
11530000	Northwest	CA	7389	0.63	13000	0	0.16	2800	0	0.34
06225500	High Plain	WY	4898	1.55	20000	0	0.59	5700	0	0
09251000	High Plain	CO	8762	1.55	10400	0.01	0.28	10900	0	0.23
09292500	High Plain	UT	342	1.22	19700	0.02	0.07	5500	0	0

3.2.2.1 Wetting capacity

The spatial distribution of wetting capacity (W_p) is shown in Figure 14. The values of wetting capacity in the Midwest are generally lower than those in other regions, which is the same as the pattern of annual values reported by *Sivapalan et. al.* [2011]. To quantify the dependence of wetting capacity on watershed properties and rainfall variabilities, the correlation between wetting capacity and the obtained physical factors described in Section 3.1.5 are calculated. In the energy-limited seasons, the wetting capacities are found to be correlated with

three factors: the saturated hydraulic conductivity (K_a) [mm/hour], the average duration of rainfall events (T_r) [day], and the average season length (L) [day]; whereas, the wetting capacities in the water-limited seasons are found to be correlated with K_a , L and $NDVI$. Wetting capacity has a positive relationship with saturated hydraulic conductivity K_a in both seasons (Figures 15a and 15c). This relationship shows that the potential value of soil wetting is positively correlated with the easiness of water going through soil layers vertically. The wetting capacities in energy-limited seasons are positively related with the average durations of rainfall events, especially when the wetting capacity is low (Figure 15b). As mentioned before, water-limited seasons are usually in the summer when vegetation coverage is maximum, and the wetting capacities have a negative relationship with the average $NDVI$ (Figure 15d).

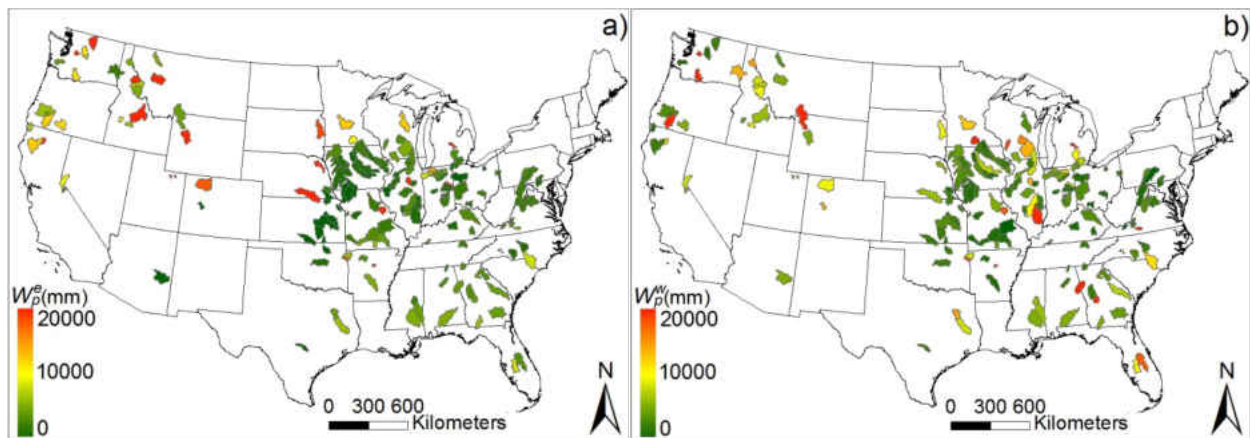


Figure 14: Spatial distribution of wetting capacity in 203 study watersheds: (a) energy-limited seasons , and (b) water-limited seasons.

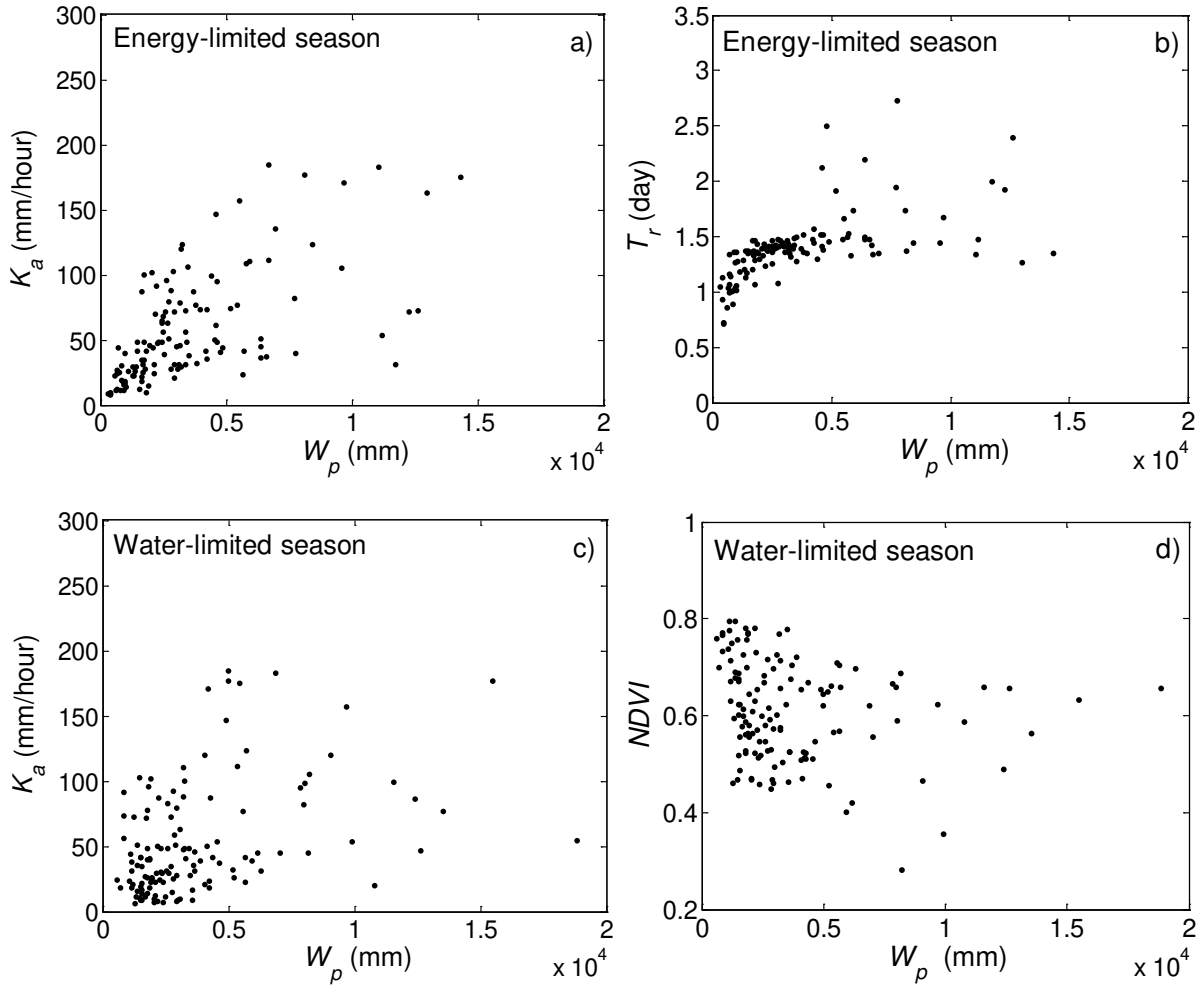


Figure 15: Relationships of W_p vs. K_a (a) and W_p vs. T_r (b) in energy-limited seasons; and W_p vs. K_a (c) and W_p vs. $NDVI_{ave}$ (d) in water-limited seasons.

The following equation is obtained for the energy-limited seasons through multiple regressions:

$$W_p^e = \begin{cases} 297L^{0.2} \cdot T_r^{1.9} \cdot K_a^{0.3} & \text{if } W_p^e \leq 4000 \text{ mm} \\ 843L^{0.2} \cdot T_r^{0.6} \cdot K_a^{0.4} & \text{otherwise} \end{cases} \quad (3.17.1)$$

The regression equation for the water-limited seasons is:

$$W_p^w = \begin{cases} 189L^{0.4} \cdot K_a^{0.3} \cdot NDVI^{-0.2} & \text{if } W_p^w \leq 4000 \text{ mm} \\ 429L^{0.4} \cdot K_a^{0.4} \cdot NDVI^{-0.1} & \text{otherwise} \end{cases} \quad (3.17.2)$$

Figure 16 shows the comparison between estimated W_p values and the computed ones by the regression equations. The regression equations capture the general trend of W_p well, especially when the W_p value is lower than 4000 mm. The regression equation in energy-limited seasons has a better performance ($R^2 = 0.71$) than that in water-limited seasons ($R^2 = 0.57$).

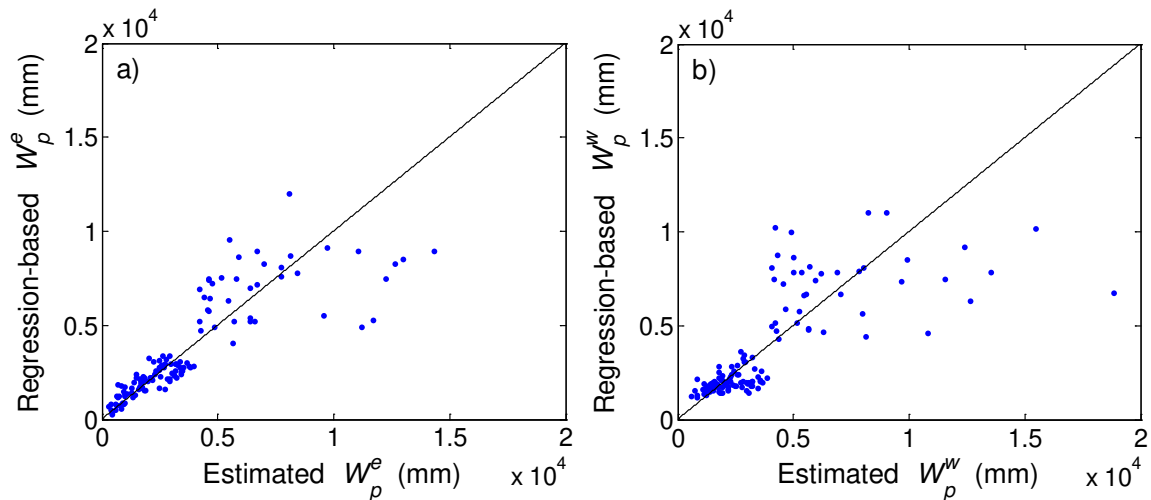


Figure 16: Comparison of wetting capacity values from the runoff model and from the regression equations in (a) energy-limited seasons and (b) water-limited seasons.

3.2.2.2 Initial wetting

The initial soil wetting (W_0) is represented as a fraction of wetting capacity ($\lambda_s W_p$). The average value of initial wetting over the study watersheds is 380 mm in the water-limited seasons and 208 mm in the energy-limited seasons. 26% of the watersheds have a initial wetting lower than 100 mm in the water-limited seasons; and 44% of the watersheds have a initial wetting lower than 100 mm in the energy-limited seasons. The spatial distribution of initial wetting is shown in Figure 17. In the Midwest and Southeast regions, the initial wettings are much higher

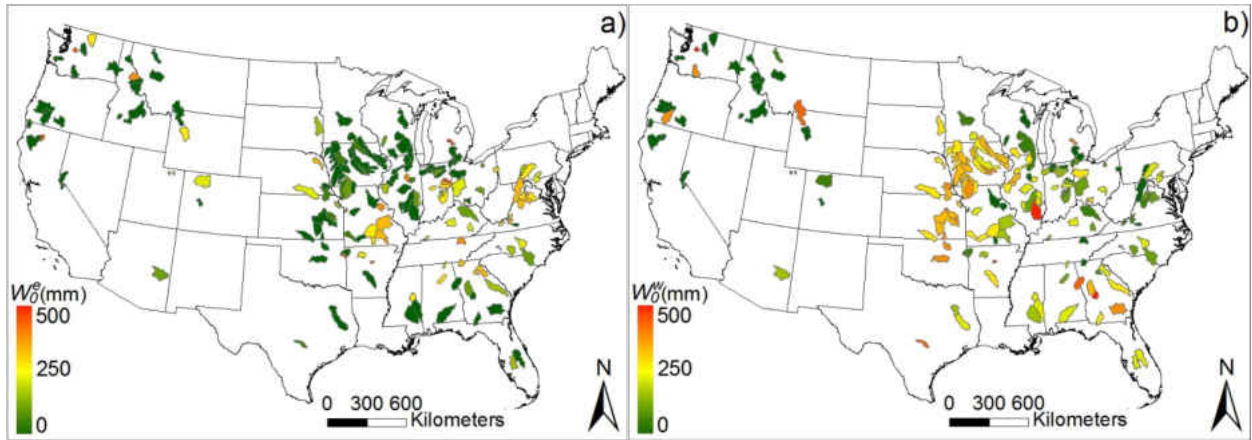


Figure 17: Spatial distribution of initial wetting in the: (a) energy-limited seasons, and (b) water-limited seasons.

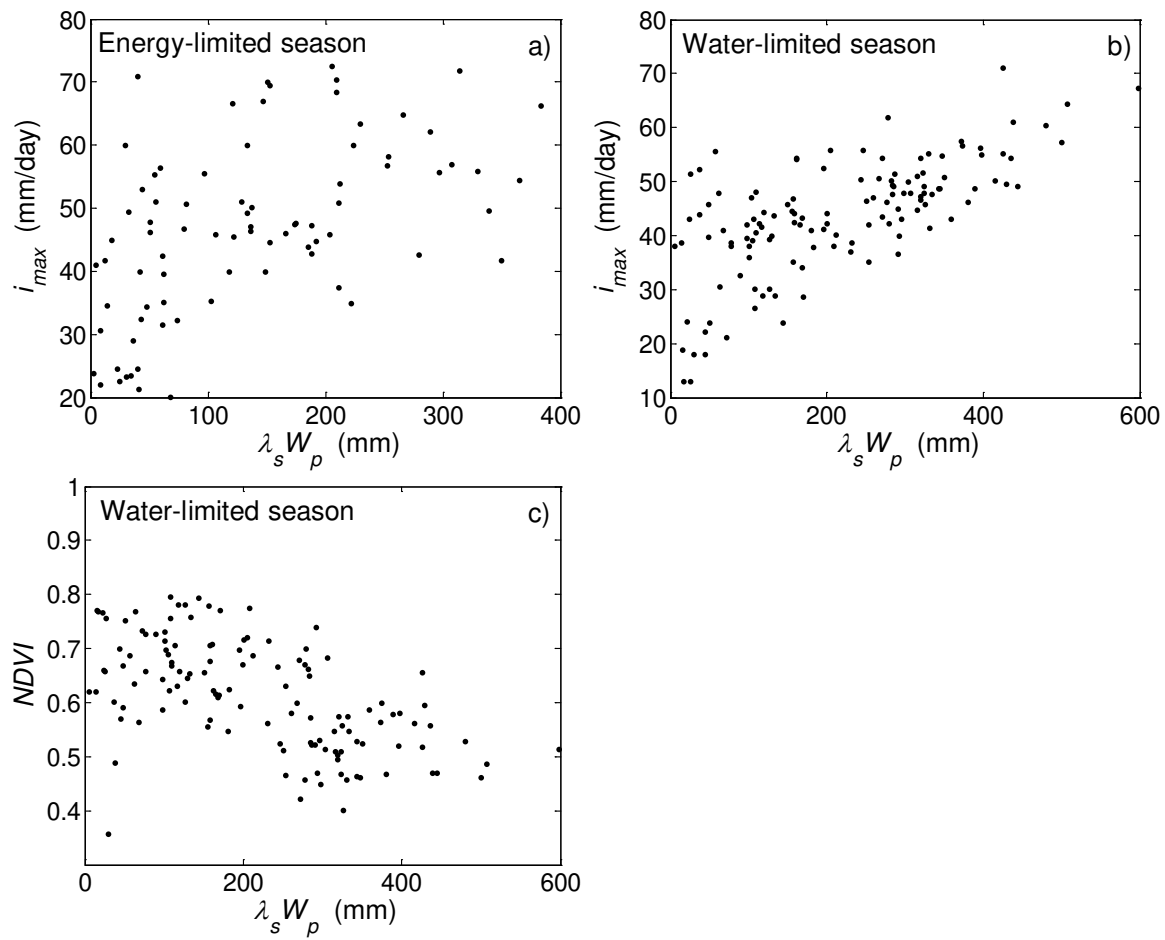


Figure 18: Relationships of (a) $\lambda_s W_p$ vs. i_{max} in the energy-limited seasons, (b) $\lambda_s W_p$ vs. i_{max} and (c) $\lambda_s W_p$ vs. $NDVI_{ave}$ in the water-limited seasons.

in the water-limited seasons than those in the energy-limited seasons. This seasonal change could be related with the seasonality of vegetation and rainfall characteristics.

Correlation between initial wetting and physical factors is quantified through a multiple regression analysis. The average season length (L) and the maximum rainfall intensity (i_{max}) are positively correlated with initial wetting in both seasons (Figure 18a and 18b). Besides these two factors, NDVI is found to be correlated with initial wetting in the water-limited seasons (Figure 18c). Through multiple regression analysis, the following equation is obtained for the energy-limited seasons:

$$W_o^e = \begin{cases} 0.1L \cdot i_{max}^{0.3} & \text{if } W_o \leq 150 \text{ mm} \\ 0.32L^{1.1} \cdot i_{max}^{0.1} & \text{otherwise} \end{cases} \quad (3.18.1)$$

and for the water-limited seasons:

$$W_o^w = \begin{cases} 0.79L^{0.7} \cdot i_{max}^{0.3} \cdot NDVI^{-0.01} & \text{if } W_o \leq 150 \text{ mm} \\ 0.89L^{0.8} \cdot i_{max}^{0.5} \cdot NDVI^{-0.01} & \text{otherwise} \end{cases} \quad (3.18.2)$$

Figure 19 compares the estimations of initial wetting through the two-stage runoff model and the regression-based ones. The R^2 of the multiple regression is 0.79 in the energy-limited seasons and 0.82 in the water-limited seasons.

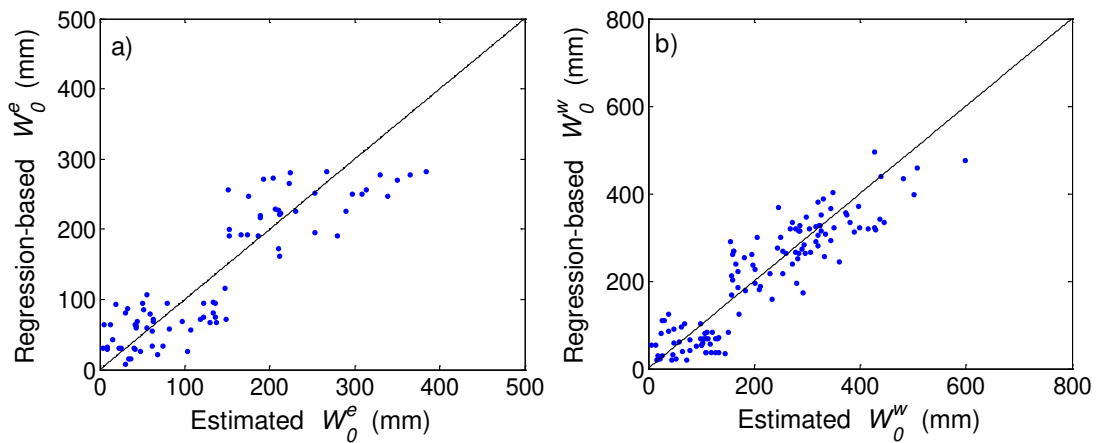


Figure 19: Comparison of initial wetting estimated from the two-stage runoff model and the regression equations in: (a) the energy-limited seasons and (b) the water-limited seasons.

3.2.2.3 Initial evaporation

Initial evaporation (E_o) is represented as a fraction of potential evaporation, i.e., $E_o = \lambda_b E_p$. The average of initial evaporation is 289 mm in the water-limited seasons and 101 mm in the energy-limited seasons. 90% of watersheds in the water-limited seasons have an initial evaporation lower than 423 mm, while 90% of watersheds in energy-limited seasons have an initial evaporation lower than 261 mm. The spatial distribution of initial evaporation is shown in Figure 20. The average number of rainfall event per season (N), seasonal average $NDVI$, and the duration of the season (L) [day] are found to be correlated with initial evaporation in both seasons. The higher value of initial evaporation in the water-limited seasons is due to the higher vegetation coverage and rainfall frequency compared with the energy-limited seasons. As expected, initial evaporation is positively correlated with $NDVI$ and N in both seasons (Figure 21). Figure 21d shows that in the water-limited season, the positive relationship between initial evaporation and $NDVI$ is not clear. This pattern is caused by the trade-off between the two components of initial evaporation: λ_b and E_p . In the water-limited seasons, $NDVI$ has a positive correlation with λ_b ($R = 0.80$) and a negative correlation with E_p ($R = -0.66$).

The following regression equation is obtained for the energy-limited seasons:

$$E_o^e = \begin{cases} 0.21N^{0.1} \cdot NDVI^{1.3} \cdot L^{1.2} & \text{if } E_o \leq 150 \text{ mm} \\ 1.18N^{0.2} \cdot NDVI^{0.8} \cdot L^{0.9} & \text{Otherwise} \end{cases} \quad (3.19.1)$$

and the following equation is obtained for the water-limited seasons:

$$E_o^w = \begin{cases} 35.7N^{0.6} \cdot NDVI^{1.5} \cdot L^{0.1} & \text{if } E_o \leq 150 \text{ mm} \\ 1.2N^{0.2} \cdot NDVI^{0.8} \cdot L^{0.9} & \text{Otherwise} \end{cases} \quad (3.19.2)$$

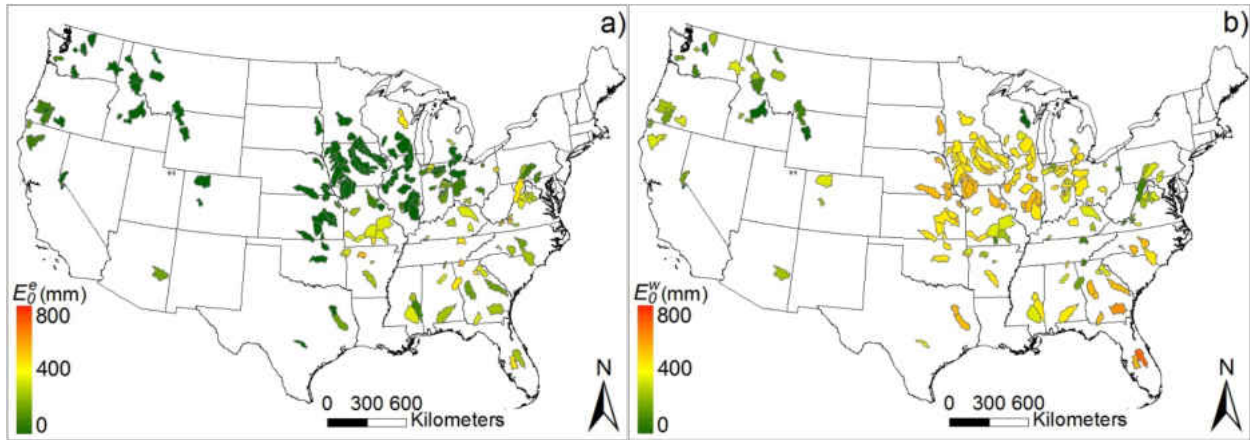


Figure 20: Spatial distribution of initial evaporation: (a) energy-limited seasons, and (b) water-limited seasons.

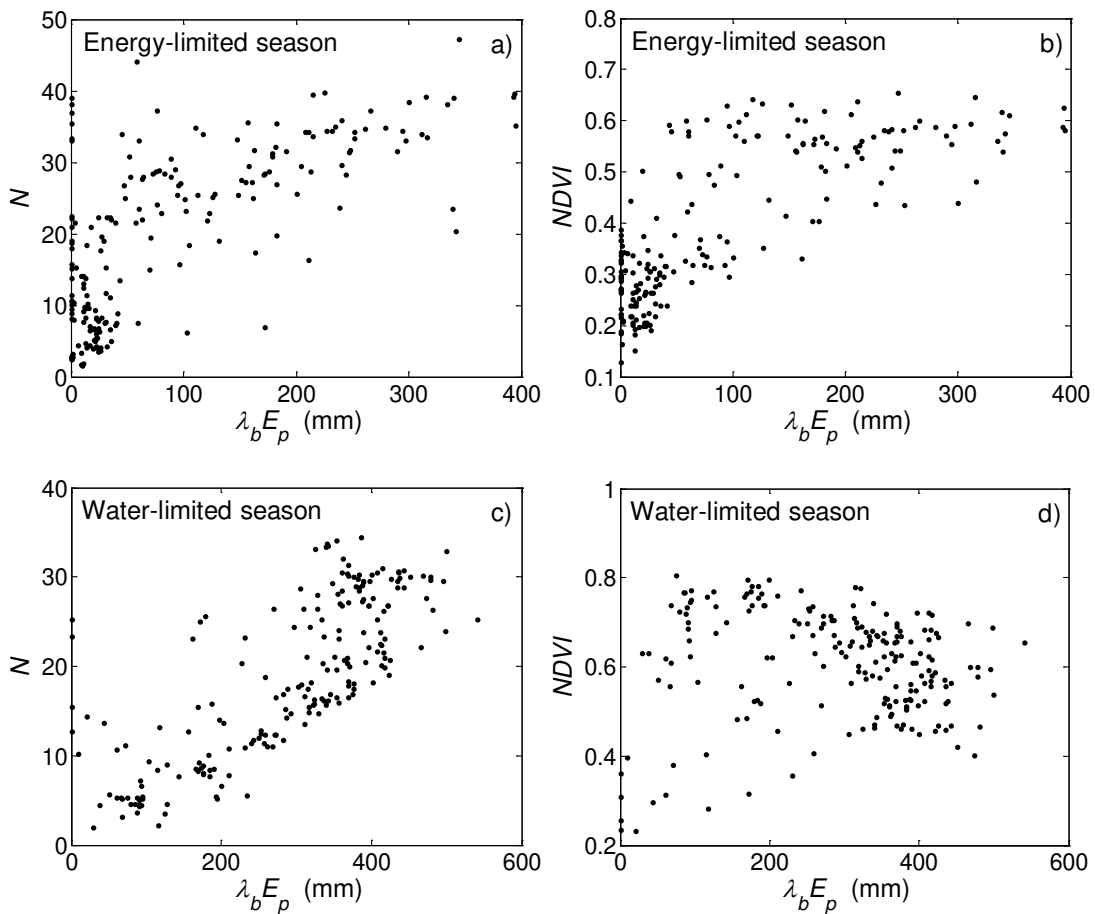


Figure 21: Correlation of (a) E_0 vs. N in the energy-limited seasons, (b) E_0 vs. $NDVI$ in the energy-limited seasons, (c) E_0 vs. N in the water-limited seasons, and (d) E_0 vs. $NDVI$ in the water-limited seasons.

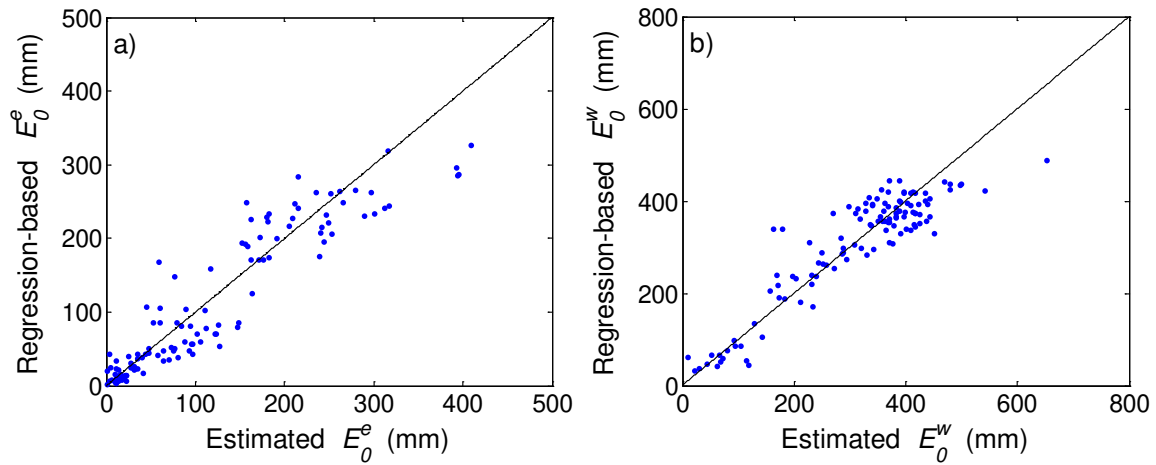


Figure 22. Comparison of initial evaporation values from the two-stage runoff model and from the regression equations: (a) energy-limited seasons and (b) water-limited seasons.

As shown in Figure 22, the regression equations for E_0 have good performance in both energy-limited seasons ($R^2 = 0.87$) and water-limited seasons ($R^2 = 0.84$). Different from initial wetting, initial evaporation has a strong positive relationship with vegetation coverage in both seasons, based on equation (3.19.1) and (3.19.2). This result reveals the difference between E_0 and W_0 . As discussed in the previous section, W_0 tends to have a negative relationship with vegetation coverage.

It should be noted that not all the physical factors computed in Section 3.1.5, such as topography factors, are included in the regression analysis due to the non-significant correlation.

CHAPTER 4 STORAGE DYNAMICS AND CONTRIBUTING AREA

Because of the difficulty to obtain evaporation and storage data for watersheds, the feasibility of using base flow recession analysis to estimate evaporation and storage change is investigated in this study as well. The evaporation estimation model used by many former studies [Szilagyi *et al.*, 2007; Kirchner, 2009; Palmroth *et al.*, 2010] was applied on 9 study watersheds in this study. Spoon River Watershed in Illinois will be the focused study watershed because of the high data availability. Furthermore, the performance and potential limitation of the model is also discussed with a focus on the newly developed concept: contributing area. Figure 23 shows the locations of the 9 study watersheds.

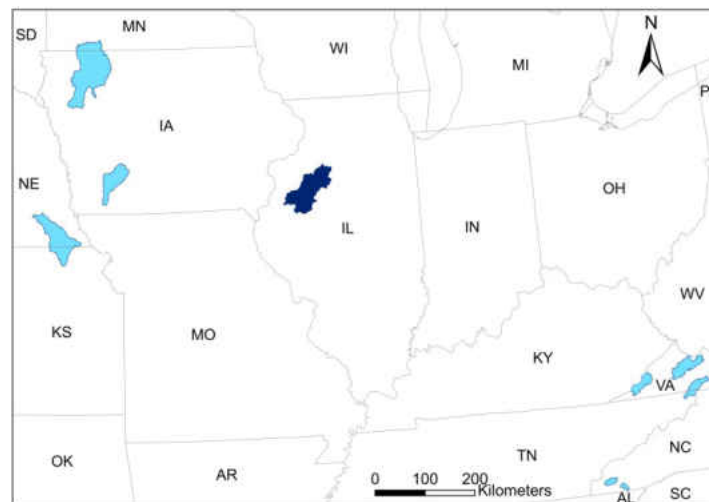


Figure 23: Locations of the 9 study watersheds with Spoon River watershed located in Illinois highlighted with dark blue.

4.1 Methodology

4.1.1 Recession analysis

Hydrograph recession analysis is usually utilized to derive water storage-discharge functions at the watershed scale. The recession analysis method proposed by *Brutsaert and Nieber* [1977] is to plot recession slope ($-dQ/dt$) as a function of discharge (Q). This method facilitates the analysis on a collective of recession events, and the impact of recession starting time on parameter estimation is minimized. As proposed by *Brutsaert and Nieber* [1977], the relationship between recession slope and discharge can be modeled as a power function:

$$-\frac{dQ}{dt} = aQ^b \quad (4.1)$$

Exponent b is dimensionless and the unit of a depends on the value of b . Q (mm/day) is groundwater discharge per unit watershed area. The data pairs $(-\frac{dQ}{dt}, Q)$ can be computed by the difference of discharges in consecutive days ($Q_t - Q_{t+1}$) and the average discharge $((Q_t + Q_{t+1})/2)$, respectively [*Brutsaert and Nieber*, 1977]. Recession periods were selected when there was no rainfall. As an example, the data pairs $(-\frac{dQ}{dt}, Q)$ for the Spoon River watershed are plotted in Figure 24.

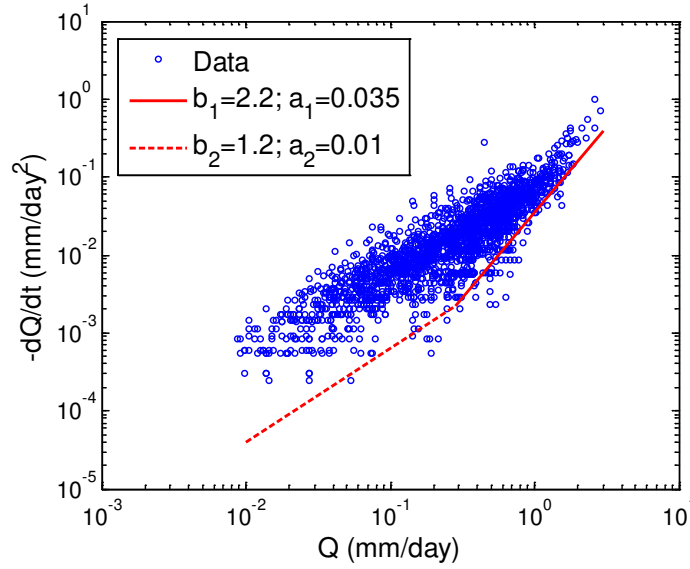


Figure 24: $-dQ/dt$ versus Q and the lower envelope for the Spoon River water based on daily streamflow data during 01/01/1983-12/31/2003.

Based on the plot of $-\frac{dQ}{dt}$ versus Q on log-log space, the function of $-\frac{dQ}{dt} = f(Q)$ and further the storage-discharge function can be constructed. Several methods have been used to estimate the parameters in the literature [Stoelzle et al., 2013]. Vogel and Kroll [1992] estimated the parameter values in equation (4.1) by linear regressions. Kirchner [2009] proposed to use polynomial functions which fit the binned data points. Therefore, the power function in equation (4.1) was not assumed a priori. Since the recession rate of groundwater discharge is smaller than other storage components, Brutsaert and Nieber [1977] proposed to place the fitted line at the lower envelope of the data points. The effect of evaporation on recession parameter estimation is minimal at the lower envelope. In this study, the lower envelope method is used for estimating the recession parameters a and b . Table 2 shows the values of parameters a and b of the 9 study watersheds.

Table 2: Watershed name, USGS gage number, drainage area, climate aridity index (E_p/P), and estimated recession parameters for the 9 case study watersheds

Watershed	USGS gage	Drainage area (km ²)	E_p/P	Recession parameter			
				a_1	b_1	a_2	b_2
Spoon River, IL	05570000	4237	1.09	0.035	2.2	0.01	1.2
Holston River, VA	03473000	785	0.61	0.02	2.3	0.03	1.4
Nantahala River, NC	03504000	134	0.39	0.0015	2.9	0.01	1.5
Little Sioux River, IA	06606600	6475	1.34	0.022	2.5	0.02	1.5
Valley River, NC	03550000	265	0.38	0.004	3	0.017	1.5
Clinch River, VA	03524000	1380	0.68	0.025	2.9	0.035	1.5
Powell River, VA	03531500	827	0.60	0.025	2.9	0.035	1.5
Nodaway River, IA	06817000	1972	1.17	0.05	2.8	0.025	1.5
Big Nemaha River, NE	06815000	3468	1.34	0.15	3	0.025	1.3

When rainfall is zero and the net groundwater flux from outside the watershed is negligible, the water balance equation during recessions can be written as:

$$\frac{dS}{dt} = -Q - E \quad (4.2)$$

where S (mm) is the depth of water storage per unit watershed area. S is the water storage contributed to observed base flow at the outlet but normalized over the entire watershed area. Therefore, E (mm) is also the depth of evaporation from the contributing storage but normalized by the watershed area. Both S and E are not the corresponding total values in the entire watershed. The storage-discharge function derived from hydrograph recession is a conceptual lumped model. The unsaturated and saturated zones are modeled by one storage term. Therefore, evaporation in equation (4.2) is assumed for the total value from unsaturated and saturated zones [Szilagyi et al., 2007; Kirchner, 2009; Palmroth et al., 2010]. The recession parameters can be estimated at the lower envelope where the impact of evaporation is minimal (Figure 24). Correspondingly, the storage-discharge relation is obtained:

$$dS = \frac{1}{a} Q^{1-b} dQ \quad (4.3)$$

Substituting dS into equation (4.2), evaporation can be estimated based on the observed recession slope and discharge [*Palmroth et al.*, 2010]:

$$E = \frac{-dQ/dt}{a} Q^{1-b} - Q \quad (4.4)$$

The effect of evaporation on hydrograph recession has been reported in many watersheds [*Federer*, 1973; *Daniel*, 1976]. The seasonal variability of recession rate is caused by seasonal pattern of evaporation [*Wittenberg and Sivapalan*, 1999].

During the late recession, the exponent, which is presented as b_2 , is usually less than 2, and the contributing storage is obtained by integrating equation (4.3):

$$S = S_m + \frac{Q^{2-b_2}}{a_2(2-b_2)} \quad (4.5.1)$$

S_m is interpreted as the minimum storage for generating base flow. During the early recession, the exponent, which is presented as b_1 , is usually larger than 2 and the contributing storage is computed as:

$$S = S_c + \frac{Q^{2-b_1}}{a_1(2-b_1)} \quad (4.5.2)$$

S_c is interpreted as the storage capacity [*Kirchner*, 2009]. Storage and discharge functions by equation (4.5), which are estimated from recession analysis as shown in Figure 24, are usually assumed to be one-to-one relationships.

Discharge at the transition point from early to late recessions is a function of recession parameters:

$$Q_0^* = \left(\frac{a_2}{a_1}\right)^{\frac{1}{b_1-b_2}} \quad (4.6)$$

For the parameters in Figure 24, Q_0^* is 0.29 mm/day for the Spoon River watershed. If $Q > Q_0^*$, the recession is at the early stage. Otherwise, it is at the late stage. According to equation (4.5), the storage capacity can be computed given S_m and Q_0^* :

$$S_c = S_m + \frac{Q_0^{*2-b_2}}{a_2(2-b_2)} - \frac{Q_0^{*2-b_1}}{a_1(2-b_1)} \quad (4.7)$$

Storages at the late and early recessions are computed by equation (4.5.1) and equation (4.5.2), respectively.

As discussed earlier, due to the effect of partial contributing storage, S in these equations is the contributing storage normalized by the watershed area. The ratio of contributing storage to total storage is represented by β :

$$\beta = \frac{S}{TS} \quad (4.8)$$

where TS (mm) is the total depth of water storage per unit watershed area. Similarly, the ratio of evaporation estimated by equation (4.4) to total evaporation is represented by:

$$\alpha = \frac{E}{TE} \quad (4.9)$$

where TE (mm) is the total evaporation per unit watershed area. The variables α and β can be interpreted as the fraction of the watershed underlain by aquifers that contributes to streamflow [Brutsaert and Nieber, 1977]. The values of α and β are indicators of hydrologic connectivity among hillslope-riparian-stream zones. The variability of β , such as seasonal variation, is one potential factor for variable storage-discharge functions, $TS = f(Q)$, at the watershed scale.

4.1.2 Estimation of α and β

In order to explore the impact of the variable contributing storage on the storage-discharge relationship, the values of α and β are estimated in the study watersheds. At each individual recession event, α is estimated as the ratio between estimated daily E by equation (4.4) and observed daily evaporation (E^{obs}) based on remote sensing data at the watershed scale: $\alpha = E/E^{obs}$. On the other hand, β is estimated as the ratio between estimated storage and total storage. For a recession segment, the value of β is estimated by the water balance described as follows. Storages at two consecutive days, $S(t_1)$ and $S(t_2)$, are computed by equation (4.5). The total watershed storage change is equal to discharge and total evaporation:

$$TS(t_1) - TS(t_2) = Q(t_2) + TE(t_2) \quad (4.10)$$

Combining equations (4.8) and (4.10), the contributing storage parameter at t_2 is computed by:

$$\beta(t_2) = \frac{S(t_2)}{[S(t_1)/\beta(t_1) - Q(t_2) - TE(t_2)]} \quad (4.11)$$

At the onset of the recession event (t_1), the value of β is assumed to be equal to the average of α during the recession, since α and β are both majorly controlled by the variation of contributing storage in the watershed. This assumption is used to determining the initial value of β in a recession event. The uncertainty of the initial β does not affect the generalization of the findings.

4.1.3 Data selection and S_m

The analysis in this study is based on recessions during the period from April to October in order to focus on the rainfall events. The following criteria are used to filter recession segments: (1) declining streamflow; 2) no rainfall during recession; 3) recession event is longer

than 4 days. The recession rate computed by $\frac{Q(t)-Q(t+2)}{2}$ is used to compute $S(t+1)$ associated with discharge $Q(t+1)$. The estimated storage in Eq. (4.5) is affected by the minimal storage S_m , which is set to 0. However, the estimation of evaporation in Eq. (4.4) is unaffected by S_m .

4.2 Results and Discussion

4.2.1 Recession analysis and parameter α and β

The values of α and β in the 9 case study watersheds shown in Table 2 are calculated using the method discussed formerly. The Spoon River watershed will be discussed with more details as mentioned before. As shown in Figure 24, the recession parameters for the Spoon River watershed are $b_1 = 2.2$ and $a_1=0.035 \text{ mm}^{-2} \text{ d}$ for the early recession and $b_2 = 1.2$ and $a_2=0.01 \text{ mm}^{-0.2} \text{ d}^{-0.8}$ for the late recession. The values of recession parameters for the other 8 watersheds are shown Table 2, and the corresponding plots of $-dQ/dt \sim Q$ can be found in the support material.

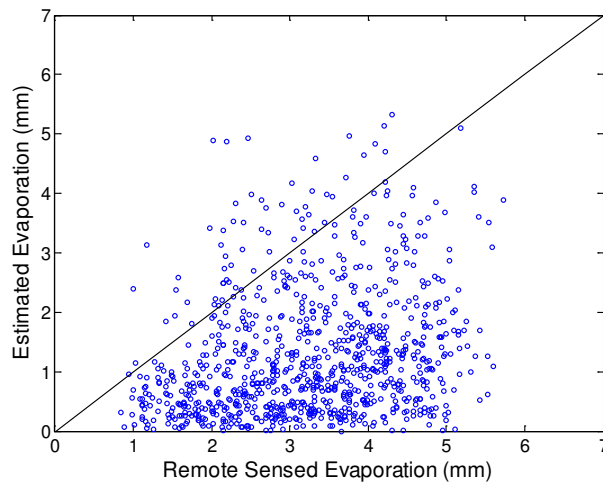


Figure 25: Comparison between estimated evaporation from recession analysis and evaporation from remote sensed data.

4.2.2 Underestimation of evaporation from base flow recession analysis

The estimated daily evaporation from the lumped storage-discharge relationship is compared with the one estimated from remote-sensing and weather stations-based data. For demonstration purpose, two recession events from: 1) the Spoon River watershed during May 1994 in Table 3; 2) and the Nodaway River watershed during May 1994 in Table 4 are shown as below. The estimated E by equation (4.4) and E^{obs} from remote sensing data are shown in columns 6 and 7, respectively. As we can see in Table 3 and 4, the estimated evaporation from recession analysis is much smaller than E^{obs} . Figure 25 plots estimated E versus E^{obs} from all the 9 watersheds. Most of the estimated values of evaporation are smaller than the remote sensed ones, and 93% of data points are below the 1:1 line in Figure 25.

Table 3: One recession event from the Spoon River watershed in Illinois

Date	P (mm/day)	Q (mm/day)	$-dQ/dt$ (mm/day ²)	S (mm)	Estimated E (mm/day)	E^{obs} (mm/day)	α	β
05/15/1994	0.40	0.84						
05/16/1994	0.00	0.78						
05/17/1994	0.00	0.71	0.0665	76.22	2.18	3.33	0.656	0.437
05/18/1994	0.00	0.65	0.0491	73.57	1.72	3.16	0.543	0.431
05/19/1994	0.00	0.61	0.0373	71.55	1.33	3.08	0.432	0.429
05/20/1994	0.00	0.57	0.0258	69.71	0.86	3.10	0.278	0.427
05/21/1994	0.00	0.56	0.0255	68.72	0.92	3.35	0.274	0.431
05/22/1994	0.00	0.52						
05/23/1994	0.81	0.50						

Table 4: One recession event from the Nodaway River watershed in Iowa

Date	P (mm/day)	Q (mm/day)	$-dQ/dt$ (mm/day ²)	S (mm)	Estimated E (mm/day)	E^{obs} (mm/day)	α	β
06/14/1995	0.51	0.70						
06/15/1995	0.00	0.65						
06/16/1995	0.00	0.60	0.0497	61.87	1.90	4.37	0.436	0.384
06/17/1995	0.00	0.55	0.0428	59.46	1.75	4.02	0.435	0.357
06/18/1995	0.00	0.51	0.0329	57.28	1.33	3.75	0.353	0.330
06/19/1995	0.00	0.49	0.0298	55.81	1.22	3.91	0.313	0.319
06/20/1995	0.04	0.45						

The mismatch between estimated E versus E^{obs} can be induced by two potential reasons. The values of E are underestimated, or the values of E^{obs} are overestimated. However, E^{obs} is not biased toward overestimating evaporation as discussed earlier, and the average RMSE of E^{obs} is 1.2 mm/day. The detailed uncertainty assessment of E^{obs} is not discussed in this study and referred to [Zhang *et al.*, 2010]. Even if 1.2 mm/day of overestimation in E^{obs} is assumed, the estimated E is still underestimated in most recession events. As shown in Table 3 and 4, the estimated E decreased from 1.72 mm/day to 0.92 mm/day during a recession event in May in the Spoon River watershed while E^{obs} remained at the level of 3.08 mm/day to 3.35 mm/day. The underestimation of E is also supported by the fact that potential evaporation of the Spoon River watershed is 6.20 mm/day and the land use is dominated by agriculture including corns and soybeans [ISWS, 2010]. It should be noted that the placement of lower envelope in Figure 24 also affects the estimation of E . If the lower envelope in Figure 24 was moved upward, the estimated evaporation will be even lower.

The underestimation of evaporation from hydrograph recession analysis can be explained by two major reasons: 1) The storage contributed to the observed base flow in the outlet is mainly from riparian groundwater during dry periods, and therefore the estimated evaporation by equation (4.4) only accounts for evaporation from the riparian zone; 2) The linkage between water storage in the unsaturated zone and base flow becomes weak while the groundwater table declining. As a result, evaporation from unsaturated zone is not included in the estimated E by recession analysis. Because of these two reasons, the value of estimated E by equation (4.4) will be underestimated, since the estimated E from riparian zone or contributing storage to base flow is normalized by the entire watershed area.

4.2.3 Temporal variability of α

The ratio between estimated E and E^{obs} , which is described as α , reflects the significance of bias in the estimated evaporation. As shown in Table 3, the value of α decreases by 58% from 0.656 to 0.274 during the recession event; and the value of α decreases by 28% from 0.436 to 0.313 during the event in Table 4. The value of α decreases with declining discharge during individual recession events in all the study watersheds. The value of α also varies with events and is dependent on the initial soil moisture and groundwater table. For example, the water table rises after a heavy rainfall and therefore more groundwater area contributes to the base flow, which is corresponding to a higher value of α . At the same time, higher discharge is corresponding to higher water table. Figure 26 plots the relation between estimated α and observed discharge from the Spoon River watershed. As it shows, the larger values of α correspond to higher discharges.

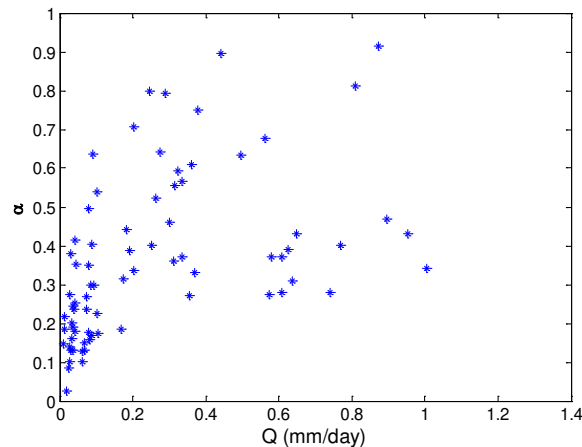


Figure 26: Estimated α versus discharge (Q) from the Spoon River watershed.

As a statistical summary on the underestimation of E , Figure 27 shows the cumulative distribution function (CDF) curve of α , in which 93.3% of the α values in the 9 study watersheds

are smaller than 1 and over 70.2% of the α values are smaller than 0.5. This result indicates a significant underestimation of evaporation based on recession analysis.

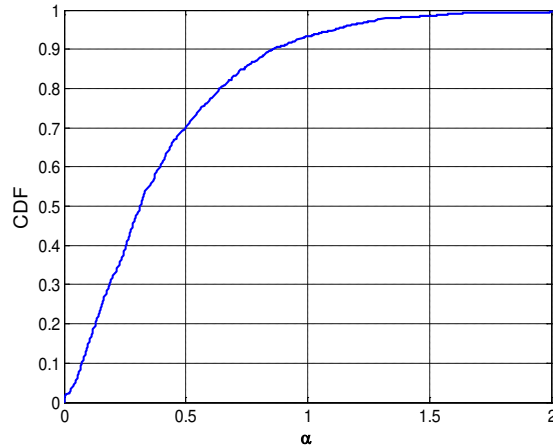


Figure 27: Cumulative distribution function of α from all the study watersheds.

4.2.4 Temporal variability of β

The underestimation of storage by storage-discharge relationship is reflected in the values of β which is the ratio of estimated storage to total storage. Figure 28 plots the CDF curve of β values in the 9 study watersheds. The values of β are less than 1.0 for 94.5% of data points, and 0.5 for 72.7% of data points. Focusing on small watersheds with drainage area less than 100 km², *Krakauer and Temimi* [2011] compared the storage inferred from the recession curve and the storage measured by GRACE and found that the variability of storage by storage-discharge functions derived from recession curves is typically smaller by a factor of 10. The effect of partial contributing storage contributes to the discrepancy was also observed in their study.

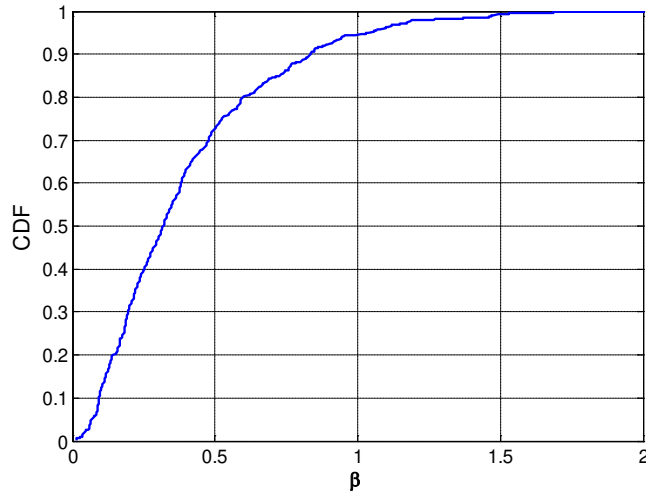


Figure 28: Cumulative distribution function of $\beta=S/TS$ from all the study watersheds.

The underestimations of both evaporation and storage change based on recession analysis are due to the partial contributing storage to base flow. Furthermore, the storage changes between two consecutive days (ΔS and ΔTS) are computed, and the ratios between them, $\Delta S/\Delta TS$, are obtained. Figure 29 plots $\Delta S/\Delta TS$ versus α (i.e., E/E^{obs}) from the Spoon River watershed. The correlation coefficient between $\Delta S/\Delta TS$ and E/E^{obs} is 0.84. Therefore, the underestimations of evaporation and storage change are highly correlated.

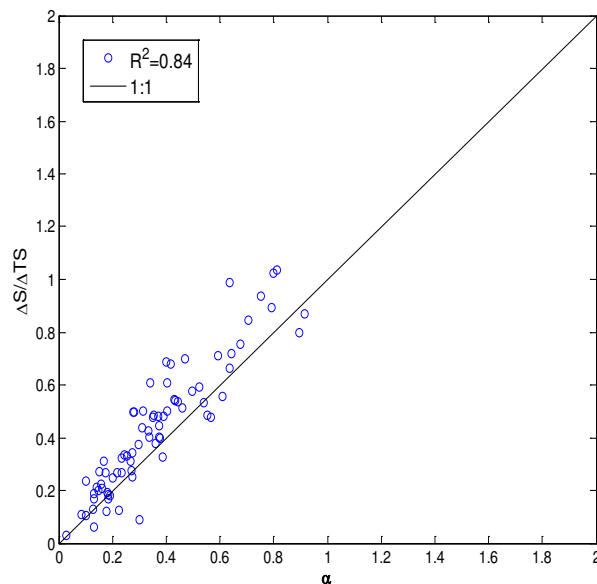


Figure 29: Correlation between $\Delta S/\Delta TS$ and α in the Spoon River watershed.

The value of β can also be interpreted as the percentage of water storage contributing to the base flow during low flow periods when riparian groundwater storage is the major source for base flow. Column 5 in Table 3 and 4 shows the computed relative storage by equation (4.5.1), and the last column shows the estimated β by equation (4.11) from water balance. As shown in the tables, β does not change significantly during a recession event. The value of β is around 0.43 for the Spoon River watershed and varies from 0.38 to 0.32 for the Nodaway River watershed. Compared with the declining trend of α during a recession event, the value of β is relatively more stable. The implication of stable value of β is that the ratio of riparian groundwater storage to total watershed groundwater storage is relatively stable during a recession event.

On the other hand, β reflects the level of shallow groundwater connectivity in the watershed. The groundwater storage connectivity is dependent on the groundwater table depth. Therefore, the value of β may be correlated with groundwater table depth. It is fortunate that the observation of the shallow groundwater table depth in the Spoon River watershed is available [Wang, 2012a]. As shown in Figure 30, the values of β decrease as the groundwater table depth increases and the correlation coefficient is 0.41, which indicates that when the groundwater table drops down, the contributing storage to base flow will decrease. The seasonal variability of water table depth is significant ranging from 86 mm to 510 mm as shown in Figure 30. Correspondingly, the seasonal variability of β is also significant ranging from 0.027 to 0.799 (Figure 28), even though the variation of β is not significant during a recession event.

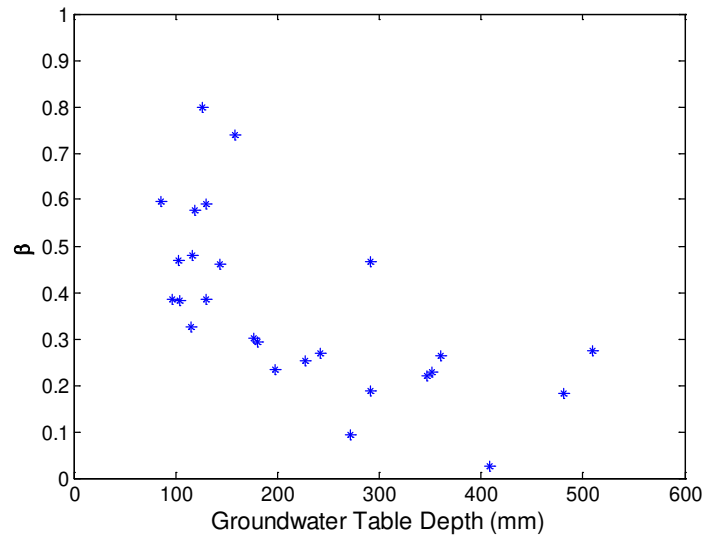


Figure 30: The relationship between estimated β and observed shallow groundwater table depth at the Spoon River watershed.

4.2.5 Variability of storage-discharge relationship

The effect of partial contributing storage induces variable storage-discharge relationship at the watershed scale. Figure 31 presents the estimated total relative storage (TS) and discharge (Q) relationship for the Spoon River watershed. The red solid line represents the storage-discharge function derived from the lower envelope of Figure 24, i.e., equation (4.5), which is equivalent to the case of $\beta = 1$. The blue circles represent the estimated total watershed relative storage by considering variable β values based on water balance at the watershed scale. The data points ($\beta < 1$) are below the red solid line ($\beta = 1$). From Figure 31, the TS - Q relation tends to follow a power law within a recession event but varies among different recession events due to the variability of β among recession event. Given the same values of discharge, the corresponding total watershed water storage may vary between recession events. Therefore, the storage-discharge relation during recession periods may not be a one-to-one function. Other

factors can also contribute to the multi-valued storage-discharge relationship [Rupp *et al.*, 2009; Haught and Meerveld, 2011; Clark *et al.*, 2011]. Sloan [2000] demonstrated that single-valued storage discharge functions are often incapable of representing the actual storage-discharge characteristics of a watershed and proposed an alternative discharge function based on hillslope groundwater hydraulics. Therefore, the effect of partial contributing storage is one of potential contributions to the variable storage-discharge relationship.

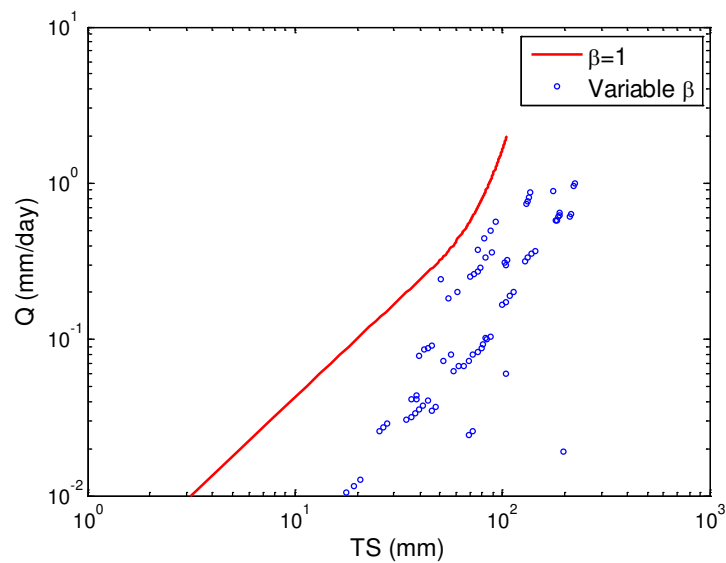


Figure 31: The impact of variable contributing storage on the total storage-discharge relationship at the Spoon River watershed.

CHAPTER 5 CASE STUDIES

5.1 Case Study at Chipola River Watershed

With the combination of the evaporation model, two-stage runoff model and water balance equations, a complete seasonal water balance model can be obtained. Totally 8 equations are included in the model: (2.6.1), (2.6.2), (3.5), (3.9), (3.12.1), (3.12.2), (3.15.1) and (3.15.2). The parameters in this model are: ϕ_w , ϕ_d , V_w , V_d , λ_d^w , λ_d^d , W_p^w , W_p^d , λ_b^w and λ_b^d . The input will be precipitation and potential evaporation in wet and dry season respectively, namely P_w , P_d , E_{pw} and E_{pd} . The output will be evaporation, storage change, surface runoff and baseflow in wet and dry season respectively, namely E_w , E_d , ΔS_w , ΔS_d , Q_d^w , Q_d^d , Q_b^w and Q_b^d .

5.1.1 General information of Chipola River Watershed

Chipola River Watershed is located in the “Pan-handle” region of Florida as shown in Figure 32. The drainage area of the watershed is 2148 km² and the aridity index (E_p/P) is 0.92. Based on the monthly aridity index developed in this study, the dry season of the watershed is from May to September, while the rest of the months are in wet season.

The historical data of 1983-2000 of streamflow and rainfall data for Chipola River Watershed is collected from local USGS gages and NOAA gages respectively. Evaporation and potential evaporation data of the same period are collected from remote-sensed database. The future projection of rainfall and temperature of the period of 2038-2070 are obtained from RCM and potential evaporation is calculated based on temperature using Hamon equation.

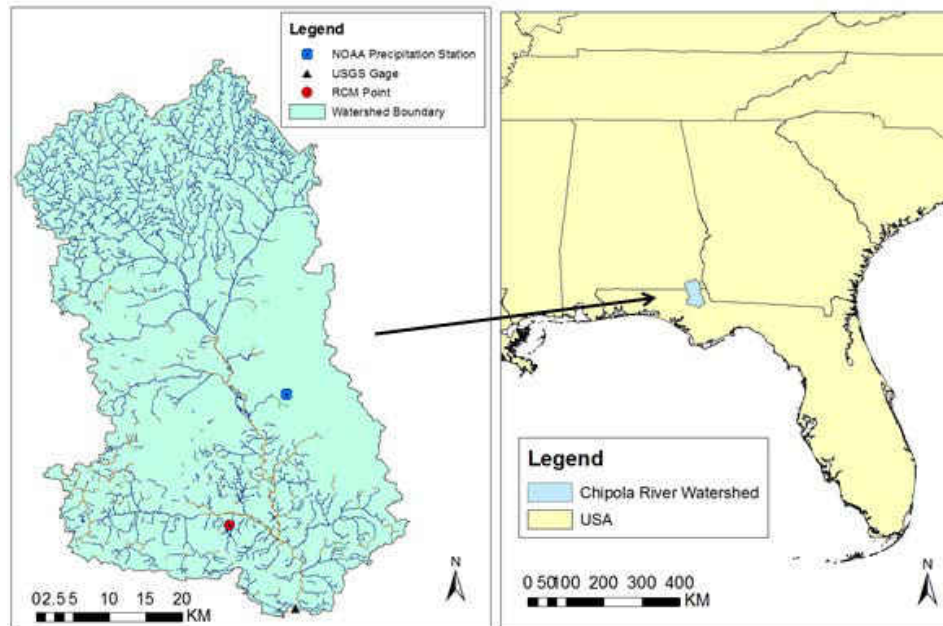


Figure 32: Chipola River Watershed.

5.1.2 Seasonal water balance simulation

Based on historical data of precipitation and evaporation during 1983~2000 in Chipola River Watershed (the information about data source is described in 4), the simulated evaporation, storage change and runoff are obtained and shown in Figure 33. As the results show, the simulation accuracy of the water balance model is high for all three outputs.

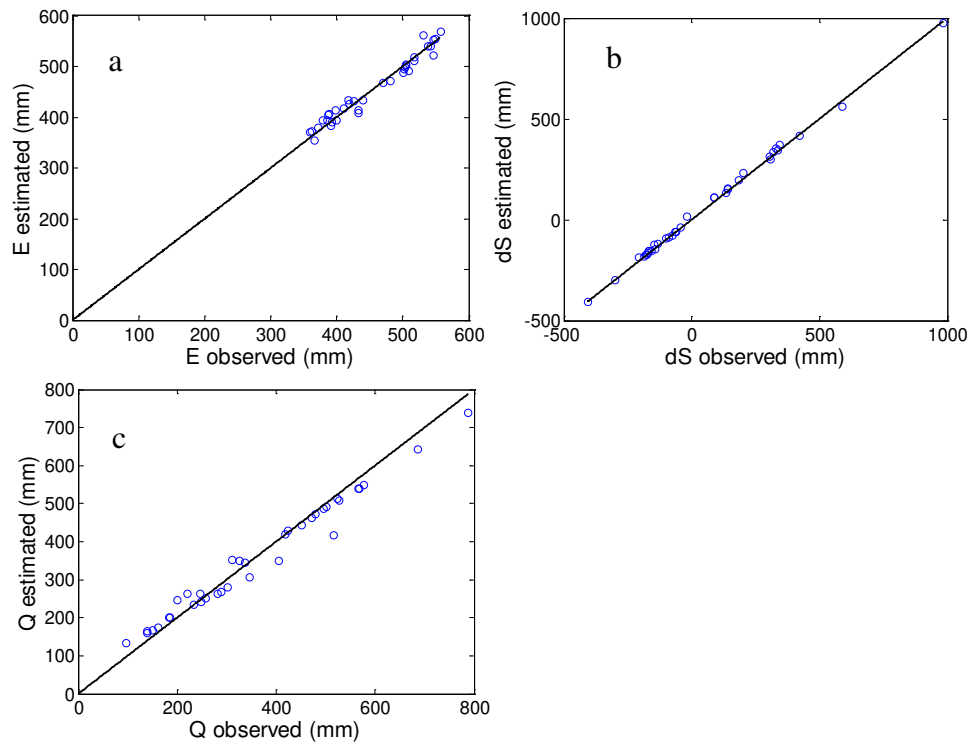


Figure 33: Simulation results in Chipola River Watershed in terms of evaporation (a), storage change (b) and runoff (c) and their comparison with the observed values respectively.

5.1.3 Seasonal water balance projection

Since the model had a high simulation accuracy of the seasonal water balance partitioning, the potential of the model is further explored in terms of future water balance project. By combining the seasonal water balance model with RCM, from where future precipitation and temperature projection from 2041 to 2068 are obtained, a water balance projection is conducted. The results of the projection are shown in Figure 34. As the figure shows, a significant increasing trend of evaporation in the future is observed, comparing with present values, in both wet and dry seasons. This increasing trend is expected since the temperature in the future will increase according to the RCM projection, which has strong positive relation with evaporation.

In terms of runoff, a slight increasing trend is shown as well, but not as significant as evaporation. The storage change in dry seasons will increase significantly in the future, but the storage change in wet seasons have no significant trend.

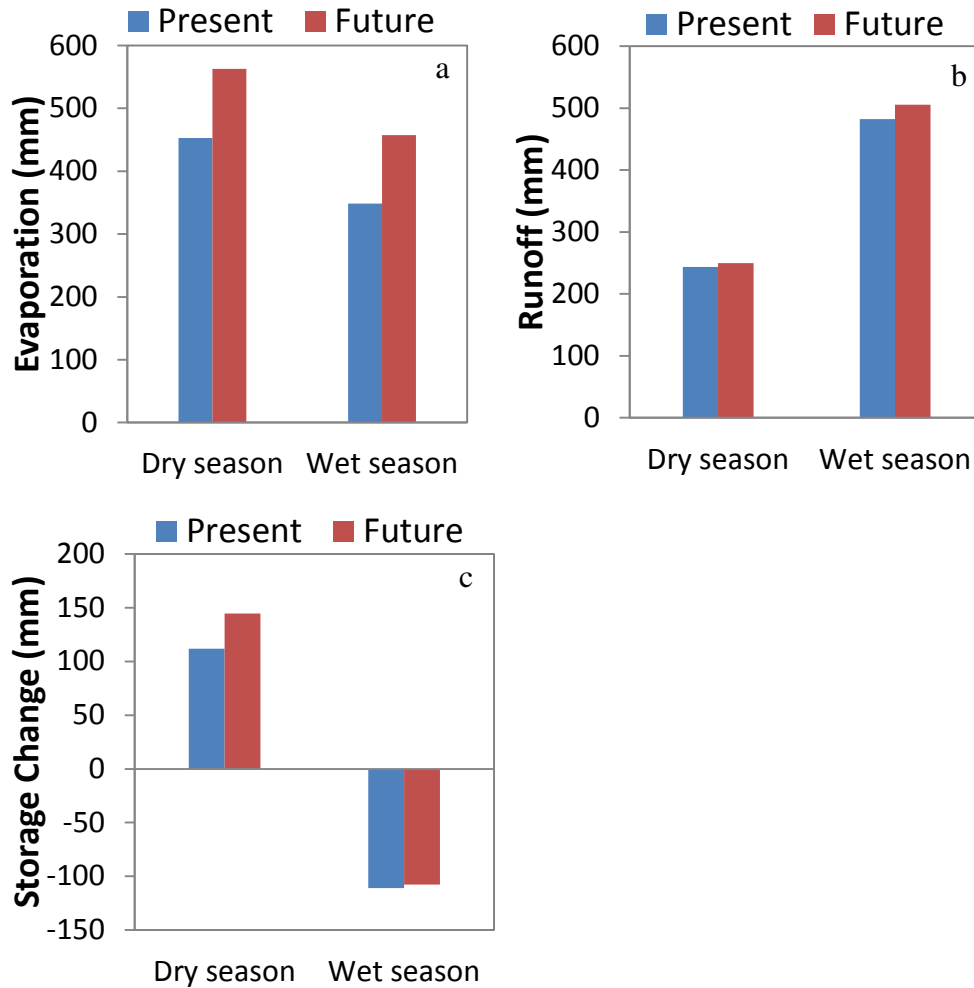


Figure 34: Projection results in Chipola River Watershed in terms of evaporation (a), storage change (b) and runoff (c) and their comparison with the present values respectively.

5.2 Case Study at Apalachicola River Watershed

5.2.1 Study area and data sources

The Apalachicola River is located at the lower part of the Apalachicola-Chattahoochee-Flint (ACF) River basin. It receives streamflow and sediment from Chattahoochee River and Flint River, and flows through the Florida Panhandle eventually draining into the Gulf of Mexico (Figure 35). It is located in the semi-humid region with a long-term climate aridity index of 0.89. Based on a digital elevation model (DEM) with a resolution of 30 meters from National Elevation Dataset (Gesch, 2007), the average slope in the region is 5.8%. As the source of 90% of the oyster production in Florida, Apalachicola Bay is an important marine nursery area (Livingston, 1984; Liu and Huang, 2009). The streamflow and sediment load from the Apalachicola River have a direct impact on the ecosystem, particularly with respect to the commercial oyster production in Apalachicola Bay. It is important to assess the impact of climate change on the Apalachicola River's streamflow and sediment load in order to form a basis to identify potential ecological effects.

The majority of the Apalachicola River basin is undeveloped nature lands. As a result, there are not many stream gages or weather stations with a long period of data records. A total of four stream gage stations monitored by the U.S. Geological Survey (USGS) are located in the area, which have a long period record of daily streamflow and sediment load (Figure 35). Among the four USGS stations, gages 2358000 and 2359000 are used as the inlet records from the Flint/Chattahoochee Rivers and the Chipola River, respectively. Gage 2358700, located at midstream and gage 2359170, located at downstream are selected for observed streamflow data

for model performance evaluation and calibration. In terms of rainfall and temperature data, three weather stations from National Climatic Data Center (NCDC) are located in the area with a long period of hourly data record (Figure 35). Based on the availability of all the data records, the baseline period is selected from 1984 to 1994. Data during 1984-1989 are used for model calibration and the last five years are used for model validation.

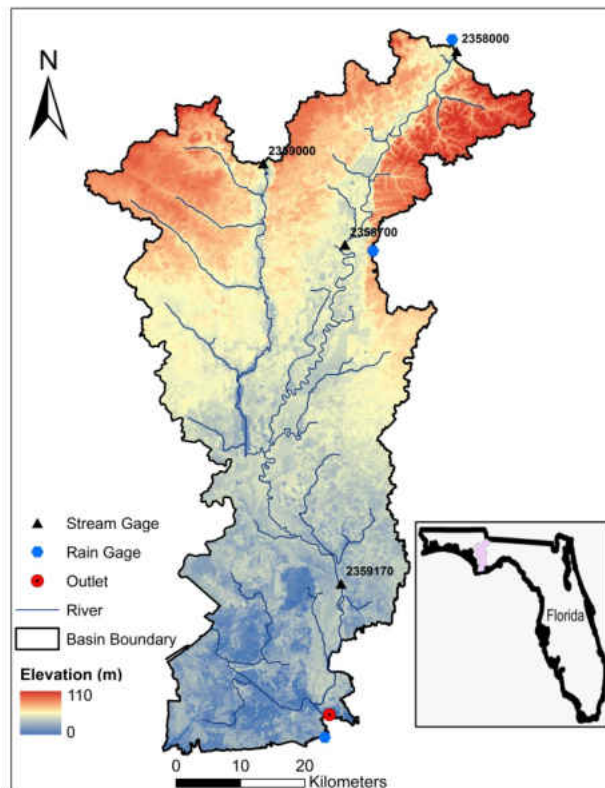


Figure 35. The basin boundary, river network, ground surface elevations, and the locations of rainfall and streamflow observation in the Apalachicola River basin.

Figure 36a shows the land use/land cover (LULC) map and the spatial distribution of soil types. The LULC data is obtained from National Land Cover Database (NLCD). Since the study period is from 1984 to 1994, LULC in 1992 is used in this study (Vogelmann *et al.*, 2001). The dominating LULC types in the region are forest (35.9%), shrub (7.5%) and agricultural

(4.4%) in the upstream area and wetland (38.9%) in the downstream area (Figure 36a). The soil data in the Apalachicola River basin, as shown in Figure 36b, is collected from Soil Survey Geographic Database (SSURGO) (USDA, 2007). The dominating soil type is Aquent, under the soil order of Entisol. With loamy or clayey-loamy texture, Aquent type soil is usually found in tidal marshes and floodplains along the rivers. As a result, loam (30.3%) and clayey loam (37.3%) are the two soil texture types that cover the largest area in the region, as shown in Figure 36b.

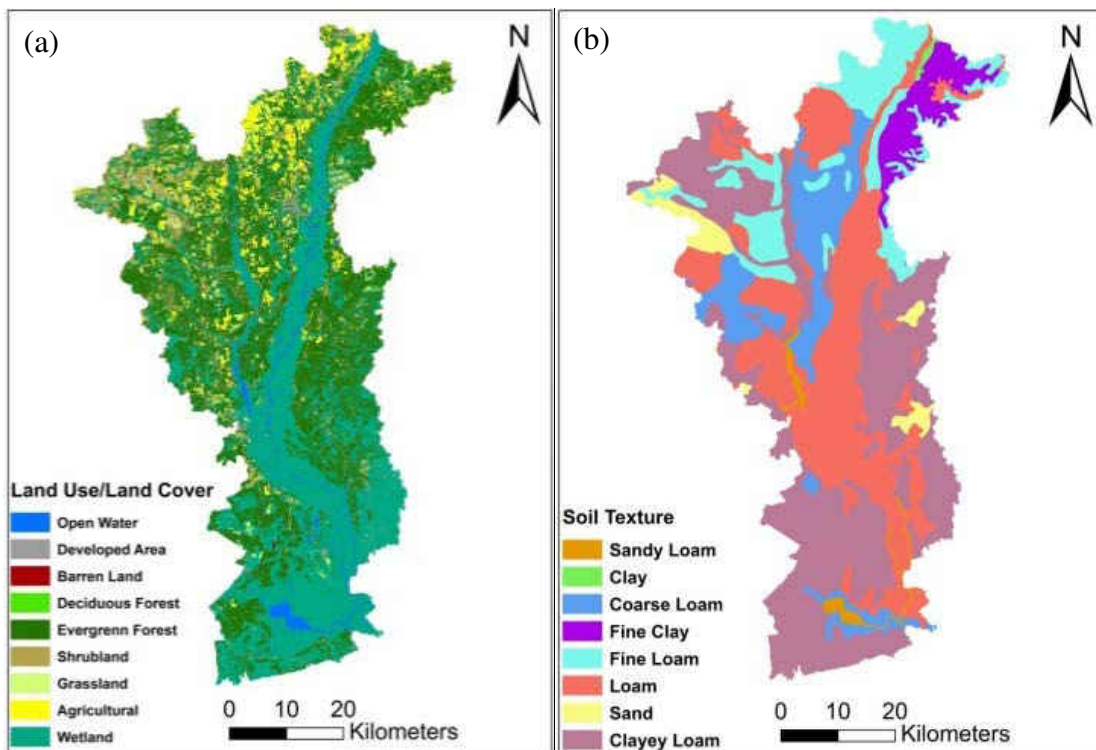


Figure 36. Land use/land cover map in 1992 (a); and soil map (b) in Apalachicola River basin.

Surrounding the Apalachicola River are the Chattahoochee River and Flint River, and the tributary Chipola River, all located upstream. The Chattahoochee River and Flint River confluence at Lake Seminole and flow into the Apalachicola River, whereas the Chipola River directly flows into Apalachicola River. In order to evaluate the contribution from the upstream

rivers and the tributary, the average daily values of observed streamflow and sediment load from the Chattahoochee River and Flint River (Gage ID: 2358000), the Chipola River (Gage ID: 2359000) and downstream in the Apalachicola River (Gage ID: 2359170) are analyzed. Results show that the Chattahoochee River and Flint River together contribute 84% of the streamflow and 46% of the sediment load in Apalachicola River, while the Chipola River contributes 6% of the streamflow and 3% of the sediment load. Therefore, the streamflow in the Apalachicola River is majorly controlled by the upstream discharge, while the local watershed contributes 10% of annual streamflow at the downstream gage. However, the local Apalachicola River basin contributes 51% of annual sediment load in the Apalachicola River. Similar results have been reported in other studies (Matraw and Elder, 1984; Stallins *et al.*, 2010; Peterson *et al.*, 2013).

5.2.2 SWAT model parameter calibration and validation

The SWAT model, which is recognized as a distributed, physically-based, daily time step, continuous-simulation model (Arnold *et al.*, 1998), is selected to simulate the streamflow and sediment load in the Apalachicola River. Additionally the model projects future streamflow and sediment load under climate change scenarios. SWAT has been used in many studies with a wide range of climate and landscape conditions (Ghaffari *et al.*, 2010; Wang *et al.*, 2011; Perrin *et al.*, 2012). In SWAT, the study watershed is divided into sub-basins based on the input DEM; the sub-basins are further divided into hydrologic response units (HRUs) based on the overlaid maps of soil type, LULC and slope. For this study, a total of 73 sub-basins and 3910 HRUs are delineated. The parameters describing the physical processes are determined based on the HRUs characteristics; values of parameter sets may vary among HRUs. The hydrologic computation in

SWAT starts from the HRU scale, and then aggregates into the sub-basin scale and the watershed scale. SWAT has been applied in various applications due to its robustness on watershed scale hydrologic modeling. These applications include land use change impact assessments, water resources management, water quality control, and sediment yield estimations. In this study, the SWAT model simulation will be focusing on streamflow and sediment yield at the seasonal and event scales.

The SWAT model uses the Soil Conservation Service (SCS) curve number method (USDA-SCS, 1985) to simulate surface runoff. Groundwater flow is simulated using a linear reservoir model. The following are the two major equations used for runoff calculations. Equations (5.1) and (5.2) are derived from the SCS curve number method and a linear reservoir model, respectively (Neitsch *et al.*, 2011):

$$Q_s = \frac{(R-0.2S)^2}{R+0.8S} \quad (5.1)$$

$$\frac{dQ_{gw}}{dt} = \alpha_{gw} * (w_r - Q_{gw}) \quad (5.2)$$

where Q_s is surface runoff (mm/day); R is daily rainfall (mm/day); S is the retention parameter (mm); Q_{gw} is base flow (mm/day); w_r is recharge rate (mm/day) to shallow groundwater; and α_{gw} is the base flow recession constant. In equation (5.1), the parameter S is a function of the curve number (CN), $S = \frac{1000}{CN} - 10$. Based on equations (5.1) and (5.2), CN and α_{gw} are the controlling factors for surface runoff and base flow, respectively. The detailed explanation on selecting key parameters for model calibration is provided in the “Results and Discussion” part.

For simulating sediment yield, the SWAT model uses the Modified Universal Soil Loss Equation (MUSLE) shown below (William, 1995):

$$Q_s = 11.8 * (Q_{sv} * q_{peak} * area_{hru})^{0.56} * K_{USLE} * C_{USLE} * P_{USLE} * LS_{USLE} * CFRG \quad (5.3)$$

where Q_s is sediment yield (metric tons/day); Q_{sv} is surface runoff depth per unit area (mm/ha); q_{peak} is peak runoff rate (m³/s); $area_{hru}$ is area of the HRU (ha); K_{USLE} is the soil erodibility factor of universal soil loss equation (USLE); C_{USLE} is cover and management factor of USLE; P_{USLE} is support practice factor of USLE; LS_{USLE} is topographic factor of USLE; and $CFRG$ is coarse fragment factor. Based on equation (5.3), the sediment yield is strongly related to surface runoff. The detailed explanations of the equations and parameters used in runoff and sediment yield simulation are provided in the SWAT Theoretical Documentation (Neitsch *et al.*, 2011).

To evaluate the performance of SWAT simulations in this study, the statistical measurement of Nash-Sutcliffe efficiency (NSE) is used.

5.2.3 RCM selection and future climate change projection

The projection of future climate change in terms of rainfall and temperature is conducted using RCMs from NARCCAP. NARCCAP is an international program to serve the needs of climate change projection in the North America region covering northern Mexico, conterminous U.S. and most of Canada (Mearns *et al.*, 2009). The RCMs provide future climate projections at the regional scale for a time period of 2038-2070. The simulation results of RCMs are presented at a grid resolution of 50 km. Therefore, the Apalachicola River basin, which has a drainage area of 3589 km², is covered by 2~3 grid points in each RCM. Wang *et al.* (2013) compared the performance of seven RCMs in Apalachicola River basin with a focus on rainfall variation. Based on their results, HRM3-HADCM3 and RCM3-GFDL have good performance for rainfall

in the Apalachicola River basin. Furthermore, the authors projected the future rainfall intensity-duration-frequency (IDF) curves in the study area based on the two selected RCMs. This study employs HRM3-HADCM3 and RCM3-GFDL for future rainfall and temperature projections. By combining the RCM projections with the calibrated SWAT model, the impact of climate change on streamflow and sediment load is investigated. Furthermore, the future IDF projections generated in Wang *et al.* (2013) are applied in the SWAT model to evaluate the climate change impact on streamflow and sediment load under extreme rainfall events.

5.2.4 Climate change projections

To evaluate the performance of the two selected RCMs, the observed temperature and daily rainfall are sorted to mean monthly values and compared with the corresponding values from the RCMs during the baseline period of 1968-2000. The monthly rainfall and temperature values illustrated in Figure 37 do not correlate very well with the observed values. To reduce the bias caused by the RCM projections, the following method is applied to correct climate change projections in the future period. Mean monthly rainfall and temperature are computed during the baseline and future periods for RCMs, respectively. The climate change factors of rainfall and temperature for each month are calculated with the following equations (Cai *et al.*, 2009):

$$\Delta P_i = \frac{\bar{P}_{f,i} - \bar{P}_{b,i}}{\bar{P}_{b,i}} \quad (5.4)$$

$$\Delta T_i = \frac{\bar{T}_{f,i} - \bar{T}_{b,i}}{\bar{T}_{b,i}} \quad (5.5)$$

where ΔP_i and ΔT_i are the climate change factors of month i for rainfall and temperature, respectively; $\bar{P}_{f,i}$ and $\bar{T}_{f,i}$ are the mean monthly rainfall and temperature during the period of 2038-2070, respectively; and $\bar{P}_{b,i}$ and $\bar{T}_{b,i}$ are the mean monthly rainfall and temperature at the baseline period, respectively. A similar bias correction procedure using monthly values has been used in former studies (Wood *et al.*, 2002; Wang *et al.*, 2013).

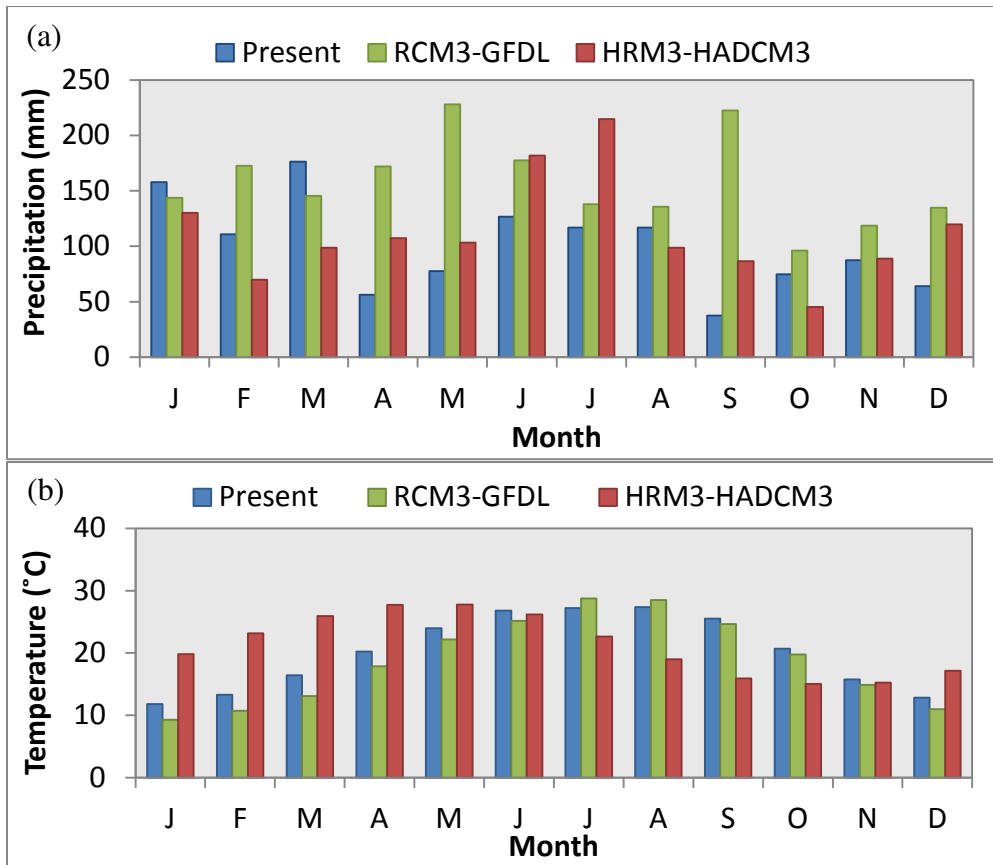


Figure 37. Comparison of observed values and RCM baseline projections of mean monthly precipitation (a) and temperature (b).

Projected daily rainfall and temperature are computed by applying the corresponding climate change factors to the observed daily values in each month:

$$P_f = P_{obs} + P_{obs} * \Delta P \quad (5.6)$$

$$T_f = T_{obs} + T_{obs} * \Delta T \quad (5.7)$$

where P_f and T_f are the projected daily rainfall and temperature; P_{obs} and T_{obs} are the observed values of daily rainfall and temperature. Based on the month of the observed daily data, the climate change factor of the corresponding month is applied. Daily values of precipitation and temperature are generated for the future period and utilized as inputs for the continuous simulation of SWAT model.

5.2.5 Projected climate changes

The future average daily rainfall based on HRM3-HADCM3 projection is 3.60 mm/day, 3.43 mm/day, and 3.40 mm/day at upstream, midstream, and downstream, respectively. The RCM3-GFDL projections for upstream, midstream, and downstream are 4.09 mm/day, 3.67 mm/day, and 3.53 mm/day, respectively. Comparing the RCM projections with the current observed daily rainfall of 3.24 mm/day at upstream, 4.27 mm/day at midstream and 4.23 mm/day at downstream indicates future rainfall at upstream will increase, and at midstream and downstream will decrease. Wang *et al.* (2013) found that the rainfall intensity will increase from upstream to downstream based on RCM3-GFDL and only increase significantly at downstream based on HRM3-HADCM3 projection. Combining the average rainfall and rainfall intensity projections, the rainfall event in the future will have a higher intensity and lower frequency. Therefore, the average level of rainfall may not change significantly, but the rainfall during extreme events may increase. For a better illustration, Figure 38a shows a comparison between the observed mean monthly values of precipitation and the future projections of the two RCMs.

As the figure shows, the maximum increase of rainfall may occur in July based on RCM3-GFDL projection.

The future temperature projection shows that the daily average temperature will increase in the future for both HRM3-HADCM3 and RCM3-GFDL projections. The peak average temperature occurs in April and May using the HRM3-HADCM3 projection, and in July and August using the RCM3-GFDL projection. Figure 38b shows the mean monthly temperature of present level based on observation and projected future level based on the two RCMs. Comparing the projected temperature with the observed value reveals RCM3-GFDL correlates better than HRM3-HADCM3 in terms of temperature projection in the Apalachicola River basin.

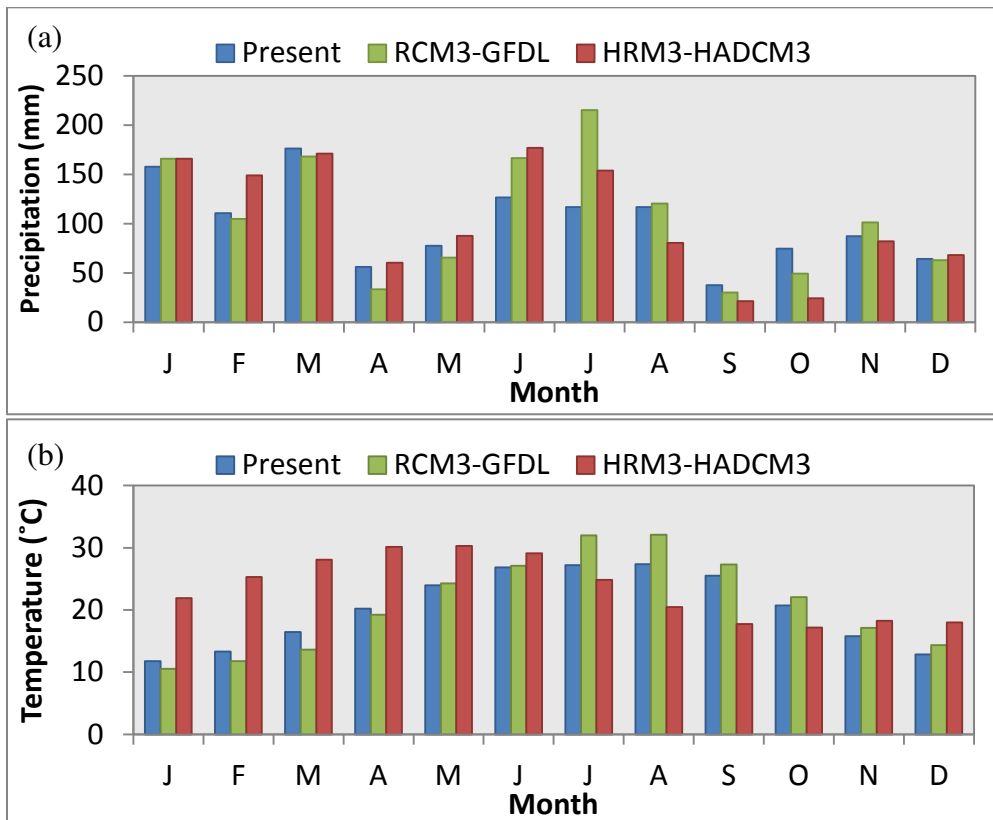


Figure 38. Comparison of observed values and RCM future projections of mean monthly precipitation (a) and temperature (b).

5.2.6 Model calibration and performance during the baseline period

During the 11-year study period, the years 1984-1989 are selected for the calibration period and 1990-1994 are used for the validation period. The selection of the calibration parameter for SWAT is based on the sensitivity of the simulation results to the parameter values. Fifteen parameters with the highest sensitivity are selected for calibration (Table 1). Among these parameters, 12 are associated with runoff simulation, and 3 are connected with sediment yield simulation. A similar list of parameters has been used in other studies for discharge simulations (Ghaffari *et al.*, 2010; Zhang *et al.*, 2011; Perrin *et al.*, 2012) and sediment load simulations (Li *et al.*, 2011; Phan *et al.*, 2011; Khoi and Suetsugi, 2014). The calibration procedure includes two steps: one for runoff and the other for sediment yield. The runoff calibration is conducted first, followed by the sediment calibration based on the calibrated runoff (Santhi *et al.*, 2001; Arnold *et al.*, 2012). The calibrated parameters are shown in Table 1. The calibration adjustment with percentages in Table 1 is to describe the changing percentage of the parameters from the original values.

The model performance during the calibration and validation periods is presented in Figure 39 and Figure 40. Figure 39a shows the simulated and observed streamflow at the gage 2359170 during the period from 1/1/1985 to 12/31/1994; Figure 39b shows the simulated and observed sediment load at the same gage station. The ramping period in the SWAT model simulation is set to the year 1984, which is not shown in the figure. The NSE values are 0.92 and 0.88 during the calibration period of 1985- 1989 and validation period of 1990-1994, respectively, indicating good performance. As shown in Figure 39b, the measurement of the sediment load is intermittent, which may affect model comparison. Although the NSE values are

0.47 and 0.36 during the calibration and validation periods respectively, the model captures the trend variability.

Table 5. Calibrated parameter values for the SWAT model

Parameter	Description	Calibration adjustment
Parameters Related to Runoff		
CN2	Curve number II	-31.6%
ESCO	Soil evaporation compensation factor	0.51
SOL_AWC	Available soil water capacity	-27.1%
SURLAG	Surface runoff lag coefficient (day)	1.2
ALPHA_BF	Base flow recession constant	0.21
SOL_Z	Soil depth (mm)	+34%
SOL_K	Saturated hydraulic conductivity (mm/hr)	+29%
CH_K2	Channel effective hydraulic conductivity (mm/hr)	115
GW_REVAP	Groundwater re-evaporation coefficient	0.16
GWQMN	Threshold depth of water in the shallow aquifer required for return flow to occur (mm)	233
REVAPMN	Threshold depth of water in the shallow aquifer for re-evaporation to occur (mm)	24
GW_DELAY	Groundwater delay (day)	5
Parameters Related to Sediment		
USLE_P	USLE support practice factor	0.042
SPCON	Sediment transport coefficient (m/s)	0.002
SPEXP	Exponent of sediment transport coefficient	1.9

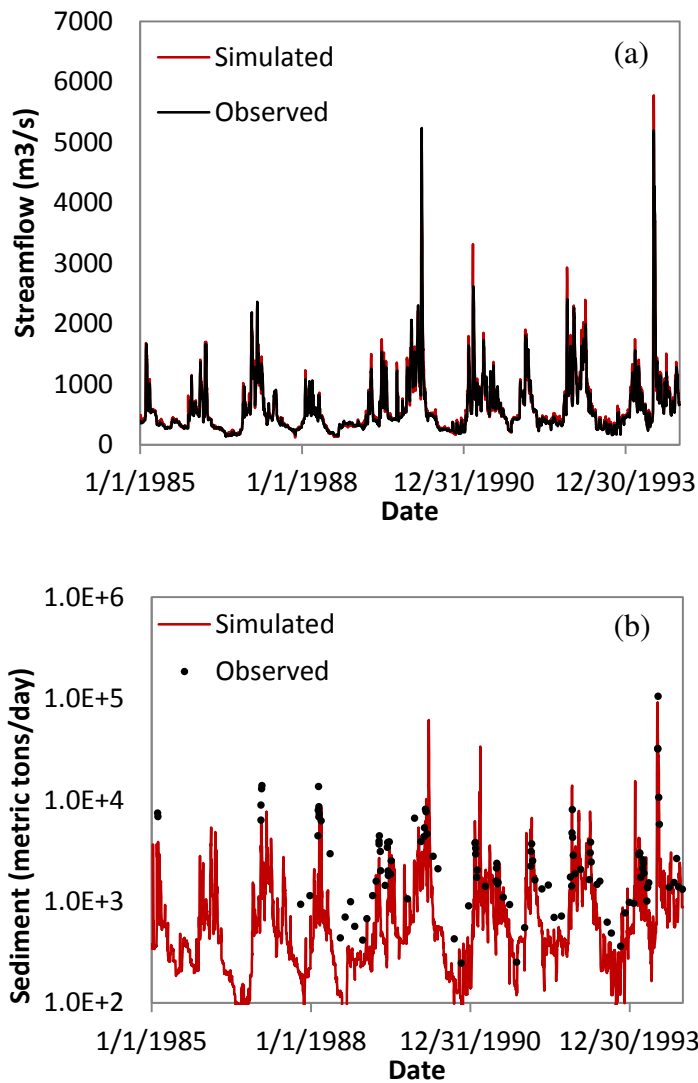


Figure 39. (a) Time series of simulated and observed streamflow at the gage 2359170; (b) time series of simulated and observed sediment load at the gage 2359170.

To further compare the simulated and observed results, Figure 40 shows the plots of observed values vs. simulated values of runoff and sediment load against the 1:1 line. The figures demonstrate that the discharge simulation performance is generally good and no significant bias is detected. The sediment load simulation results tend to underestimate the observed values when the sediment load is low. Since the sediment load is positively related to

surface runoff, this bias may also be interpreted as the simulation underestimates the sediment load when the surface runoff is low. A possible reason for this underestimation is that the sediment calculation in SWAT is primarily controlled by surface runoff, as shown in equation (5.3). The contribution of groundwater flow and lateral flow is calculated by the following equation:

$$sed_{lat} = \frac{(Q_{lat} + Q_{gw}) * area_{hru} * conc_{sed}}{10000} \quad (5.8)$$

where sed_{lat} is the sediment load from groundwater and lateral flow (metric tons/day); Q_{lat} is the lateral flow (mm/day); and $conc_{sed}$ is the concentration of sediment in groundwater and lateral flow (mg/L). Comparing equation (5.3) with equation (5.8) shows the sediment load relation to groundwater flow is linear, while it has a power law relation with surface runoff; this may be a possible explanation for the underestimation of sediment load during low flow periods.

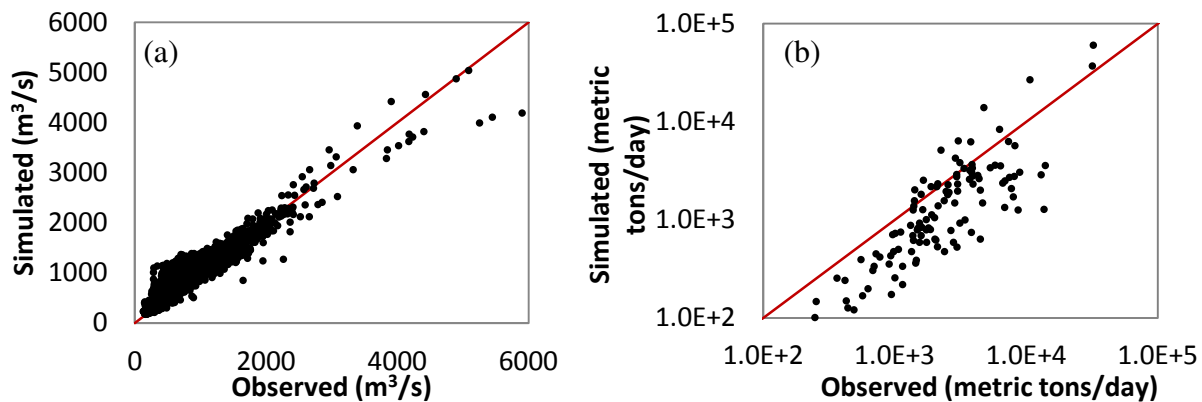


Figure 40. (a) 1:1 plot of simulated runoff versus observed streamflow; (b) 1:1 plot of simulated and observed sediment load.

5.2.7 Runoff and sediment load under climate change scenarios

The calibrated SWAT model is then used for assessing potential climate change impacts on runoff and sediment projection. The average daily runoff increased by 5% from 702 m³/s to 737 m³/s using HRM3-HADCM3 model, but slightly decreased by 0.9% using the RCM3-GFDL model. Furthermore, the mean monthly runoff is computed for the two RCMs, and the results are shown in Figure 41a. The maximum increase in rate of runoff occurs in July (34%) using the RCM3-GFDL model. This indicates that in the RCM3-GFDL climate change scenario, the average runoff generation will slightly decrease although the peak flow will increase in the summer. This result can be explained by the rainfall pattern change in the Apalachicola River basin, i.e., the rainfall event will have a lower frequency but a higher intensity (Wang *et al.*, 2013). Sediment results are shown in Figure 41b. The average daily sediment load in the future may slightly decrease from 1124 metric tons/day to 1123 metric tons/day using the HRM3-HADCM3 projection. Using the RCM3-GFDL projection, the average daily sediment load may increase to 1189 metric tons/day. As shown in equation (5.3), sediment yield is sensitive to the peak flows. Therefore, the increase rate in the RCM3-GFDL projection is much more significant than in the HRM3-HADCM3 projection (Figure 41b).

In general, the climate change impact on runoff and sediment is not very significant in terms of mean monthly level. However, the rainfall pattern change illustrated in the RCM projections, especially with RCM3-GFDL, may cause the peak flow of runoff and the corresponding peak sediment load to significantly increase. To investigate this issue further, the following section demonstrates the climate change impact on runoff and sediment during extreme rainfall events based on IDF curve projections.

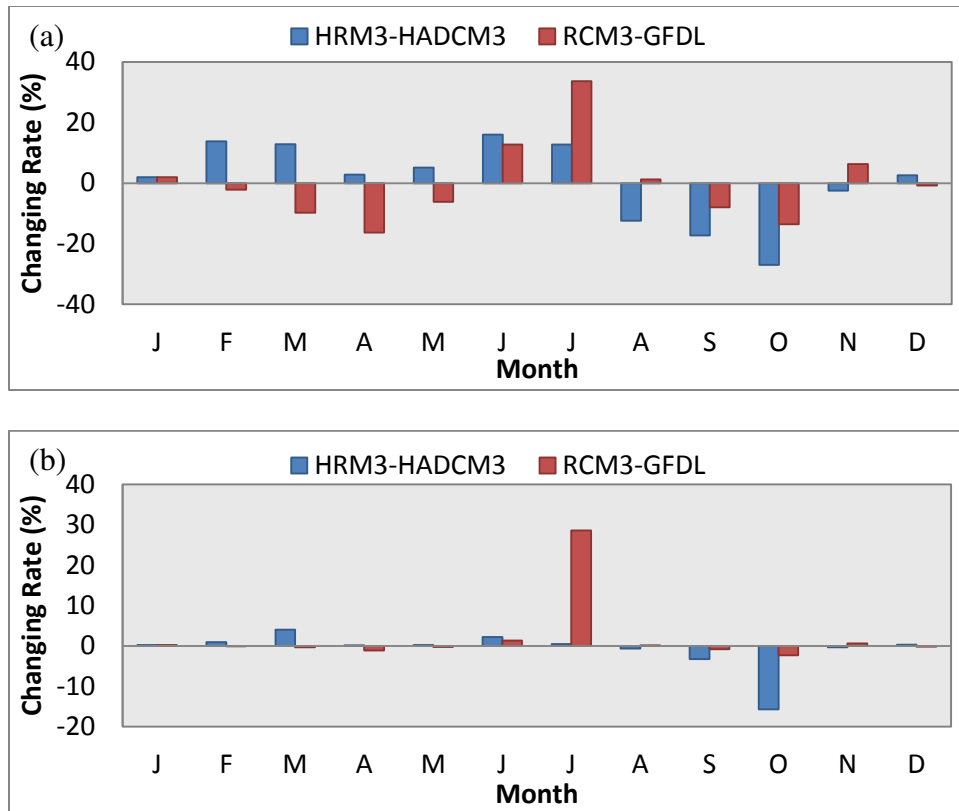


Figure 41. The mean monthly changing rate of discharge (a) and sediment load (b) under climate change impact based HRM3-HADCM3 and RCM3-GFDL.

5.2.8 Runoff and sediment load during extreme events under climate change

To evaluate the climate change impact during extreme events, a 24-hour rainfall event on March 2, 1991 with a return period of 25 years is selected as the baseline event. The rainfall intensity distribution from upstream to downstream in the Apalachicola River basin on March 2, 1991 is shown in Figure 42. The future extreme event projection is conducted using the future IDF curve in the Apalachicola River basin generated by Wang *et al.* (2013). This IDF curve is used to project the extreme event due to its ability to capture the characteristics of extreme events with much more detail. For each RCM, three IDF curves were generated to represent different

locations in the river basin: upstream, midstream and downstream (Wang *et al.*, 2013). Based on the IDF curves, the future rainfall intensities at different locations during a 24-hour rainfall event with a return period of 25 years are computed. The projected future extreme rainfall event is used as weather data input for the calibrated SWAT model.

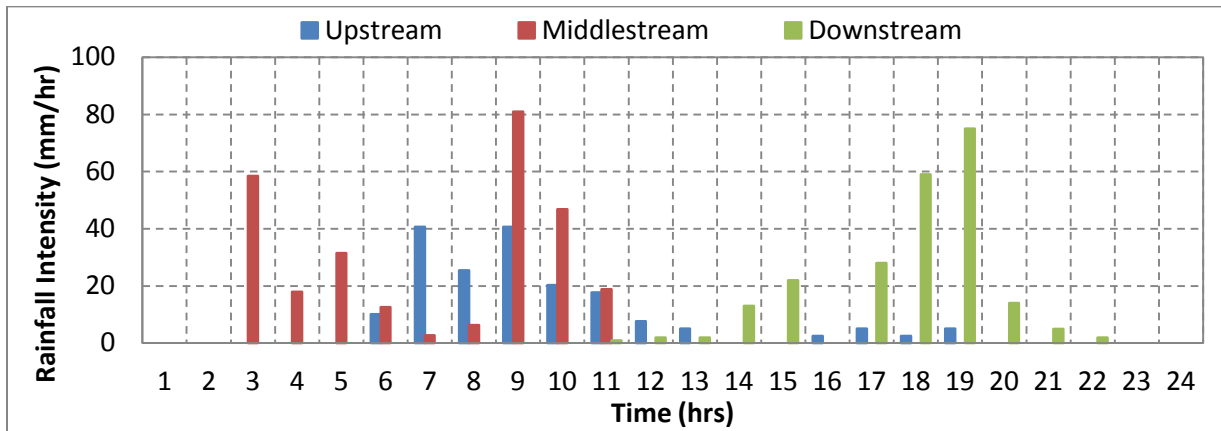


Figure 42. Hyetograph of the sample storms at three different locations in the Apalachicola River basin at 3/2/1991.

The simulated runoff and sediment load during the projected extreme event are compared with the observed values during the baseline period. As shown in Figure 43a, the peak flow based on the HRM3-HADCM3 model is 3621 m³/s, which is 8% higher than the baseline peak flow of 3360 m³/s; for the RCM3-GFDL projection, the peak flow is 5029 m³/s, which is 50% higher than the baseline value. In terms of sediment load (Figure 43b), the peak load for the HRM3-HADCM3 projection is very close to the baseline peak load of 12,110 metric tons/day. However, for the RCM3-GFDL projection, the peak load is 22,830 metric tons/day, which is 89% higher than the present level.

These results indicate that the climate change impact on runoff and sediment load in the Apalachicola River basin may be much more severe during extreme rainfall events. As shown in

previous section, the future projected average daily runoff and sediment load are similar to the current level with a change rate of less than 5%. However, under the 24-hr event with a 25-year return period, the peak streamflow and peak sediment load may be dramatically increased by 50% and 89%, respectively due to climate change. One possible reason for this change is that the rainfall event in the RCM projections, especially for RCM3-GFDL, is less frequent but has higher intensity compared to the current rainfall pattern. Another possible explanation is that the seasonality is altered due to the climate change impact, which will significantly affect the characteristics of the hydrologic system (Chen *et al.*, 2013).

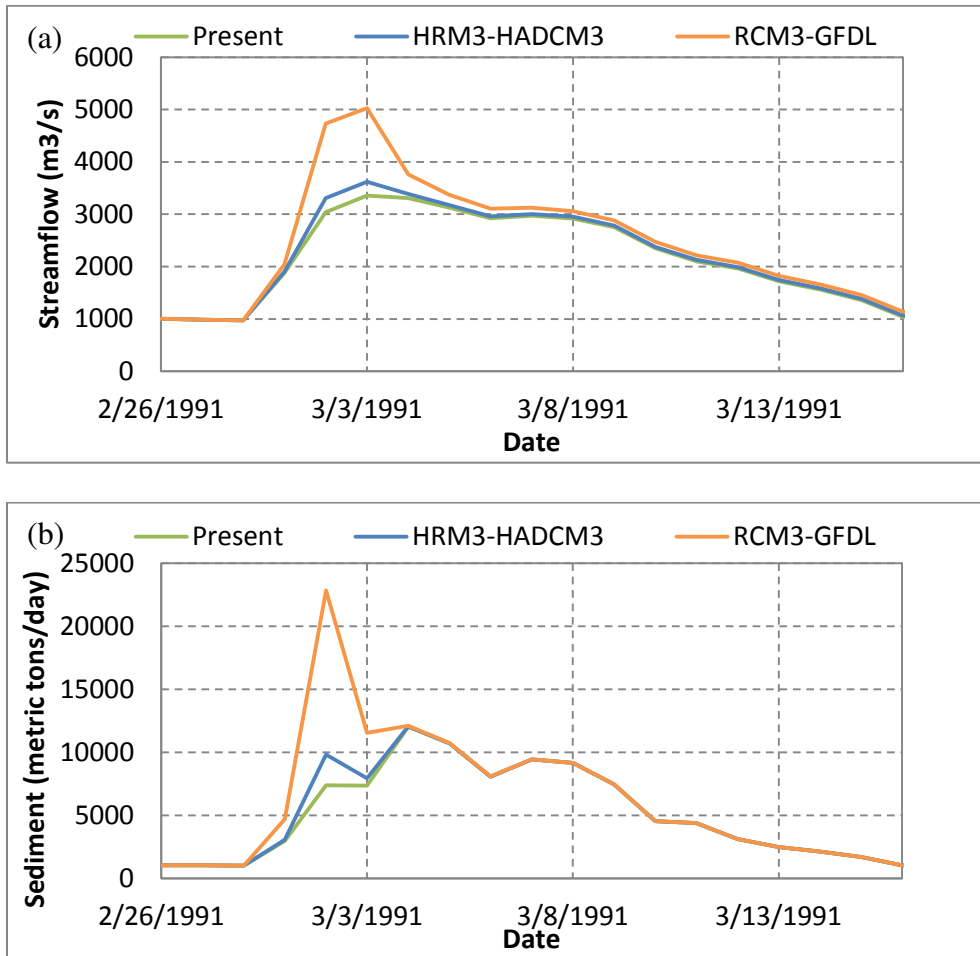


Figure 43. Future projections of discharge (a) and sediment load (b) during the extreme event under climate change impact projection.

CHAPTER 6 SUMMARY

The catchment scale hydrologic system is an important topic that directly relates to human's daily life, in terms of drinking water, storm water, recreational water, agricultural water and many other aspects. As a result, the complex watershed system has been studied with every angle and scale by hydrologists. The purpose of this study is to use simple models that are developed based on the "top-down" approach to gain a comprehensive understanding on the watershed scale hydrologic system at the seasonal scale, which is a part that has not been fully studied yet.

Three major processes in the hydrologic cycle are the foundation of this study, namely water/energy exchange, runoff generation and storage dynamics. In the study, the model of water/energy exchange at the seasonal scale is developed based on the Budyko framework; the model of runoff generation at the seasonal scale is developed based on the proportionality hypothesis; and the model to describe seasonal storage dynamics is developed based on base flow recession analysis. All the 3 models developed in this study show good performance. The modified Budyko model and seasonal runoff model both have around 90% of the study watersheds with NSE higher than 0.5. For the seasonal storage dynamics model, the simulated contributing area and contributing storage matches well with the observed streamflow and groundwater table depth respectively.

Furthermore, at the seasonal scale, the effects of storminess, infiltration capacity, soil water storage, and topography becomes more significant. Therefore, the relationship between the seasonal model parameters and the physical factors is also investigated. Several key

controlling factors are identified in the study: vegetation, average rainfall duration, number of rainfall events, average saturated hydraulic conductivity and maximum rainfall intensity.

Two case studies focusing on the seasonal hydrologic system modeling are conducted as well, namely the Chipola River Watershed case study and the Apalachicola River Watershed case study. In the Chipola River Watershed case study, a complete seasonal water balance model is obtained by combining the modified Budyko model and seasonal runoff model. The model has a good performance on seasonal hydrologic cycle simulation. For the Apalachicola River Watershed, the SWAT model is used for hydrologic simulation. Again, a good model performance on runoff and sediment load simulation is obtained in the study. For both case studies, the future climate projections from RCMs are applied to the calibrated hydrologic model to evaluate the potential future climate change impact on the watershed systems. The result shows that the climate change impact on runoff and sediment is not significant (<5%) on the seasonal average level for both cases. However, the peak runoff and sediment load during extreme rainfall events may significantly increase under climate change scenarios.

The methodology of this study provides a guideline for seasonal time scale hydrologic modeling, and the results of the study shows that the complex watershed system can be modeled with simple equations, as long as the key controlling factors are well defined.

REFERENCES

- Ajami, H., P. A. Troch, T. Maddock III, T. Meixner, and C. Eastoe (2011), Quantifying mountain block recharge by means of catchment-scale storage-discharge relationships, *Water Resour. Res.*, 47, W04504, doi:10.1029/2010WR009598.
- Arnold, J. G., D. N. Moriasi, P. W. Gassman, K. C. Abbaspour, M. J. White, R. Srinivasan, C. Santhi, R. D. Harmel, A. van Griensven, M. W. Van Liew, N. Kannan, and M. K. Jha (2012), SWAT: model use, calibration, and validation, *T. ASABE*, 55(4), 1491-1508.
- Arnold, J. G., R. Srinivasan, R. S. Muttiah, and J. R. Williams (1998), Large-area hydrologic modeling and assessment: Part I. Model development, *J. Am. Water Resour. As.*, 34(1), 73-89.
- Barnett, T.P., D. W. Pierce, H. G. Hidalgo, C. Bonfils, B. D. Santer, T. Das, G. Bala, A. W. Wood, T. Nozawa, A. A. Mirin, D. R. Cayan, and M. D. Dettinger (2008), Human induced changes in the hydrology of the Western United States, *Science*, 319(5866), 1080-1083.
- Bauwens, A., C. Sohler, and A. Degré (2011), Hydrological response to climate change in the Lesse and the Vesdre catchment: contribution of a physically based model (Wallonia Belgium), *Hydrol. Earth Syst. Sc.*, 15, 1745-1756.
- Biswal, B., and M. Marani (2010), Geomorphological origin of recession curves, *Geophys. Res. Lett.*, 37, L24403, doi:10.1029/2010GL045415.
- Blyth, K., and J. C. Rodda (1973), A stream length study, *Water Resour. Res.*, 9(5), 1454-1461.
- Brutsaert, W., and J. L. Nieber (1977), Regionalized drought flow hydrographs from a mature glaciated plateau, *Water Resour. Res.*, 13(3), 637-644, doi:10.1029/WR013i003p00637.
- Budyko, M. I. (1958), *The heat balance of the earth's surface*, US Department of Commerce, Washington, DC.
- Budyko, M. I. (1974), *Climate and Life*, 508 pp., Academic Press, New York.
- Buttle, J. M., P. J. Dillon, and G. R. Eerkes (2004), Hydrologic coupling of slopes, riparian zones and streams: an example from the Canadian Shield, *J. Hydrol.*, 287, 161-177.
- Cai, X., D. Wang, and R. Laurent (2009), Impact of soil moisture under climate change on crop yield – a case study of rainfed corn in central Illinois, *J. Appl. Meteorol.*, 48(9), 1968-1881. DOI: 10.1175/2009JAMC1880.1.
- Changnon, S. A., F. A. Huff, and C. Hsu (1988), Relations Between Precipitation and Shallow Groundwater in Illinois, *J. Climate*, 1(12), 1239-1250.

- Chen, S., W. Huang, W. Chen, and X. Chen (2011), An enhanced MODIS remote sensing model for detecting rainfall effects on sediment plume in the coastal waters of Apalachicola Bay, *Mar. Environ. Res.*, 72, 265-272.
- Chen, X., N. Alimohammadi, and D. Wang (2013), Modeling interannual variability of seasonal evaporation and storage change based on the extended Budyko framework, *Water Resour. Res.*, 49, 6067–6078, doi:10.1002/wrcr.20493.
- Cheng, L., Z. Xu, D. Wang, and X. Cai (2011), Assessing Inter-annual Variability of ET at the Catchment Scale Using Satellite-Based ET Datasets, *Water Resour. Res.*, 47, W09509, doi:10.1029/2011WR010636.
- Choudhury, B. J. (1999), Evaluation of an empirical equation for annual evaporation using field observations and results from a biophysical model, *J. Hydrol.*, 216, 99-110.
- Christopher, J.M., J. J. Maleski, and M. F. Miller (2012), Trends in precipitation and temperature in Florida, USA. *J. Hydrol.*, 452-453, 259-281.
- Clark, M. P., D. E. Rupp, R. A. Woods, H. J. Tromp-van Meerveld, N. E. Peters, and J. E. Freer (2009), Consistency between hydrological models and field observations: Linking processes at the hillslope scale to hydrological responses at the watershed scale, *Hydrol. Process.*, 23(2), 311-319, doi:10.1002/hyp.7154.
- Clark, M. P., H. K. McMillan, D. B. G. Collins, D. Kavetski, and R. A. Woods (2011), Hydrological field data from a modeller's perspective: Part 2: process-based evaluation of model hypotheses, *Hydrol. Process.*, 25, 523-543, doi:10.1002/hyp.7902.
- Daniel, J. F. (1976), Estimating groundwater evaporation from streamflow records, *Water Resour. Res.*, 12(3), 360–364, doi:10.1029/WR012i003p00360.
- Day, J. C. (1978), International Aquifer Management: The Hueco Bolson on the Rio Grande River, *National Resource Journal*, 18(1), 163-179.
- Demissie, M., L. Keefer, Y. Lian, and F. Yue (2007), The importance of managing sedimentation in the Cache River wetlands. In Kabbes, K. C. (Ed.) Restoring our natural habitat: proceedings of the 2007 World Environmental and Water Resources Congress: May 15-19, 2007, Tampa, Florida. Reston, VA: American Society of Civil Engineers. (10 pages), doi:10.1061/40927(243)626.
- Detto, M., Molini, A., Katul, G., Stoy, P., Palmroth, S., and Baldocchi, D. (2012), Causality and persistence in ecological systems: a nonparametric spectral granger causality approach, *Am. Nat.*, 179(4), 524-535.
- Donohue, R. J., M. L. Roderick, and T. R. McVicar (2007), On the importance of including vegetation dynamics in Budyko's hydrological model, *Hydrol. Earth Syst. Sci.*, 11, 983-995.

- Donohue, R. J., M. L. Roderick, and T. R. McVicar (2010), Can dynamic vegetation information improve the accuracy of Budyko's hydrological model, *J. Hydrol.*, 390(1-2), 23-34.
- Donohue, R. J., M. L. Roderick, and T. R. McVicar (2011), Assessing the differences in sensitivities of runoff to changes in climatic conditions across a large basin, *J. Hydrol.*, 406, 234-244.
- Donohue, R. J., M. L. Roderick, and T. R. McVicar (2012), Roots, storms and soil pores: Incorporating key ecohydrological processes into Budyko's hydrological model, *J. Hydrol.*, 436-437, 35-50.
- Duan, Q., J. Schaake, V. Andréassian, S. Franks, G. Goteti, H. V. Gupta, Y. M. Gusev, F. Habets, A. Hall, L. Hay, T. Hogue, M. Huang, G. Leavesley, X. Liang, O. N. Nasonova, J. Noilhan, L. Oudin, S. Sorooshian, T. Wagener, and E. F. Wood (2006), The Model Parameter Estimation Experiment (MOPEX): An overview of science strategy and major results from the second and third workshops, *J. Hydrol.*, 320(1-2), 3-17.
- Engle, R. F., and Granger, C. W. J. (1987), Co-integration and error correction: representation, estimation, and testing, *Econometrica*, 55(2), 251-276.
- Federer, C. A. (1973), Forest transpiration greatly speeds streamflow recession, *Water Resour. Res.*, 9(6), 1599-1604.
- Feng, X., G. Vico, and A. Porporato (2012), On the effects of seasonality on soil water balance and plant growth, *Water Resour. Res.*, 48, W05543, doi:10.1029/2011WR011263.
- Florida Department of Environmental Protection (2013), Apalachicola National Estuarine Research Reserve Management Plan, Florida Department of Environmental Protection, Florida.
- Fowler, H.J., M. Ekstrom, C. G. Kilsby, and P. D. Jones (2005), New estimates of future changes in extreme rainfall across the UK using regional climate model integrations. 1. Assessment of control climate, *J. Hydrol.*, 300(1-4), 212-233.
- Fu, B. P., 1981. On the calculation of the evaporation from land surface, *Scientia Atmospherica Sinica*, 5, 23-31 (in Chinese).
- Fuelberg, H.E., and D. G. Biggar (1994), The preconvective environmental of summer thunderstorms over the Florida Panhandle, *Weather and Forecast.*, 9(3), 316-326.
- Gentine, P., P. D'Odorico, B. R. Lintner, G. Sivandran, and G. Salvucci (2012), Interdependence of climate, soil, and vegetation as constrained by the Budyko curve, *Geophys. Res. Lett.*, 39, L19404, doi:10.1029/2012GL053492.

- Gerrits, A. M., H. H. G. Savenije, E. J. M. Veling, and L. Pfister (2009), Analytical derivation of the Budyko curve based on rainfall characteristics and a simple evaporation model, *Water Resour. Res.*, 45, W04403, doi:10.1029/2008WR007308.
- Gesch, D.B. (2007), The National Elevation Dataset, in Maune, D., ed., Digital Elevation Model Technologies and Applications: The DEM User's Manual, 2nd Edition, *ASPRS*, Maryland.
- Ghaffari, G., S. Keesstra, J. Ghodousi, and H. Ahmadi (2010), SWAT-simulated hydrological impact of land-use change in the Zanjanrood Basin, Northwest Iran, *Hydrol. Process.*, 24, 892-903.
- Githui, F., W. Gitau, F. Mutua, and W. Bauwens (2009), Climate change impact on SWAT simulated streamflow in western Kenya, *Int. J. Climatol.*, 29, 1823-1834.
- Granger, C. W. J. (1969), Investigating causal relations by econometric models and cross-spectral methods, *Econometrica*, 37(3), 424-438.
- Gregory, P. W. (1976), The water quality of streamflow from Ponderosa pine forests on sedimentary soils, *M. S. Thesis*.
- Harman, C. J., M. Sivapalan, and P. Kumar (2009), Power law catchment-scale recessions arising from heterogeneous linear small-scale dynamics, *Water Resour. Res.*, 45, W09404, doi:10.1029/2008WR007392.
- Harman, C., and Troch, P. A. (2013), Darwinian hydrology: can the methodology Charles Darwin pioneered help hydrologic science?, *Hydrol. Earth Syst. Sci. Discuss.*, 10, 6407-6444, doi:10.5194/hessd-10-6407-2013, 2013.
- Hought, D. R. W., and H. J. van Meerveld (2011), Spatial variation in transient water table responses: differences between an upper and lower hillslope zone, *Hydrol. Process.*, 25, 3866-3877, doi:10.1002/hyp.8354.
- Hickel, K., and L. Zhang (2006), Estimating the impact of rainfall seasonality on mean annual water balance using a top-down approach, *J. Hydrol.*, 331, 409-424.
- Hollinger, S. E., and S. A. Isard (1994), A soil moisture climatology of Illinois, *J. Climate*, 7(5), 822-833.
- Illinois Department of Natural Resources (1998), *Spoon River Area Assessment: Volume 1: Geology*, IDNR, Springfield, IL.
- Illinois State Water Survey (2010), Illinois Monthly Evaporation Data, <http://www.isws.illinois.edu/atmos/statecli/Pan-Evap/panevapx.htm>.

- IPCC (2013), The physical science basis: Contribution of working group I to the fifth assessment report of the Intergovernmental Panel on climate change, Cambridge University Press, Cambridge, UK and New York, NY.
- Istanbulluoglu, E., T. Wang, O. M. Wright, and J. D. Lenters (2012), Interpretation of hydrologic trends from a water balance perspective: The role of groundwater storage in the Budyko hypothesis, *Water Resour. Res.*, 48, W00H16, doi:10.1029/2010WR010100.
- Jencso, K. G., B. L. McGlynn, M. N. Gooseff, S. M. Wondzell, K. E. Bencala, and L. A. Marshall (2009), Hydrologic connectivity between landscapes and streams: Transferring reach- and plot-scale understanding to the catchment scale, *Water Resour. Res.*, 45, W04428, doi:10.1029/2008WR007225.
- Jha, M., Z. Pan, E. S. Takle, and R. Gu (2004), Impacts of climate change on streamflow in the Upper Mississippi River Basin: A regional climate model perspective, *J. Geophys. Res.*, 109, D09105.
- Jothityangkoon, C., and M. Sivapalan (2009), Framework for exploration of climatic and landscape controls on catchment water balance, with emphasis on inter-annual variability, *J. Hydrol.*, 371, 154-168.
- Khoi, D., and T. Suetsugi (2014), The responses of hydrological processes and sediment yield to land-use and climate change in the Be River Catchment, Vietnam, *Hydrol. Process.*, 28, 640-652.
- Kim, U., and J. J. Kaluarachchi (2009), Climate change impacts on water resources in the upper Blue Nile river basin, Ethiopia, *J. Am. Water Resour. As.*, 45(6), 1361-1378.
- Kirchner, J. W. (2009), Watersheds as simple dynamical systems: watershed characterization, rainfall-runoff modeling, and doing hydrology backward, *Water Resour. Res.*, 45:W02429, doi:10.1029/2008WR006912.
- Koster, R. D., and M. J. Suarez (1999), A Simple Framework for Examining the Interannual Variability of Land Surface Moisture Fluxes, *J. Climate*, 12, 1911-1917.
- Krakauer, N. Y., and M. Temimi (2011), Stream recession curves and storage variability in small watersheds, *Hydrol. Earth Syst. Sci.*, 15, 2377-2389.
- L'vovich, M. I. (1979), *World Water Resources and Their Future*, translated from Russian by R. L. Nace, 415 pp., AGU, Washington, D. C.
- Legates, D. R., and G. J. McCabe Jr. (1999), Evaluating the use of "goodness-of-fit" Measures in hydrologic and hydroclimatic model validation, *Water Resour. Res.*, 35(1), 233-241, doi:10.1029/1998WR900018.

- Li, Y., B. Chen, Z. Wang, and S. Peng (2011), Effects of temperature change on water discharge, and sediment and nutrient loading in the lower Pearl River basin based on SWAT modeling, *Hydrolog. Sci. J.*, 56(1), 68-83.
- Liu, X., and W. Huang (2009), Modeling sediment resuspension and transport induced by storm wind in Apalachicola Bay, USA. *Environ. Modell. Softw.*, 24, 1302-1313.
- Livingston, R. J. (1984), The ecology of the Apalachicola Bay system: an estuarine profile, National Coastal Ecosystem Team, *US Fish and Wildlife Service*, Washington, DC.
- Lu, G., H. Xiao, Z. Wu, S. Zhang, and Y. Li (2013), Assessing the impacts of future climate change on hydrology in Huang-Huai-Hai region in China using the PRECIS and VIC models, *J. Hydrol. Eng.*, 18, 1077-1087.
- Mattraw, H. C., and J. F. Elder (1984), Nutrient and Detritus Transport in the Apalachicola River, Florida. *U.S. Geological Survey Water Supply Paper*, 2196-C.
- McDonnell, J.J., D. Brammer, C. Kendall, N. Hjerdt, L. Rowe, M. Stewart, and R. Woods (1998), Flow pathways on steep forested hillslopes: the tracer, tensiometer and trough approach. In: Tani, M., (Ed.), *Environmental Forest Science*, Kluwer, Dordrecht, pp. 463–474.
- McGlynn, B. L., and J. J. McDonnell, Quantifying the relative contributions of riparian and hillslope zones to catchment runoff, *Water Resour. Res.*, 39(11), 1310, doi:10.1029/2003WR002091, 2003.
- Mearns, L. O., W. Gutowski, R. Jones, R. Leung, S. Mcginnis, A. Nunes, and Y. Qian (2009), A regional climate change assessment program for North America, *Eos. Trans. AGU*, 90(36), 311-312.
- Milly, P. C. D. (1993), An analytic solution of the stochastic storage problem applicable to soil water, *Water Resour. Res.*, 29(11), 3755–3758.
- Milly, P. C. D. (1994a), Climate, interseasonal storage of soil-water, and the annual water-balance, *Adv. Water Resour.*, 17 (1-2), 1-24.
- Milly, P. C. D. (1994b), Climate, soil water storage, and the average annual water balance, *Water Resour. Res.*, 30, 2143-2156.
- Milly, P. C. D., and K. A. Dunne (2002), Macroscale water fluxes 2. Water and energy supply control of their interannual variability, *Water Resour. Res.*, 38(10), 1206, doi:10.1029/2001WR000760.

- Milly, P. C. D., and R. T. Wetherald (2002), Macroscale water fluxes, 3, Effects of land processes on variability of monthly river discharge, *Water Resour. Res.*, 38(11), 1235, doi:10.1029/2001WR000761.
- Milly, P. C. D., J. Betancourt, M. Falkenmark, R.M. Hirsch, Z. W. Kundzewicz, D. P. Lettenmaier, and R. J. Stouffer (2008), Stationarity is dead: whither water management? *Science*, 319(5863), 573-574.
- Molénat, J., C. Gascuel-Oudou, L. Ruiz, and G. Gruau (2008), Role of water table dynamics on stream nitrate export and concentration in agricultural headwater catchment, *J. Hydrol.*, 348, 364-378.
- Moriasi, D. N., J. G. Arnold, M. W. Van Liew, R. L. Bingner, R. D. Harmel, and T. L. Veith (2007), Model evaluation guidelines for systematic quantification of accuracy in watershed simulations, *T. ASABE*, 50(3): 885–900.
- Mulholland, P. J., G. R. Best, C. C. Coutant, G. M. Hornberger, J. L. Meyer, P. J. Robinson, J. R. Stenberg, R. E. Turner, F. Vera-Herrera, and R. G. Wetzel (1997), Effects of climate change on freshwater ecosystems of the south-eastern United States and the Gulf Coast of Mexico, *Hydrol. Process.*, 11(8), 949-970.
- Nagy, R. C., B. G. Lockaby, L. Kalin, and C. Anderson (2012), Effects of urbanization on stream hydrology and water quality: the Florida Gulf Coast, *Hydrol. Process.*, 26, 2019-2030.
- Nash, J. E., and J. V. Sutcliffe (1970), River forecasting using conceptual models. 1: A discussion of principles, *J. Hydrol.*, 10, 280– 290.
- Nathan, R. J., and T. A. McMahon (1990), Evaluation of automated techniques for base flow and recession analyses, *Water Resour. Res.*, 26(7), 1465-1473.
- Neitsch, S. L., J. G. Arnold, J. R. Kiniry, and J. R. Williams (2011), *Soil and Water Assessment Tool Theoretical Documentation*, Texas Water Resources Institute, Texas.
- Ocampo, C. J., M. Sivapalan, and C. E. Oldham (2006), Hydrological connectivity of upland-riparian zones in agricultural catchments: Implications for runoff generation and nitrate transport, *J. Hydrol.*, 331, 643-658.
- Palmroth, S., G. G. Katul, D. Hui, H. R. McCarthy, R. B. Jackson, and R. Oren (2010), Estimation of long-term basin scale evaporation from streamflow time series, *Water Resour. Res.*, 46, W10512, doi:10.1029/2009WR008838.
- Peterson, R. N., W. C. Burnett, S. P. Opsahl, I. R. Santos, S. Misra, and P. N. Froelich (2013), Tracking suspended particle transport via radium isotopes (²²⁶Ra and ²²⁸Ra) through the Apalachicola-Chattahoochee-Flint River system, *J. Environ. Radioactiv.*, 116, 65-75.

- Phan, D. B., C. C. Wu, and S. C. Hsieh (2011), Impact of climate change on stream discharge and sediment yield in northern Viet Nam, *Water Resour.*, 38(6), 827-836.
- Pike, J. G. (1964), The estimation of annual runoff from meteorological data in a tropical climate, *J. Hydrol.*, 2, 116– 123.
- Ponce, V. M., and A. V. Shetty (1995), A conceptual model of catchment water balance. 1. Formulation and calibration, *J. Hydrol.*, 173, 27–40.
- Ponce, V. M., and R. H. Hawkins (1996), Runoff curve number: has it reached maturity? *J. Hydraul. Eng.-ASCE*, 1(1), 11-19.
- Porporato, A., E. Daly, and I. Rodriguez-Iturbe (2004), Soil water balance and ecosystem response to climate change, *Am. Nat.*, 164(5), 625– 632.
- Potter, N. J., and L. Zhang (2009), Interannual variability of catchment water balance in Australia, *J. Hydrol.*, 369, 120-129.
- Potter, N. J., L. Zhang, P. C. D. Milly, T. A. McMahon, and A. J. Jakeman (2005), Effects of rainfall seasonality and soil moisture capacity on mean annual water balance for Australian catchments, *Water Resour. Res.*, 41, W06007, doi:10.1029/2004WR003697.
- Priestley, C. H. B., and R. J. Taylor (1972), On the assessment of surface heat flux and evaporation using large-scale parameters, *Mon. Weather Rev.*, 100:81-82.
- Roderick, M. L., and G. D. Farquhar (2011), A simple framework for relating variations in runoff to variations in climatic conditions and catchment properties, *Water Resour. Res.*, 47, W00G07, doi:10.1029/2010WR009826.
- Rodhe, A., and J. Seibert (2011), Groundwater dynamics in a till hillslope: flow directions, gradients and delay, *Hydrol. Process.*, 25, 1899-1909, doi:10.1002/hyp.7946.
- Rupp, D. E., J. Schmidt, R. A. Woods, and V. J. Bidwell (2009), Analytical assessment and parameter estimation of a low-dimensional groundwater model, *J. Hydrol.*, 377, 143–154.
- Sankarasubramanian, A., and R. V. Vogel (2002), Annual hydroclimatology of the United States, *Water Resour. Res.*, 38, 1083. doi:10.1029/2001WR00061.
- Sankarasubramanian, A., and R. V. Vogel (2003), Hydroclimatology of the continental United States, *Geophys. Res. Lett.*, 30(7), 1363, doi:10.1029/2002GL01593.
- Santhi, C., J. G. Arnold, J. R. Williams, W. A. Dugas, and L. Hauck (2001), Validation of the SWAT model on a large river basin with point and nonpoint sources, *J. Am. Water Resour. As.*, 37(5), 1169-1188.

- Sayama, T., J. J. McDonnell, A. Dhakal, and K. Sullivan (2011), How much water can a watershed store? *Hydrol. Process.*, 25(25), 3899–3908, doi:10.1002/hyp.8288.
- Scott, R. W., E. C. Krug, and S. L. Burch (2010), Illinois Soil Moisture under Sod Experiment, *J. Hydrometeor.*, 11, 683-704, doi:10.1175/2009JHM1130.1.
- Seibert, J., K. Bishop, A. Rodhe, and J. J. McDonnell (2003), Groundwater dynamics along a hillslope: A test of the steady state hypothesis, *Water Resour. Res.*, 39(1), 1014,doi:10.1029/2002WR001404.
- Sivapalan, M. (2005), Patterns, process and function: Elements of a unified theory of hydrology at the catchment scale, in: *Encyclopedia of Hydrological Sciences*, John Wiley and Sons.
- Sivapalan, M., G. Blöschl, L. Zhang, and R. Vertessy (2003), Downward approach to hydrological prediction, *Hydrol. Process.*, 17, 2101-2111, doi: 10.1002/hyp.1425.
- Sivapalan, M., H. H. G. Savenije, and G. Blöschl (2012), Socio-hydrology: A new science of people and water, *Hydrol. Process.*, 26, 1270-1276, doi: 10.1002/hyp.8426.
- Sivapalan, M., M. A. Yaeger, C. J. Harman, X. Xu, and P. A. Troch (2011), Functional model of water balance variability at the catchment scale: 1. Evidence of hydrologic similarity and space-time symmetry, *Water Resour. Res.*, 47, W02522, doi:10.1029/2010WR009568.
- Sloan, W. T. (2000), A physics-based function for modeling transient groundwater discharge at the watershed scale, *Water Resour. Res.*, 36(1), 225-241.
- Spence, C., Guan, X. J., Phillips, R., Hedstorm, N., Granger, and G., Reid, B. (2010), Storage dynamics and streamflow in a catchment with a variable contributing area, *Hydrol. Process.*, 24, 2209-2221, doi:10.1002/hyp.7492.
- Stallins, A. J., M. Nesiuis, M. Smith, and K. Watson (2010), Biogeomorphic characterization of floodplain forest change in response to reduced flows along the Apalachicola River, Florida, *River Res. Appl.*, 26, 242-260.
- Stoelzle, M., K. Stahl, and M. Weiler (2013), Are streamflow recession characteristics really characteristic? *Hydrol. Earth Syst. Sci.*, 17, 817-828.
- Swenson, S., P. J.-F. Yeh, J. Wahr, and J. Famiglietti (2006), A comparison of terrestrial water storage variations from GRACE with in situ measurements from Illinois, *Geophys. Res. Lett.*, 33, L16401, doi:10.1029/2006GL026962.
- Szilagyi, J., Z. Gribovszki, and P. Kalicz (2007), Estimation of catchmentscale evaporation from baseflow recession data: Numerical model and practical application results, *J. Hydrol.*, 336, 206–217.

- Teuling, A. J., I. Lehner, J. W. Kirchner, and S. I. Seneviratne (2010), Catchments as simple dynamical systems: Experience from a Swiss prealpine catchment, *Water Resour. Res.*, 46, W10502, doi:10.1029/2009WR008777.
- Troch, P. A., G. Carrillo, M. Sivapalan, T. Wagener, and K. Sawicz (2013), Climate-vegetation-soil interactions and long-term hydrologic partitioning: signatures of catchment co-evolution, *Hydrol. Earth Syst. Sci.*, 17, 2209–2217.
- Tromp-van Meerveld, H. J., and J. J., McDonnell (2006a), Threshold relations in subsurface stormflow: 1. A 147-storm analysis of the Panola hillslope, *Water Resour. Res.*, 42, W02410. doi:10.1029/2004WR003778.
- Tromp-van Meerveld, H. J., and J. J., McDonnell (2006b), Threshold relations in subsurface stormflow: 2. The fill and spill hypothesis, *Water Resour. Res.*, 42, W02411. doi:10.1029/2004WR003800.
- Tu, T. (2009), Combined impact of climate and land use changes on streamflow and water quality in eastern Massachusetts, USA, *J. Hydrol.*, 379, 268-283.
- Tucker, C.J., J. E. Pinzon, M. E. Brown, D. Slayback, E. W. Pak, R. Mahoney, E. Vermote, and N. El Saleous (2005), An extended AVHRR 8-km NDVI data set compatible with MODIS and SPOT vegetation NDVI data. *Int. J. Remote Sens.*, 26(20), 4485-5598.
- Turc, L. (1954), Le bilan d'eau des sols: Relation entre les précipitations, l'évaporation et l'écoulement, *Ann. Agron.*, 5, 491-569.
- US Department of Agriculture (USDA) (2007), Soil survey geographic database, USDA, Washington, DC. Available online at <http://websoilsurvey.nrcs.usda.gov/>. Last Accessed [04/23/2013].
- US Department of Agriculture Soil Conservation Service (USDA SCS), 1985. National Engineering Handbook, Section 4: Hydrology. SCS, Washington, D.C.
- US Department of Agriculture Soil Conservation Service (USDA SCS) (1985), *National Engineering Handbook, Section 4: Hydrology*, SCS, Washington, DC.
- Vidon, P. (2012), Towards a better understanding of riparian zone water table response to precipitation: surface water infiltration, hillslope contribution or pressure wave processes? *Hydrol. Process.*, 26, 3207-3215, doi:10.1002/hyp.8258.
- Vidon, P., and A. R. Hill (2004), Landscape controls on nitrate removal in stream riparian zones, *Water Resour. Res.*, 40, W03201, doi:10.1029/2003WR002473.
- Vogel, R., and C. Kroll (1992), Regional geohydrologic-geomorphic relationships for the estimation of low-flow statistics, *Water Resour. Res.*, 28, 2451–2458.

- Vogelmann, J. E., S. M. Howard, L. Yang, C. R. Larson, B. K. Wylie, and J. N. Van Driel (2001), Completion of the 1990's National Land Cover Data Set for the conterminous United States, *Photogramm. Eng. Remote Sens.*, 67, 650-662.
- Wang, D. (2011), On the base flow recession at the Panola Mountain Research Watershed, Georgia, USA, *Water Resour. Res.*, 47, W03527, doi:10.1029/2010WR009910.
- Wang, D. (2012a), Evaluating interannual water storage changes at watersheds in Illinois based on long-term soil moisture and groundwater level data, *Water Resour. Res.*, 48, W03502, doi:10.1029/2011WR010759.
- Wang, D. (2012b), Assessing the impact of subsurface storage contributing area on the watershed scale storage-discharge function derived from baseflow recession at the Spoon River in Illinois, *ASCE-World Environmental and Water Resources Congress in Albuquerque, New Mexico - May 20-24, 2012*.
- Wang, D. and Y. Tang (2014), A one-parameter Budyko model for water balance captures emergent behavior in Darwinian hydrologic models, *Geophys. Res. Lett.*, 41, doi:10.1002/2014GL060509.
- Wang, D., and M. Hejazi (2011), Quantifying the relative contribution of the climate and direct human impacts on mean annual streamflow in the contiguous United States, *Water Resour. Res.*, 47, W00J12, doi:10.1029/2010WR010283.
- Wang, D., and N. Alimohammadi (2012), Responses of annual runoff, evaporation, and storage change to climate variability at the watershed scale, *Water Resour. Res.*, doi:10.1029/2011WR011444.
- Wang, D., M. Hejazi, X. Cai, and A. J. Valocchi (2011), Climate change impact on meteorological, hydrological, and agricultural drought in central Illinois, *Water Resour. Res.*, 47, W09527, doi:10.1029/2010WR009845.
- Wang, D., S. C. Hagen, and K. Alizad (2013), Climate change impact and uncertainty analysis of extreme rainfall events in the Apalachicola River basin, Florida, *J. Hydrol.*, 480, 125-135.
- William, J. R. (1995), The EPIC model. In *Computer models of watershed hydrology*, Singh, V.P. (ed.), Water Resources Publications.
- Wittenberg, H., and M. Sivapalan (1999), Watershed groundwater balance estimation using streamflow recession analysis and base flow separation, *J. Hydrol.*, 219(1-2), 20-33.
- Wood, A.W., E. P. Maurer, A. Kumar, and D. P. Lettenmaier (2002), Long-range experimental hydrologic forecasting for the eastern United States, *J. Geophys. Res.*, 107(D20), 4429.

- Xu, X., D. Yang, and M. Sivapalan (2012), Assessing the impact of climate variability on catchment water balance and vegetation cover. *Hydrol. Earth Syst. Sci.*, 16, 43–58, doi:10.5194/hess-16-43-2012.
- Yang, D., F. Sun, Z. Liu, Z. Cong, G. Ni, and Z. Lei (2007), Analyzing spatial and temporal variability of annual water-energy balance in nonhumid regions of China using the Budyko hypothesis, *Water Resour. Res.*, 43, W04426, doi:10.1029/2006WR005224.
- Yang, H., and D. Yang (2011), Derivation of climate elasticity of runoff to assess the effects of climate change on annual runoff, *Water Resour. Res.*, 47, W07526, doi:10.1029/2010WR009287.
- Yang, H., D. Yang, Z. Lei, and F. Sun (2008), New analytical derivation of the mean annual water-energy balance equation, *Water Resour. Res.*, 44, W03410, doi:10.1029/2007WR006135.
- Yokoo, Y., M. Sivapalan, and T. Oki (2008), Investigating the roles of climate seasonality and landscape characteristics on mean annual and monthly water balances, *J. Hydrol.*, 357, 255-269.
- Zanardo, S., C. J. Harman, P. A. Troch, P. S. C. Rao, and M. Sivapalan (2012), Intra-annual rainfall variability control on interannual variability of catchment water balance: A stochastic analysis, *Water Resour. Res.*, 48, W00J16, doi:10.1029/2010WR009869.
- Zhang, C., C. A. Shoemaker, J. D. Woodbury, M. Cao, and X. Zhu (2013), Impact of human activities on stream flow in the Biliu River basin, China, *Hydrol. Process.*, 27, 2509-2523.
- Zhang, K., J. S. Kimball, R. R. Nemani, and S. W. Running (2010), A continuous satellite-derived global record of land surface evapotranspiration from 1983 to 2006, *Water Resour. Res.*, 46, W09522, doi:10.1029/2009WR008800.
- Zhang, L., N. Potter, K. Hickel, Y. Zhang, and Q. Shao (2008), Water balance modeling over variable time scales based on the Budyko framework – Model development and testing, *J. Hydrol.*, 360, 117-131.
- Zhang, L., W. R. Dawes, and G. R. Walker (2001), Response of mean annual evapotranspiration to vegetation changes at catchment scale, *Water Resour. Res.*, 37(3), 701-708.
- Zhang, X., R. Srinivasan, J. G. Arnold, R. C. Izaurralde, and D. D. Bosch (2011), Simultaneous calibration of surface flow and baseflow simulations: a revisit of the SWAT model calibration framework, *Hydrol. Process.*, 25, 2313-2320.
- Zhang, Y., and F. H. S. Chiew (2009), Relative merits of different methods for runoff predictions in ungauged catchments, *Water Resour. Res.*, 45, W07412, doi:10.1029/2008WR007504.

Zhu, Y., X. Lu, and Y. Zhou (2008), Sediment flux sensitivity to climate change: A case study on the Longchuanjiang catchment of the upper Yangtze River, China, *Global Planet. Change*, 60, 429-442.